TELEOPERATION SYSTEM DESIGN OF A ROBOT ASSISTED ENDOSCOPIC PITUITARY SURGERY

A Thesis Submitted to
the Graduate School of Engineering and Sciences of
İzmir Institute of Technology
in Partial Fulfillment of the Requirements for the Degree of

MASTER OF SCIENCE

in Mechanical Engineering

by
Gizem ATEŞ

July 2018
İZMİR

We approve the thesis of **Gizem ATEŞ**

Examining Committee Members:

Assoc. Prof. Dr. Mehmet İsmet Can DEDE
Department of Mechanical Engineering
İzmir Institute of Technology

Assoc. Prof. Dr. Tolga AYAV
Department of Computer Engineering
İzmir Institute of Technology

Assoc. Prof. Dr. Levent ÇETİN
Department of Mechatronics Engineering
İzmir Katip Çelebi University

10/07/2018

Assoc. Prof. Dr. Mehmet İsmet Can DEDE
Supervisor
Mechanical Engineering
Izmir Institute of Technology

Prof. Dr. Metin TANOĞLU
Head of the Department of
Mechanical Engineering

Prof. Dr. Aysun SOFUOĞLU
Dean of the Graduate School of
Engineering and Sciences

ACKNOWLEDGMENTS

I would like to start expressing my gratitude with my dear parents Bahattin and Ayşen Ateş, and my lovely sister İzel Ateş for their immeasurable support, patience, and encouragements every single day of my life besides this research period.

I owe a deep sense of gratitude to my dear advisor Dr. Mehmet İsmet Can Dede for his invaluable guidance throughout my years at IZTECH Mechanical Engineering Department as well as his support at every stage of my research.

It is a privilege to thank my precious friends Çağhan Kirişci and Ronny Majani for their inestimable encouragements. Their prompt suggestions, both technical and moral support made a significant contribution in completing my thesis.

It is also a genuine pleasure to express my thanks to Ruhi Dede for his priceless knowledge, timely suggestions with kindness and patience.

Moreover, I would like to thank my dear friends in IZTECH Robotics Laboratory and IZTECH Prototyping Laboratory. Also, I would like to express many thanks to my dear professors who have supported NeuRoboScope project with their valuable experiences, Dr. Gökhan Kiper, Dr. Tolga Ayav, Dr. Barbaros Özdemirel, Prof. Dr. Enver Tatlıcıoğlu.

In particular, I would like to extend special thanks to my dearie friend Neslihan Kutlu for her eternal support and keeping up my motivation high anytime I need.

This study is funded by *The Scientific and Technological Research Council of Turkey (TÜBİTAK)* with the project name *NeuRoboScope - Robot Assisted Endoscope Control that can be Controlled by the Surgical Tools* and grant number *115E726*.

ABSTRACT

TELEOPERATION SYSTEM DESIGN OF A ROBOT ASSISTED ENDOSCOPIC PITUITARY SURGERY

Teleoperation, also named telerobotics, is defined as controlling a robot over a distance by a remote controller. In a teleoperation setting, the human operator controls the master system(s) in order to send command(s) to the slave system(s) via wired or wireless communication channel. Generally, in bilateral teleoperation, the human operator is informed about the slave environment via feedback signals (haptic, visual or audio) sent back from the slave environment.

Commonly, teleoperated systems are more preferable in hazardous environments to protect the human operator; nevertheless, there many other fields where the teleoperated systems are employed for various tasks. One of these areas, where teleoperation technology is becoming more popular, is the medical area. Telesurgical equipments allow more precise performance than a human can achieve especially in minimally invasive surgeries.

The purpose of this thesis is to develop a novel teleoperation system architecture which will be used to support the endoscopic pituitary surgery procedures which are classified under minimally invasive surgeries. Even though, the surgeon has only two hands, the proposed system aims to enable the surgeon to operate with three different surgical tools simultaneously including the endoscope. The type of work is categorized under collaborative surgical robots, which incorporates a teleoperation system setup. The master control unit is a ring-shaped remote controller which consists of an inertial measurement unit and a wireless module. Surgeon wears the master system during the operation while holding a surgical tool such as the aspirator, and delivers the voluntary commands to the slave system by triggering a foot pedal. The slave is the endoscope holder robot which is a 8 degrees-of-freedom manipulator whose 3 degrees-of-freedom are active and the rest of them are passive. There is also an indicator panel which is used to provide visual feedback to the surgeon indicating the states of the surgery and excessive force application on the tissue.

ÖZET

ROBOT YARDIMLI ENDOSKOPİK HİPOFİZ AMELİYATININ TELEOPERASYON SİSTEMİ TASARIMI

Teleoperasyon, bir diğer adıyla telerobotik, bir robotun uzaktan kumanda edilmesi olarak tanımlanmaktadır. Bir teleoperasyon sisteminde, insan operatörü bağımlı sistemi kontrol etmek için kablolu veya kablosuz iletişim kanalı yoluyla ana sistem tarafından komutlar gönderir. Genel olarak, çift yönlü teleoperasyonda, insan operatörü geri besleme sinyalleri vasıtatısla (haptik, görsel veya işitsel) bağımlı ortam hakkında bilgilendirilir.

Genel olarak teleoperatör sistemler insan operatörünü korumak için tehlikeli ortamlarda tercih edilmesine rağmen teleoperatif sistemlerin çeşitli görevlere dahil olduğu birçok farklı alan vardır. Teleoperasyon teknolojisinin gittikçe daha populerleştiği bu alanlardan biri ise sağlık sektörüdür. Uzaktan kumanda edilebilen ekipmanlar özellikle minimal invaziv cerrahilerde insan ögesine nazaran çok daha hassas performans sağlar.

Bu tezin amacı, minimal invaziv cerrahi altında sınıflandırılan endoskopik hipofiz cerrahisinde kullanılacak cerraha yardımcı bir özgün bir teleoperasyon sistemi geliştirmektir. Önerilen sistem, cerrahın iki elini kullanarak aynı anda, endoskop da dahil olarak, üç farklı cerrahi araçla eş zamanlı olarak çalışmasını sağlamaktadır. Önerilen sistemin çalışma türü, teleoperasyon sistemi kurulumunu da içeren işbirlikçi cerrahi robotlar altında kategorize edilir. Ana kontrol ünitesi, atalet ölçüm birimi ve kablosuz modülden oluşan halka şeklinde bir uzaktan kumandadır. Cerrah ameliyat süresince bu kumanda sistemini takar ve aspiratör gibi bir cerrahi aleti tutarken bir ayak pedalı tetiklemesi ile el hareketlerini bağımlı sisteme kablosuz olarak iletir. Bağımlı sistem, 3 serbeslik derecesi tahriklenmiş ve geri kalan mafsalları tahriklenmemiş, 8 serbestlik dereceli bir manipülatör olan bir endoskop tutucu robottur. Ayrıca, sistemin anlık durumlarını ileten, dokuya/kemiğe aşırı baskı uygulandığı sırada cerraha görsel geri bildirim sağlayan bir de gösterge paneli bulunmaktadır.

I would like to dedicate this thesis to my dear parents
Ayşen and Bahattin ATEŞ, and my lovely sister İzel.

TABLE OF CONTENTS

LIST OF FIGURES

LIST OF TABLES

LIST OF ABBREVIATIONS

ADD ..... Emergency Button (Tr: **A**cil **D**urum **D**üğmesi)
AGA ..... Main Power Button (Tr: **A**na **G**üç **A**nahtarı)
AKS ..... Main Control Unit (TR: **A**na **K**umanda **S**istemi)
ASB ..... Surgery Zone Button (Tr: **A**meliyat **S**ınır **B**ölgesi Düğmesi)
BLE ..... Bluetooth Low Energy
CEK ..... Surgeron Holds Endoscope (Tr: **C**errah **E**ndoskobu **K**avradı)
CSRS ..... Collaborative Surgical Robotic System
DMA ..... Direct Memory Access
DoF ..... Degrees of Freedom
F/T ..... Force/Torque
GPIO ..... General Purpose Input/Output
HAS ..... Communication System (TR: **Ha**berleşme **S**istemi)
HCI ..... Host Controller Interface
HTM ..... Homogenous Transformation Matrix
IC ..... Integrated Circuit
IMU ..... Inertial Measurement Unit
IoT ..... Internet of Things
IRQ ..... Interrupt Request
ISR ..... Interrupt Service Routine
KAR ..... User Interface (TR: **K**ullanıcı **A**ra**y**üzü)
KEY ..... Active Endoscope Holder (TR: A**k**tif **E**ndoskop **Y**önlendirici)
MEMS ..... Micro Electro-Mechanical System
MIS ..... Minimally Invasive Surgery
MISO ..... Master-Input Slave-Output
MKB ..... Manual Control Button (Tr: **M**aunel **K**ontrol **B**utonu)
MOSFET ..... Metal-Oxide Semiconductor Field-Effect Transistor
MOSI ..... Master-Output Slave-Input
OPAMP ..... Operational Amplifier
PCB ..... Printed Circuit Board
PEK ..... Passive Balanced Arm (TR: **P**asif D**e**ngelenmiş **K**ol)
SCK ..... System Clock
SoC ..... System-on-Chip

CHAPTER 1

INTRODUCTION

Robotic surgery is defined as having surgical tasks executed by a robot operating autonomously, with partial or no human involvement. It is getting more preferable due to its accuracy and dexterity (Kim, 2014). They provide better vision and more precise movements than a human can do. By introducing new approaches to the surgeries, the capability of clinicians and the success rates of the surgeries are enhanced based on the meta-analyses and comparative systematic reviews (Kockerling, 2014). For that reason, there have been many robotic solutions proposed for the literature (Ballantyne, 2002; Lanfranco et al., 2004; Kim, 2014). For example, Finlay (1989) discussed about 400 applications that use robots in the medical area. ThinkSurgical (2018)

In 1978, one of the most commonly used industrial robot called PUMA 560 (Programmable Universal Machine for Assembly) robot was developed by Victor Scheinman at Unimation (Kim, 2014; Austin, Edmund; Fong, 1987). It is a smaller version of the first industrial robot Unimate which was patented in 1954 (granted in 1961) (Rosheim, 1994; Devol, 2 10). It was used in the field of medicine in 1985 for the first time by Kwoh et al. (1988). With 0.05mm accuracy, a stereotactic needle brain biopsy was achieved by using PUMA robot. Moreover, the first robot-assisted surgical procedure was performed in 1983 by Arthrobot to be used in orthopedic procedures (Mohammad, 2013). In 1988, ROBODOC system was introduced for total hip surgeries. It is also the first FDA-approved surgical robot in the history(ThinkSurgical, 2018). Further, ACROBOT surgical robot which has a similar design to ROBODOC was employed for the first knee replacement surgery (Jakopec et al., 2002).

In the 1990s, according to Kim (2014), Surgeon-Assistant Robot for Prostatectomy (SARP) system was developed as the first robot used in a prostate surgery. Further development of SARP, other robots for prostate surgery are developed as well. For instance PROBOT (Prostate Robot, (Davies et al., 1991) has a 4-DoF with a rotating blade as the end effector. It was developed by Imperial College, London, worked through a 3D image of the prostate. After the surgeon determines the boundaries of the resection area on the 3D image, PROBOT uses those data to execute the procedure without further intervention from the surgeon. CARLP (Computer-Assisted Transurethral Laser Resection of the Prostate, (Ho et al., 2001) has a similar structure, however, it has a laser endpoint

for resection.

While Scott Fischer (computer scientist) in National Air and Space Administration (NASA) Ames Research Center working on virtual reality area developed a 3D head-mounted display (HDM) to be attached on the helmet in aerospace missions, Dr. Joseph Rosen was experimenting on a dexterity-enhancing surgical telemanipulator. Afterwards, Joseph Rosen and Scott Fischer built upon these to develop telesurgery system to operate surgeries remotely by combining the idea of HMD at NASA and the robotic telepresence system which Dr. Joseph Rosen was using at Stanford Research Institute (Kim, 2014).

The first telesurgical experiment was performed by Jon Bowersox, who is a vascular surgeon, on an ex vivo subject via Stanford Research Institute's teleoperated system (Bowersox et al., 1996). On the surgeon's side, a full-color stereoscopic (3D) image of the operation is provided while two master robot arms grasped by the two hands of the surgeon. By these two master robot arms, he makes the robot perform the operation by teleoperation.

From spin-offs of NASA, AESOP and HERMES robotic systems were introduced to literature by Computer Motion company. AESOP is a voice-controlled endoscope holder arm, and HERMES is an integrated operating room control system. Later, ZEUS robotic system was introduced as a combination of AESOP and HERMES. It was a master-slave system which allowed the surgeon to control a robotic slave device (AESOP) remotely by a console of HERMES (Nathan et al., 2006).

Moreover, Beasley (2012) identified 9 distinct medical fields to use robots: neurological, orthopedics, general laparoscopy, percutaneous, steerable catheters, radio-surgery, emergency response, prosthetics & exoskeletons and assistive & rehabilitation systems. These robotic systems have been developed for many different medical procedures and their design varies according to their purpose and type of the surgery. Among the variety of medical procedures, minimally invasive surgery is a methodology which is receiving increased attention and where new systems are continuously being introduced.

1.1. Minimally Invasive Surgery

Minimally Invasive Surgery (MIS) is an operation type offered to reduce the side effects of the conventional surgeries. It can be performed either by making small incisions, which is called laparoscopic process or entering from the body's neutral spaces which are endoscopic or colonoscopic processes. Despite some doubts about advantages in overall perspective, in all the above-mentioned operations, MIS override conventional

surgeries considering the comfort of patients in their healing period (Hernandez-Vaquero et al., 2012) since the incisions made are relatively small with respect to the open-surgery procedures as it can be depicted from Figure 1.1. Since the workspace in MIS is unquestionably small compared to open surgeries, the freedom of action for the surgeon is confined. Even though the surgeons have relatively better eye-hand coordination, for some MIS areas such as inside the skull, there is a higher risk to damage other tissues or organs. For instance, in pituitary surgeries, the working area is in the vicinity of visual nerves by a couple of millimeters.

Figure 1.1. Open surgery vs minimally invasive surgery
(Source: www.pauljeffordsmd.com/minimally-invasive-surgical-mis-tlif)

1.2. Pituitary Gland, Adenoms, and Resection

The pituitary gland, also called hypophysis or ”master gland”, is a significant member of the endocrine system. It is a ductless gland and secretes hormones directly into the bloodstream. It makes or stores many different hormones. Stimulated actions of the by pituitary gland can be summarized as follows:

- *Prolactin* - Regulation of sex hormone levels in both genders, as well as fertility.
- *Growth hormone (GH)* - Production of growth in childhood and maintains muscle mass and bone mass.
- *Adrenocorticotropin (ACTH)* - Production of cortisol by the adrenal glands. It helps to maintain blood pressure and blood glucose (sugar) levels.

- *Thyroid-stimulating hormone (TSH)* - Production of thyroid hormones, which regulate the body's metabolism, energy balance, growth, and nervous system activity
- *Luteinizing hormone (LH)* - Testosterone production in men and egg release (ovulation) in women.
- *Follicle-stimulating hormone (FSH)* - Promotion of sperm production in men and production of estrogen and develop eggs in women. LH and FSH work together to enable the normal function of the ovaries and testes.
- *Antidiuretic hormone (ADH)* -Regulation of water balance in the body.
- *Oxytocin* – Milk production of breastfeeding women.

The pituitary gland is about 1 cm diameter pea-sized tiny gland lies in the middle of the skull and covered by a bony structure called the sella turcica, which is behind the nose and just below the hypothalamus (see Figure 1.2).

Pituitary tumors (also called pituitary adenomas) are located on the anterior part of the pituitary. They are 3^{rd} most common intra-cranial tumor type Jane et al. (2005). Also Ezzat et al. (2004) states that prevalence of pituitary adenomas are found 22.5% in radiologic studies and 14.4% in autopsy studies. Depending on their size, they are broadly classified into two categories:

- pituitary microadenoma: less than 10 mm in size
- pituitary macroadenoma: greater than 10 mm in size

It is also important to note that larger tumors can lead to hormonal imbalance due to mass effect rather than secretion (Pisaneschi and Kapoor, 2005). Since pituitary has a critical role in regulating the hormonal balance of the whole body, patients who suffer from this disease may experience following symptoms: headaches, vision problems, unexplained tiredness, mood changes, irritability, changes in menstrual cycles in women, impotence etc.

Nowadays, pituitary adenomas resections can be performed by three different methods; conventional open-skull surgeries, microscopic transsphenoidal surgeries and endoscopic endonasal surgeries. Among these methods, depending on the placement and the size of the tumor, the endoscopic method is more preferable due to its low-recovery period, cost-efficiency and less hospitalization duration (Komotar et al., 2011; Ezzat et al., 2004; Berker et al., 2013). In this method, an optical system called the endoscope is inserted through and directed inside the nostril to move through the nasal cavity to the

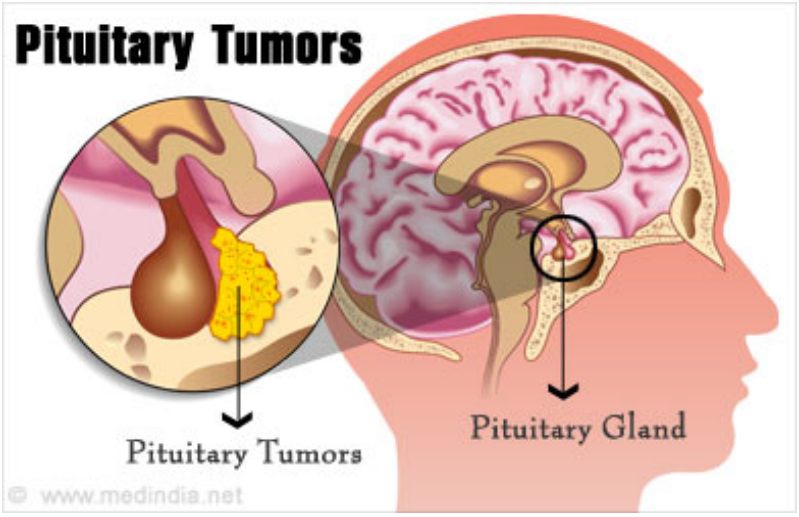

Figure 1.2. Pituitary gland and location of adenoms
(Source: www.medindia.net/patients/patientinfo/pituitary-tumors.htm))

sphenoid sinus, which is in front of the sella turcica. Then, the tumor is resected by the special surgical tools, which are also inserted through the nostrils as shown in Figure 1.3.

1.3. Problem Statement

Although endoscopic pituitary surgeries are superior to other conventional methods in some aspects (Almeida et al., 2015; Komotar et al., 2011; Berker et al., 2014), they have still drawbacks mostly on the surgeon's side. For an average of 2-4 hours surgery duration, the surgeon has to hold the endoscope for the whole operation process and he/she is only able to use one hand to operate with the other surgical tools. This problem results in longer operation duration and fatigue of the surgeon, and the constraint to use only one hand for the other surgical tools decrease the efficiency of the surgery. Generally, while the surgeon executes this operation, one or more assistants help him/her in holding the endoscope in case the surgeon needs to use both hands at the same time. Nevertheless, synchronization problems between the surgeon and the assistant produce a less efficient surgical process compared to the surgeon having the endoscope controlled by himself/herself. As seen in Figure 1.4 that the surgeon and the assistant should work cooperatively when the second and third tools are needed during the process.

In order for the surgeon to operate with two surgical tools at the same time, the surgeon needs a third hand, which is to be controlled by the surgeon himself/herself that holds and positions the endoscope. There are some proposed ideas and developed systems

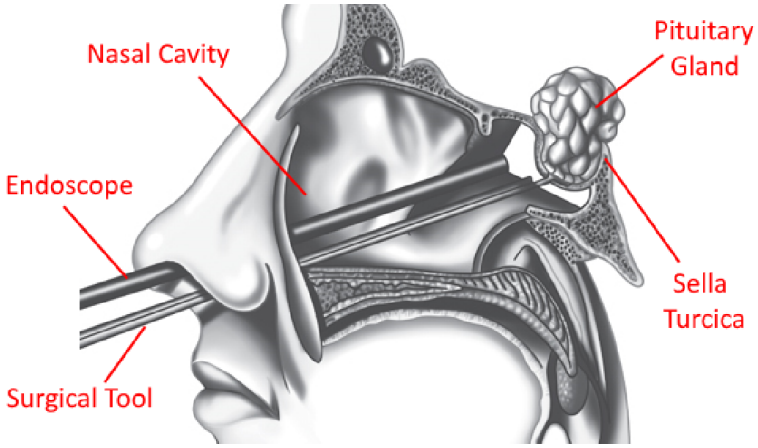

Figure 1.3. Endoscopic pituitary surgery process
(Source: www.pearsonitcertification.com/articles/article.aspx?p=2165279)

that address this problem in the literature and they are explained in Chapter 2. However, these previously developed systems fail to provide a solution that enables the surgeon to operate efficiently without any interruptions and thus, they did not become a common solution in these type of surgeries.

Figure 1.4. A photo from the endsocopic pituary tumor surgery

1.4. NeuRoboScope Project

This thesis study is based on the work carried out within the ”Robot-Assisted Endoscope Control that can be Controlled by the Surgical Tools” (NeuRoboSope) project supported by TÜBİTAK, *The Scientific and Technological Research Council of Turkey*

(Turkish: Türkiye Bilimsel ve Teknolojik Araştırma Kurumu), under the project 115E726. TÜBİTAK is a national agency in Turkey supporting the developments in ”science, technology and innovation” and conducting research, in Turkey. It was founded in 1963 as an autonomous public institution, governed by a Science Board.

The aim of NeuRoboScope project is to develop a precise robotic system to be used in minimally invasive pituitary surgeries which will provide a third hand for the surgeon to hold and position the endoscope.

Under this project, there are three subcategories of work carried out by different project teams;

- Mechanical design of the 8 DoF (3-DoF active and 5-DoF passive) endoscope holder robotic arm (by the mechanical team),
- Electronic and software design of both main PCB board and the master controller for teleoperation scheme in between the master and slave systems (by electronic & software team)
- Control algorithms of the whole system (by control team).

1.5. Aim of the Thesis

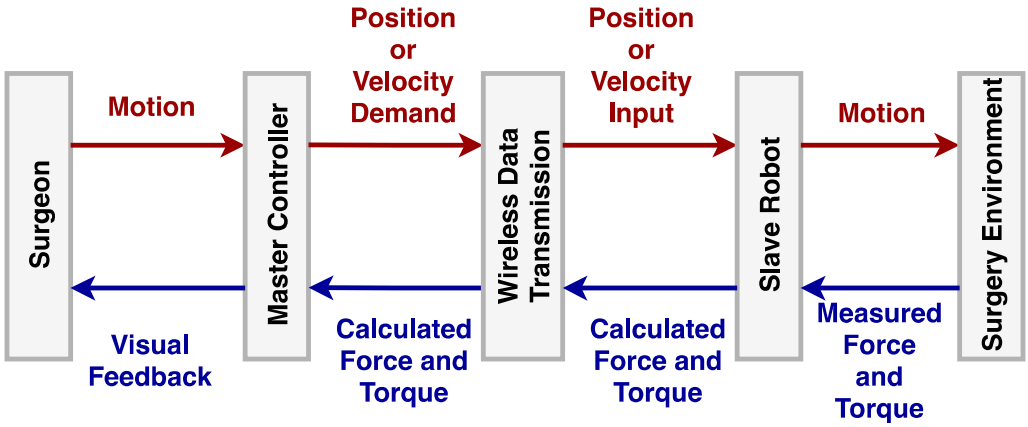

Figure 1.5. Flow diagram of the proposed teleoperation scheme

A novel teleoperation system architecture has been developed within the scope of this thesis. This study involves the teleoperation system design in both electronic and soft-

ware aspects, and feasibility studies of this system for the use in the endoscopic pituitary surgery.

Moreover, the operation scenario of this robotic endoscopic pituitary surgery system is developed within the scope of this thesis. In order to accomplish this, all the possible operation modes are identified from the initiation until the termination of the operation in order to efficiently and safely conduct the surgery.

One of the main points of this thesis is proposing an ergonomic usage for the surgeons between master and slave systems. Therefore in the experimental procedure, the system is tested in different modes in order to enhance the ergonomy.

Proposed teleoperation system's components and the information flow between them are depicted in Figure 1.5. According to this proposed design, the master controller captures the hand gestures of the surgeon using an IMU (Inertial Measurement Unit) and transmits this information wirelessly (via Bluetooth Low Energy). This transmitted information is later processed on the slave side as a velocity or position demand of the active endoscope holder. In other words, this active endoscope holder is positioned during the surgery according to surgeon's online demands issued by the master controller. As a response from the slave system, the interaction force level is sent back to the master side and displayed on an LED panel.

1.6. Outline

In Chapter 2, previously proposed solutions in literature for the problem stated in section 1.3 are presented and they are examined for their feasibilities when used in endoscopic pituitary surgery. Further, a background of teleoperation systems is given and the design process of these systems is explained in Chapter 2. The subsystems of the proposed teleoperation system are introduced by describing their purposes and components respectively in Chapter 3. The experimentations carried out to determine the active workspace of the active endoscope holder are described and their results are discussed in Chapter 4.

Moreover, in Chapter 5, system operation modes are explained in three sections; teleoperation information flow alternatives, master system's command computation alternatives, and overall system's operation states. Finally, user evaluation experiments are proposed and their results are shared in Chapter 6. The main text of this thesis is concluded by discussion feasibility of the proposed teleoperation system design for endoscopic pituitary surgery in Chapter 7.

In additions to the aforementioned sections, the overall system's peripheral setups, algorithms implemented on the microprocessor and the teleoperation scheme with operation states are given in Appendix A, B and C respectively. Furthermore, auxiliary circuits designed in order to optimize the system and enhance the sensor measurements are given in Appendix E.

CHAPTER 2

LITERATURE REVIEW

There are many different surgical robotic systems in literature proposed for many distinct purposes. It is better to narrow them which have been developed for MIS.

Under surgical robotic systems developed to be used in MIS, a variety of classifications have been proposed so far. Moustris et al. (2011) categorized these surgical robots into four subsections: *passive robots, semi-active robots, active robots* and *remote manipulators*. Passive robots are mainly support elements in the surgery room without any actuation. Semi-active robots can be also considered as support elements but they have some specific actuation capabilities besides their passive behavior. Furthermore, active robots and remote manipulators are considered as a replacement for an assistant surgeon or in some applications they are even considered as the main surgeon in the whole operation.

On the other hand, Yip and Das (2017) extend this classification approach as shown in Figure 2.1 and they categorized surgical robots into 4 sections: direct control, shared control, supervised autonomy, full autonomy.

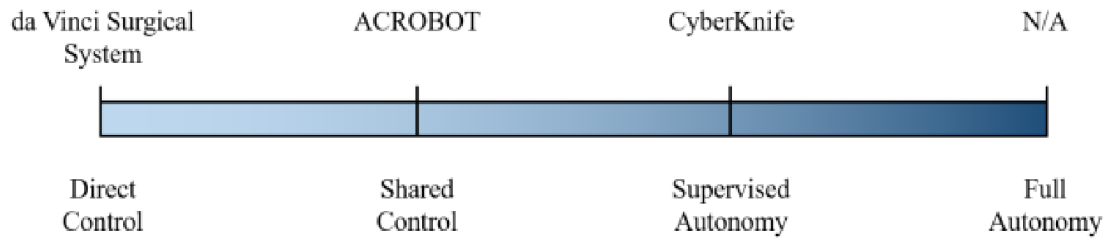

Figure 2.1. Classification of surgical robots in autonomy aspect
(Source: Yip and Das (2017))

Today there is no example of fully autonomous surgical robotic systems. In the definition of *Full Autonomous*, the robotic system can pre-plan the operation and perform it by itself without any human intervention. Since this last classification is a relatively new way of classification, the next subsections are designed in this way of classification.

2.0.1. Supervised Autonomous Surgical Robotic Systems

There are some robotic systems which can perform the operation by themselves after a preliminary process of the operation by the surgeon. These kinds of systems are included in the *Supervised Aunotomy*classification. One of the well-known examples of such systems is ROBODOC (ThinkSurgical, 2018) hip surgery system by Think Surgical, which is shown in Figure 2.2. It is an active robot to carry out the whole knee surgery after a preplanned process. Any CAD software can be used for this preplanning process and then, the robot performs the operation standalone.

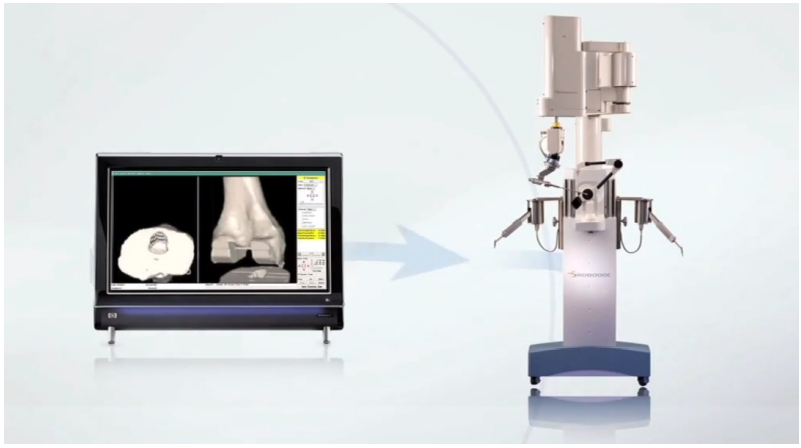

Figure 2.2. ROBODOC surgical system
(Source: www.seelio.com/w/1a2u/robodoc-inertial-measurement-system-integration-patent-pending)

Moreover, PROBOT is another example of preplanned active surgical robots designed for prostate resection (Harris et al. (1997)). The CyberKnife system developed in Stanford University also performs radiotherapy to terminate tumors after a preplanned process supervised by a surgeon (Moustris et al., 2011).

CASPAR (Computed Assisted Surgical Planning Robotics) is another example of this category with its usage in knee and hip surgeries. It is a direct competitor of the ROBODOC system. It requires a preoperative plan based on computed tomography in contrast to ROBODOC's pre-operative plan on a CAD software. Afterwards, it can perform bone drilling autonomously (Petermann et al., 2000). However, there are not many clinical studies that use CASPAR reported in the literature since it is no longer commercially available.

2.0.2. Shared Controlled Surgical Robotic Systems

In the category of *Shared Control* surgical robotic systems, the control of different types of surgical tool motions are simultaneously distributed between the human and robot. For example, Steady Hand robot is a system designed for precise manipulation tasks such as retinal microsurgery developed at Johns Hopkins University (Taylor et al. (1999)). This system, which is shown in Figure 2.3, has a haptic control by applying counteractive force proportional to the force sensed by the tool tip in order to correct for tool deflections and implement a micro-force guided cooperative control algorithm. On the surgeon side, he/she controls all the movements of the surgical instrument through the assistance of the feedback force (Kapoor et al., 2003).

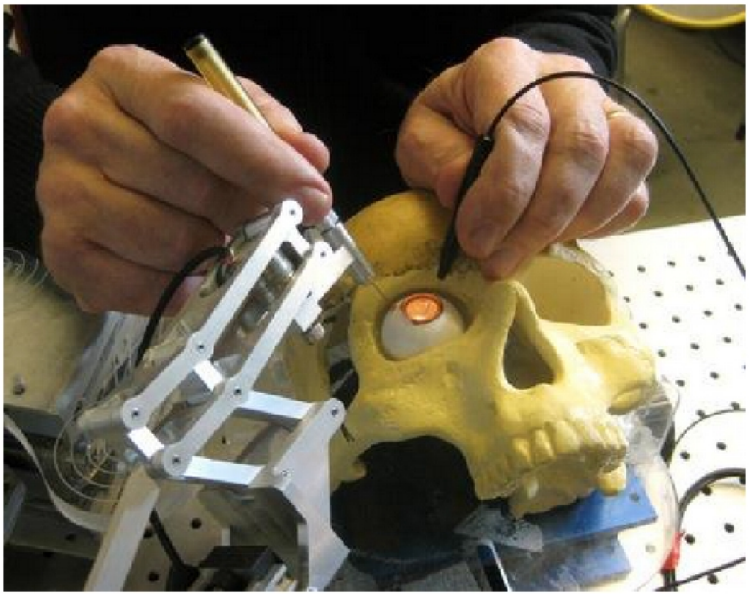

Figure 2.3. Steady-hand eye robot
(Source: Hamed et al. (2012))

Another example of this category, Endobot, is a 4-DoF semi-active surgical robot developed for MIS (Wen (2001)). It is designed for ligation of vessels and knot tying. It works collaboratively with the surgeon under shared control while the surgeon commands have a higher priority. Even though it is stated that it was designed so that the device can operate autonomously as well, they have not presented any autonomous operation study in the literature so far.

2.0.3. Directly Controlled Surgical Robotic Systems

Within the area of *Direct Control*, surgeons have the complete control of the system. They can perform the operation either manually or a by a teleoperated robotic manipulator. The manual systems are often endoscope holder type of fully passive mechanisms. They can be manually driven by the surgeon to the desired location and can be fixed at that location during the operation. On the other hand, teleoperated systems can be categorized as **off-site** and **collaborative (on-site)** robotic systems. In off-site systems, while the slave robot is working on the patient, the surgeon controls it over a certain distance. In other words, there is no physical contact between the surgeon and the patient. One of the best-known examples of this category is the Da Vinci Surgical Robotic Systems, by Intuitive Surgical, which is a computer-enhanced teleoperated system used in laparoscopic surgeries since 2000 (IntuitiveSurgical, 2018).

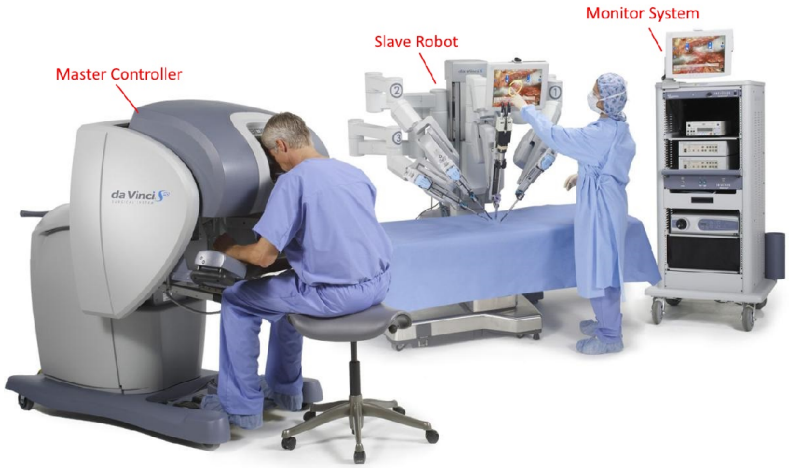

Figure 2.4. Da Vinci surgical robotic system
(Source: www.davincisurgery.com)

Three commercial models have been released so far. As shown in Figure 2.4, mainly it has three parts; the console (master system) where the surgeon sits, robotic manipulator working on the patient (slave robot) and the monitor system. On the master side, the console consists of gripper hand pedals and foot buttons to be controlled by the surgeon. On the slave side, the robot has three or four actuated arms where mostly two arms hold two different cameras for 3D imaging and the rest of the arms hold surgical tools and perform the operation as commanded by the surgeon. Monitor system provides the surgeon with a 3D visual feedback to create an environment for more precise and

realistic control (Kim (2014)).

Also, in 2009 Titan Medical's announced a directly controlled off-site surgical system SPORT (TitanMedical, 2018), similar to Da Vinci Surgical Systems, however, it has a simpler structure. It has two-joystick controllers and five foot pedals on the surgeon side (shown in Figure 2.5.a) as well as the 3D vision system. It performs the minimally invasive surgery from one incision with a multi-articulated gripper instrument (shown in Figure 2.5.b).

(a) Master system of Titan Medical Unveils Surgical Robotic System

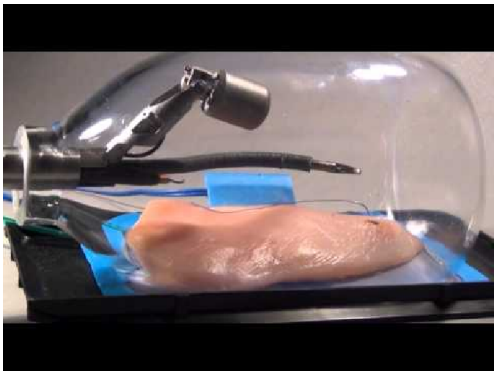

(b) Slave system of Titan Medical Unveils Surgical Robotic System

Figure 2.5. Titan Medical Unveils Surgical Robotic System (Source: www.medgadget.com/2016/02/titan-medical-unveils-sport-surgical-robotic-system.html)

Although there are these two successful commercially available off-site systems, still there are many doctors who do not like the idea of being physically away from the patient in case of any emergency situations.

On the other hand, in **collaborative systems**, the robot and surgeon work on the same patient at the same time while the robot serves an assistant to the surgeon. Although, I have already introduced some collaborative surgical robot examples in the previous Chapter, *Collaborative Surgical Robotic Systems* (CSRS) can be investigated in more detail according to the command type of the surgeon such as foot/hand pedal or joystick controlled, voice controlled, image-processed and body-motion controlled.

2.0.3.1. CSRS Controlled by Joystick and Foot/Hand Pedals

A CSRS that is controlled by a joystick is LAPMAN by Polet and Donnez (2008) for gynecologic surgery. It composed mainly two parts: the manipulator which is an

articulated arm construction on a rolling unit and the interface. They offered two different interfaces to control the manipulator. One is the remote control, which is also called the nurse's unit, to be used during the phase of alignment of the LAPMAN with the patient's umbilicus. Second is the hand controller, which is also called LAPSTICK, hold by the surgeon.

(a) LAPMAN surgical system

(b) Surgeon's controller, LAPSTICK

Figure 2.6. LAPMAN gynocologic surgery system
(Source: Polet and Donnez (2008))

Other than the LAPMAN system, Naviot is a remote-controlled laparoscope directing manipulator system (Yoshino et al., 2005). It consists of an automatic micro zoom endoscope, called Naviot, which is a special endoscope held by a five-bar mechanism and a two-thumb controller as shown in Figure 2.7. The manipulator has two actuation for horizontal and vertical directions with 25 degrees for each axis. The surgeon is able to zoom the lens and control the camera position by the thumb controller attached to the holding area of the forceps.

Nevertheless, by some surgeons using a joystick and leaving surgical instruments could not be approved due safety concerns in case of an emergency.

2.0.3.2. CSRS Controlled by Voice Commands

Another well known commercial example of directly controlled surgical robots is the Viky robotic assistance system shown n Figure 2.8 (Takahashi et al. (2017)). It is

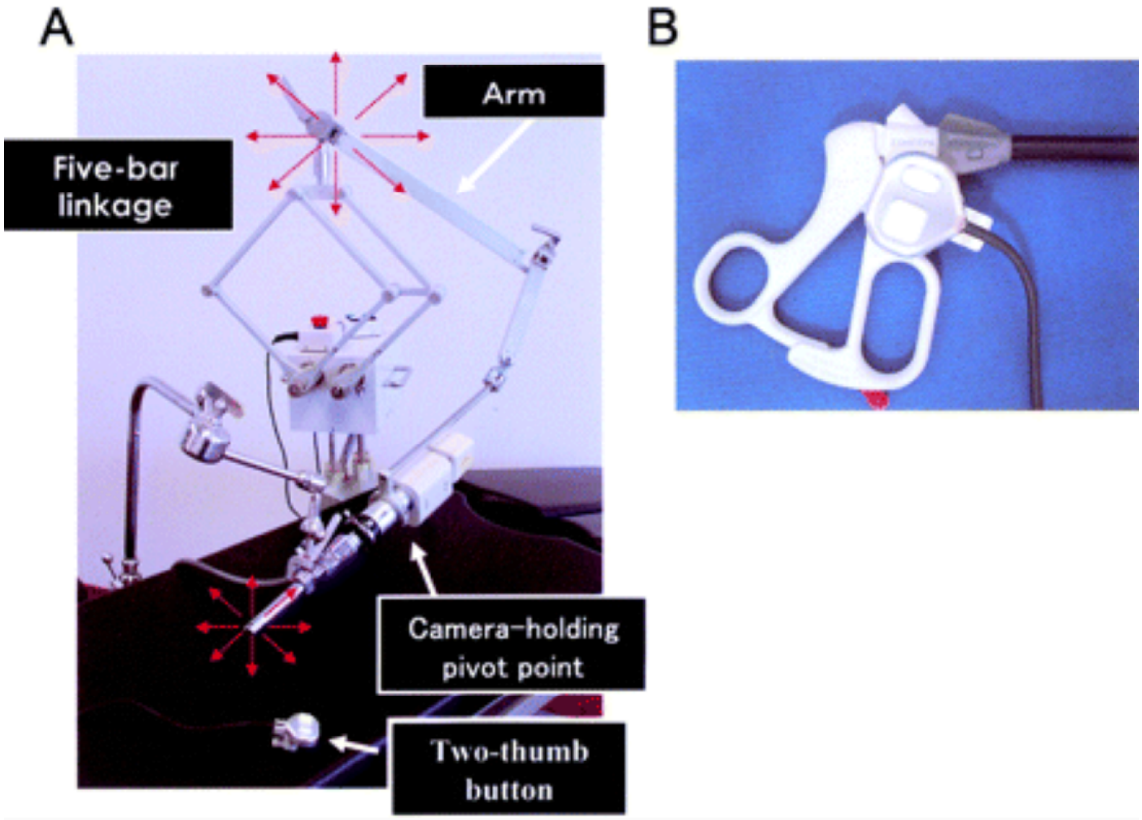

Figure 2.7. Remote-controlled laparoscope manipulator system, Naviot
(Source: Yoshino et al. (2005))

a voice controlled positioner system designed for laparoscopic surgeries. There are two commercial products based on this system: Viky EP for endoscope positioning and Viky UP for uterus positioning. Also, as mentioned in Chapter 1, AESOP is a voice-controlled example of surgical robots (Nathan et al. (2006)). Although voice controlled methods are more intuitive, they are still not precise enough for endoscopic surgeries. When the doctor gives a voice command, the robot moves one step size of the voice command. Higher step size reduces the precision and lower step sizes cause more effort for the surgeon to reach further distances.

2.0.3.3. CSRS Controlled by Image Processing Methods

There are also some surgical robots controlled by image processing methods. As a very early example of these type of robots was designed in the University of Lausanne in 1991. The robot Mirvera directs tools into the brain under the real-time computed tomography guidance. It was used until 1993 but due to the limitation of single-dimensional

Figure 2.8. Voice Commanded Viky Endoscope Positioner
(Source: Takahashi et al. (2017)))

motion and its need for real-time computed tomography (Glauser et al., 1995a).

Wei et al. (1997) designed a real-time visual servoing system for laparoscopic surgeries controlling the robot motions with color image segmentation. Also, Viky has a control method of imaging as well stated in Voros et al. (2010). They detect and track the surgical instrument from image analysis and control the positioner robot by this information. Casals et al. (1996) proposed an image analysis control method by tracking the surgical tools of the surgeon and the control system generates the robot trajectories.

Although this type of control is relatively intuitive, these systems could not be placed in surgery rooms due to their and high-cost and too many system requirements for setup.

2.0.3.4. CSRS Controlled by Body Motions

Apart from the previous three methods, Primus et al. (1991) proposed an interface which lets the surgeon control the surgical devices and conditions of the operating room by a transmitter that is worn on the head of the surgeon. In front of the surgeon, there is a monitor with the endoscope view. There is a cursor on the same monitor that is moved by the pointer signal transmitted from the master device worn by the surgeon. The pointer

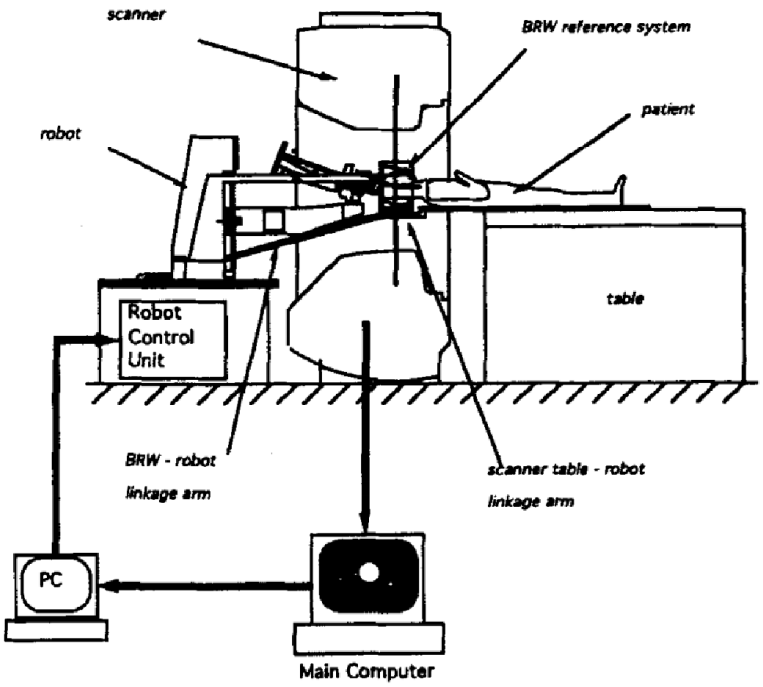

Figure 2.9. General view of the Mirvera robotized system
(Source: Glauser et al. (1995b))

signal is a laser which is directed to a screen that is located adjacent to a detection camera.

Moreover, another example of head controlled CSRS is FreeHand (FreeHandSurgeon, 2018), formerly named EndoAssist, which is an endoscope positioning system. It has an improvement with respect to EndoAssist by providing one more DoF for zooming by using a foot pedal.

Up to now, only head motions were used to generate the demand from the surgeon side in this category. However, this control method by using the head motion was not preferred by surgeons because it requires too much effort to hold the head stable throughout the whole surgery.

2.1. Combined Category

Two different categories can also be combined for improved results. A unique example to this is developed by Steinhart et al. (2015) as a computer navigation guided and remotely controlled robotic system for paranasal sinus surgeries. The workflows for both fully automated and telemanipulation surgery are conceptually identical. In the operation protocol of this system, firstly, an autonomous pre-operation imaging procedure

(a) Slave system of FreeHand CSRS

(b) Master head controller system of FreeHand CSRS

Figure 2.10. FreeHand CSRS
(Source: www.youtube.com/watch?v=BUE9xg8AmmE)

is executed by CT data for pre-planning. Computed tomographic (CT) images derived before operation are transferred to the planning station for further processing.

Secondly, telemanipulation mode with joystick control (SpaceBall, 3D Connexion Inc, Seefeld, Germany) is available as well. This function allows the doctor to perform small fractions. After opening of the sphenoid sinus autonomously, the finishing touches are performed done manually. The robot stops at the predetermined end point of the trajectory, and the drill powers down. The surgeon then moves the robot manually along the trajectory to get an overview of either the external sphenoid wall or the sinus cavity by joystick control.

As it is clearly observed from the examples in the literature, modern solutions cannot provide a solution to the problem stated in Section 1.3. Within the scope of this thesis, a new teleoperated system architecture design is proposed for a specific type of surgery to provide a solution to the mentioned problems of surgeon command transmission stated under CSRS category. For that reason, it is useful to mention some background on teleoperation systems and their design procedures.

2.2. Overview of Teleoperation Systems

Fong and Thorpe (2001) defines teleoperation ”to operate a vehicle or a system over a distance”. This distance can be either in the line-of-sight area or in between completely different locations. The overall system consists of three subsystems: master, slave and communication channel.

Master is the human operator who gives commands to the system. The *slave*

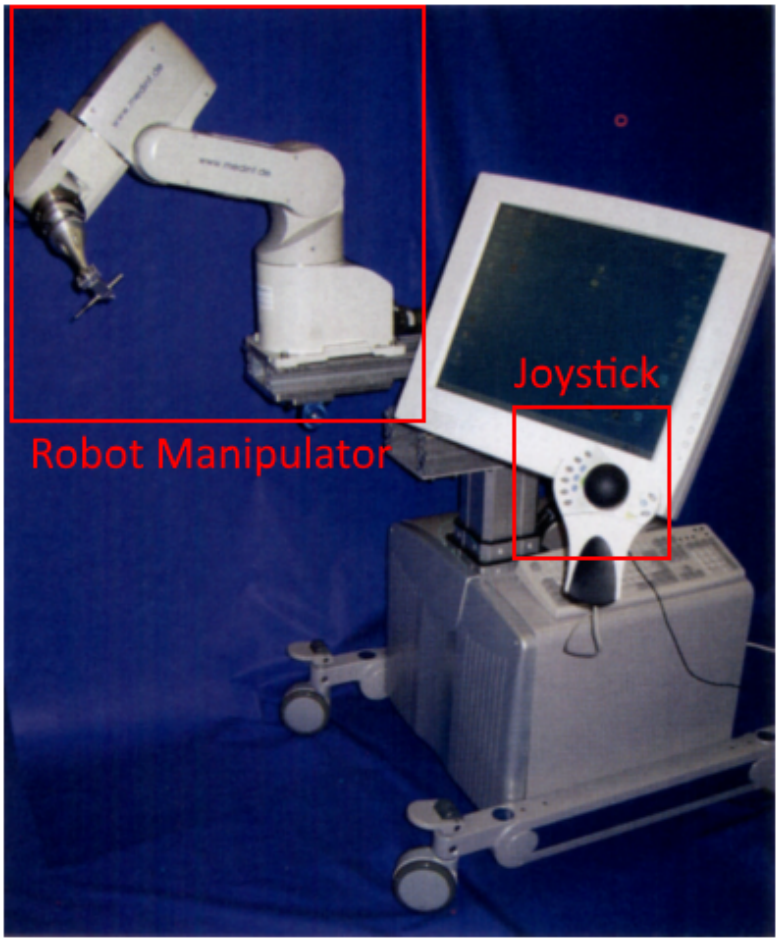

Figure 2.11. ”Stand Alone” version, 6-DoF articulating arms robot, mounted on trolley with hydraulic column for height adjustment. Operating control consists of thin film transistor touch-screen monitor and joystick mouse (Source: Steinhart et al. (2015))

system, on the other hand, is driven by these commands transmitted through the *communication channel*. Master and slave can be connected via a cable which is a wired communication channel or without any physical connections which is a wireless communication channel. Moreover, slave system can return feedback signal(s) to the master through the same communication channel or through a completely different path.

The very first teleoperated system was constructed in the 1940s. The master of this first teleoperation system sends the commands to the slave via mechanical linkages. At the beginning of the 1950s, it is seen that connection in between master and slave was evolved from mechanical structures to electrical servomotors, which allows the operator to control the systems further (Vertut and Coiffet, 1986).

Telesurgery is another developing research field where the remote control is required. In robotic surgery technology, teleoperation is a very common method in oper-

ating the system as it is described in Section 1. The surgeon and telerobot work in a master-slave relationship. However, telerobotic surgical systems have not been a part of commonly used surgical equipment in surgery rooms yet except the *Da Vinci Surgical System*.

Therefore, although there are many robotic systems for different purposes in general surgical robotics area, there is still a need for new designs of teleoperated surgical instruments for operation rooms. The first step of designing such a system is to understand the teleoperation basics.

2.2.1. Unilateral Teleoperation

In general, a teleoperated system is supposed to have a signal flow in both directions in between the master and the slave. However, some systems have a signal flow only from the master to slave. This type of teleoperation architecture is called as *unilateral teleoperation*.

In such systems, the operator transmits the command signal by the master system as shown in Figure 2.12 where the arrows show the signal flow direction and does not get any feedback from the slave environment. However, generally, there is a local closed-loop control system on the slave side to enhance the performance as shown in Figure 2.12 with a dashed arrow.

Figure 2.12. Unilateral teleoperation architecture

In literature, there are not many application examples for such a scheme. Since there is no feedback signal for the human operator to evaluate the execution of the command, the overall system might not be as reliable as in a bilateral teleoperation.

2.2.2. Bilateral Teleoperation

In bilateral teleoperation, the human operator can be stimulated to sense the slave environment by supplying him/her different types of feedback signals such as visual, aural

or haptic. The transmission of these signals to the master provides more realistic control opportunity to the user.

Depending on the signal type and amount of command signals, bilateral teleoperation architectures are usually classified as *two-channel architecture* and *four-channel architecture* Dede (2007). However, the channel configuration in bilateral teleoperation systems is still an active area of research (Kubo et al., 2007).

2.2.2.1. Two-Channel Teleoperation

In this type of teleoperation architecture (see Figure 2.13), the human operator usually sends position or velocity commands and receives force feedback via the master system. It is often referred to as "position-force" architecture. The slave system, on the other hand, moves according to the motion demand received from the master side and returns force or torque information due to the interaction with its environment.

Figure 2.13. Simplified two-channel bilateral teleoperation architecture

2.2.2.2. Four-Channel Teleoperation

Four-channel model (see figure 2.14) is preferred when the information flow is not sufficient enough for a stable teleoperation. In this architecture, the master sends both position or velocity data as well as force or torque data. The response of the slave system has the same type of information as the feedback signal.

2.3. Teleoperation System Configuration

As is seen in previous sections there are various types of teleoperation architectures. Depending on the system requirements, the most suitable system architecture

Figure 2.14. Simplified four-channel bilateral teleoperation architecture

should be employed. It does not mean always having more command or feedback signals result in a better performance of the system. More complex architectures with more signals between the two systems call for more attention in fault-tolerance of all the signal providers (sensors).

Dede (2007) introduced a chart (in Figure 2.15) for the design process of a teleoperation system. There are many parameters to receive the optimal performance from the system such as fault tolerant system design, time delay, communication loss. Within the scope of the main project that this thesis work is conducted under, bold and green highlighted path shows the design path that is followed.

Following the path on the Figure 2.15, teleoperation starts. Since there is no component failure compensation, classical design methods are applied. The teleoperation direction is two-sided; the motion commands are sent my the doctor's ring and visual feedback returns from the slave environment. Only one type of signal is delivered and returned. For that reason, this system is categorized under 2-channel bilateral teleoperation. The teleoperation channel in fast enough to neglect the effect of time delay. Classical control algorithms are applied within the scope of the NeuRoboScope project. In case of communication loss, velocity and force observers are designed to compensate it.

2.4. Discussion

In this chapter, surgical robotic systems are introduced by giving detailed examples. Moreover, surgical robotic systems are categorized into *supervised autonomous, shared controlled* and *directly controlled*. Also, directly controlled surgical robotic systems are further categorized for the first time in the literature with respect to the surgeons' location aspect; *on-site (collaborative)* and *off-site* systems. Since in this thesis work, the focus is on designing a CSRS, the control command types of such CSRSs are examined by giving examples from the literature.

Furthermore, a brief introduction to teleoperation system design is given. Types of teleoperation systems are examined in order to design an optimal system for the CSRS that is in the focus of this thesis.

According to the terminology and background of surgical robotic systems presented in this Chapter, the system developed in the NeuRoboScope project falls into the category of *Two-Channel Bilaterally Teleoperated Collaborative Surgical Robotic System Controlled by Body Motions*. The next Chapter describes the subsystems and their components to construct the above-defined surgical system.

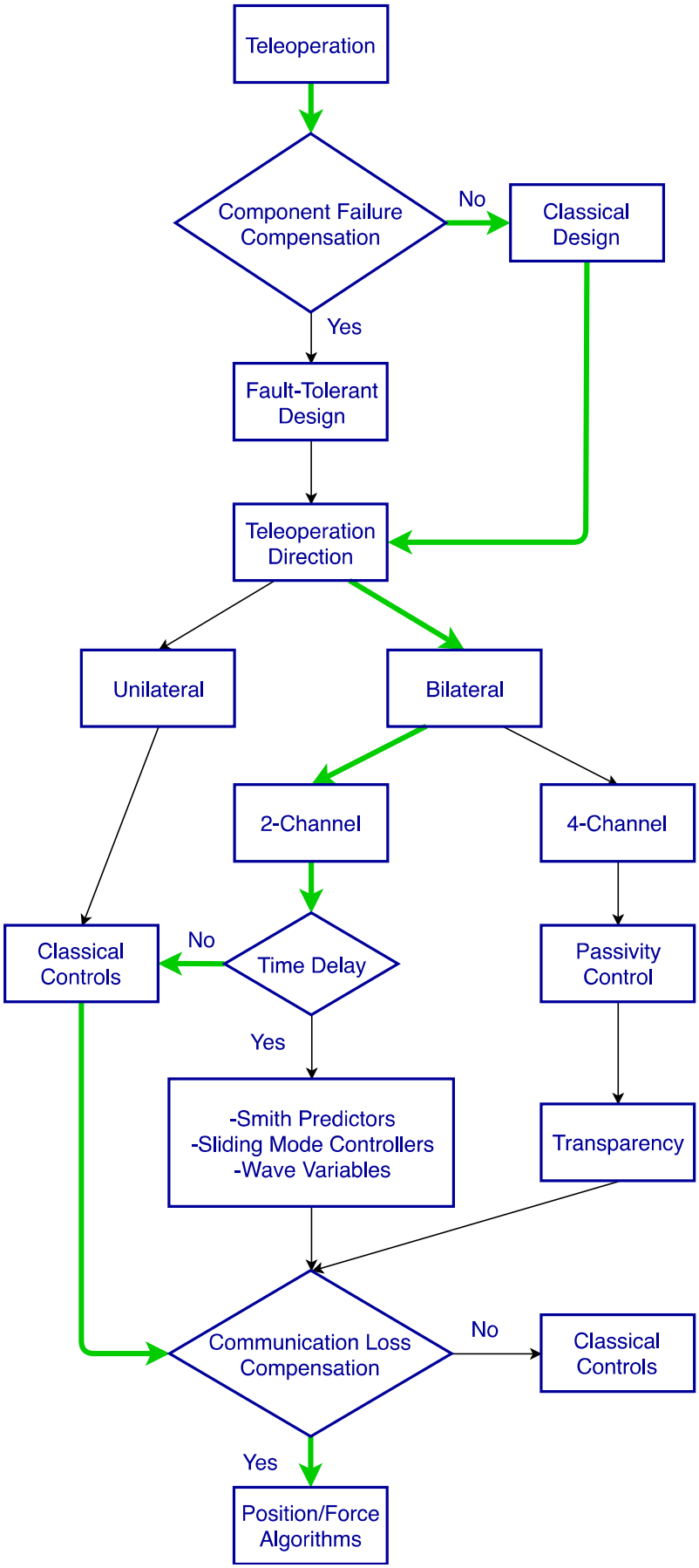

Figure 2.15. Flow chart of designing a teleoperation system

CHAPTER 3

SYSTEM OVERVIEW

This thesis introduces teleoperated CSRS specifically for minimally invasive pituitary surgeries. It is proposed as a bilateral teleoperation scheme for an endoscope holder and positioner robotic system which is the slave system. Additionally, this slave system can be handled and directed by the surgeon during the operation directly without the need of a teleoperation. The slave system includes the main processor card where the surgical system algorithm is executed. This main processor is responsible to acquire all the sensory information from the slave system, receive the commands from the master system wirelessly and issue driving command to the actuators of the slave robot. The master system is composed of a wearable ring controller that sends the command to the slave wirelessly, a foot pedal that initiates the data exchange and has a wired connection to the main processor card as shown in Figure 3.1. Besides these an LED indicator panel named as *User Interface* to provide visual feedback information to the surgeon.

In Section 3.1, subsystems of the overall scheme are introduced. Firstly, the methodology for constructing of the system architecture is explained. Later, components of these subsystems are introduced. The detailed signal flow between these subsystems are provided in Appendix C

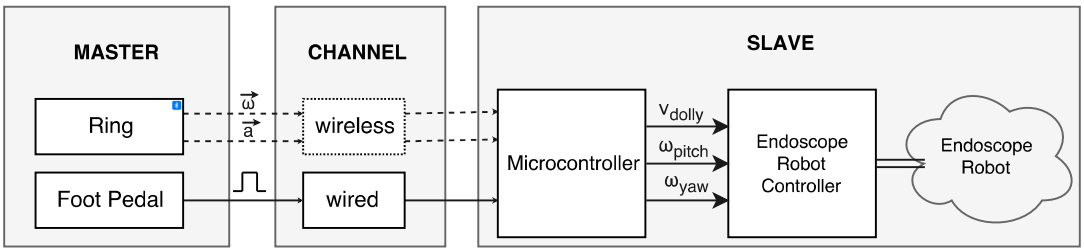

Figure 3.1. Conceptual overview of the system

3.1. Subsystems of the Surgical System

The overall system itself consists of five main subsystems. Two of them are PEK and KEY, which compose the robotic arm that holds and positions the endoscope. The

other three subsystems are *Communication System* , *Main Control Unit* and *User Interface* . Four subsystems are shown in Figure 3.2 except for HAS. The master elements of the system, wireless ring and foot pedal, is not visible on the figure directly but the placement is indicated with dashed arrows.

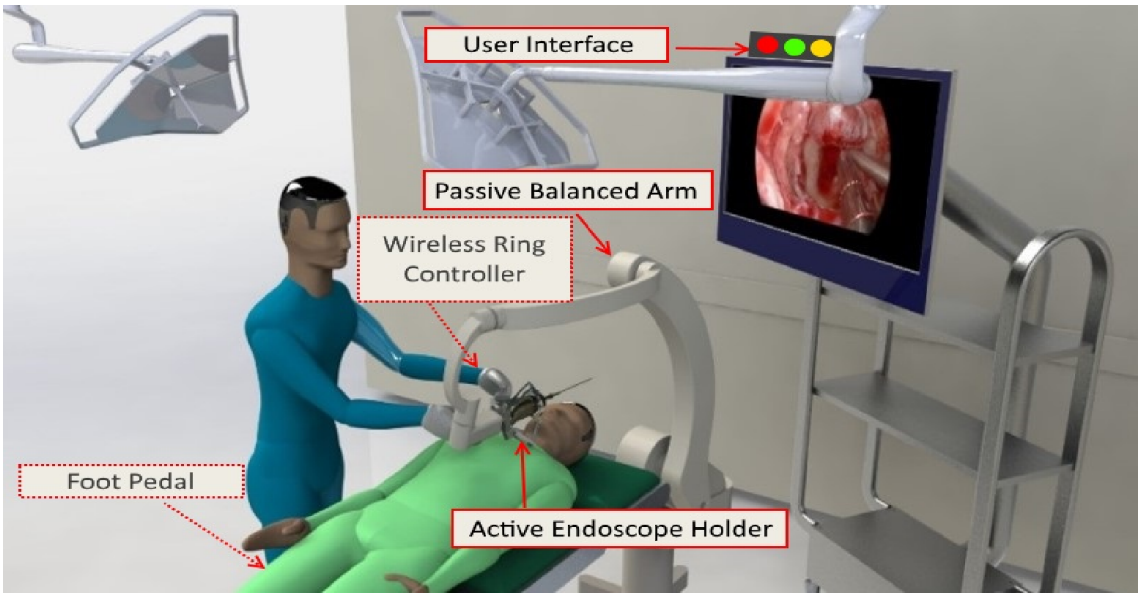

Figure 3.2. Overall system of NeuRoboScope project

3.1.1. Passive Balanced Arm - PEK

Passive Balanced Arm - (PEK) name is derived from the acronym of its Turkish translation ***P**asif **D**engelenmis **K**ol*. It is a statically balanced 6 DoF manipulator with only one actuated joint. Its main purpose is carrying KEY (see section 3.1.2) and providing an inertial frame to KEY during the surgery unless the surgeon wants to use the system in manual mode (for details about the modes please see section 5.3)

As it is seen in Figure 3.3, PEK has a portable structure which can be connected to the operation table. It has one prismatic actuated joint as the very first joint that moves vertically relative to the operating table so that the surgical team can adjust the height of KEY attached to the tip point of PEK before the surgery starts. This linear motor works completely standalone with its own power supply and it is not considered as a part of PEK that enables the manual mode back-driving of KEY during operation.

Beside the prismatic actuated joint, there are 5 non-actuated revolute joints in PEK in which an electromagnetic brake and an angular position sensor are placed. The angular

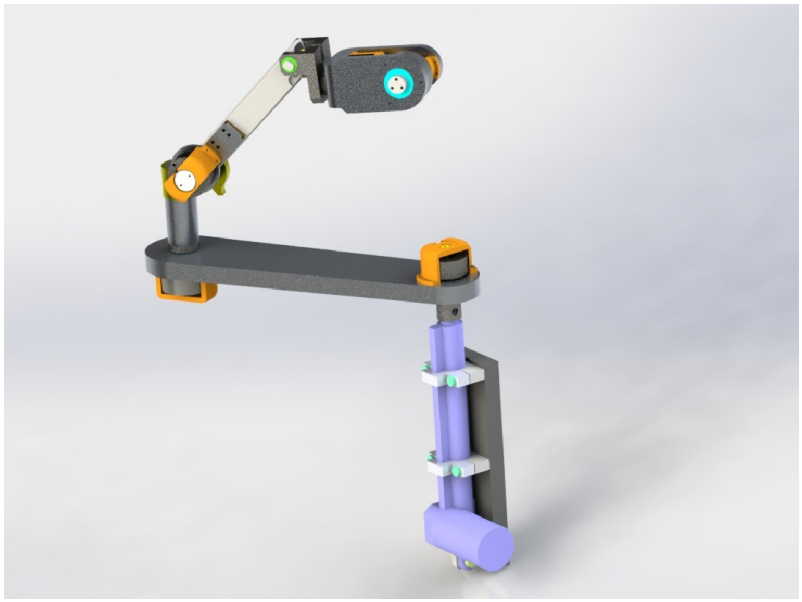

Figure 3.3. Rendered image of the *Passive Balanced Arm*

position sensor on these joints are absolute encoders with 12-bit resolution (see section 3.2.4). These measurements are used in forward kinematics to calculate the pose of KEY, which is used in control algorithms of the overall system to identify if the KEY is within the surgical area.

PEK has a back-drivable mechanical structure in order to allow the surgeon to use the system manually in case of an emergency. According to the operation states of the system, either some of those brakes are locked while some are released (in manual state or passive state) or all are locked (inactive state) (see section 5.3 and appendix E for more details).

3.1.2. Active Endoscope Holder - KEY

Active Endoscope Holder is the actuated part of the robotic arm which is design to hold and position the endoscope according to the commands received from the master system. It has a 3 DoF parallel kinematic structure 2R1T (2 revolute and 1 translational) mobile platform motion as shown in Figure 3.4 (Yaşır and Kiper (2018)). The actuated joints are shown in red rectangles and labeled as A_0 B_0 and C_0. The actuation axis on B_0 joint is placed perpendicular to the other two actuation axes to provide translational motion.

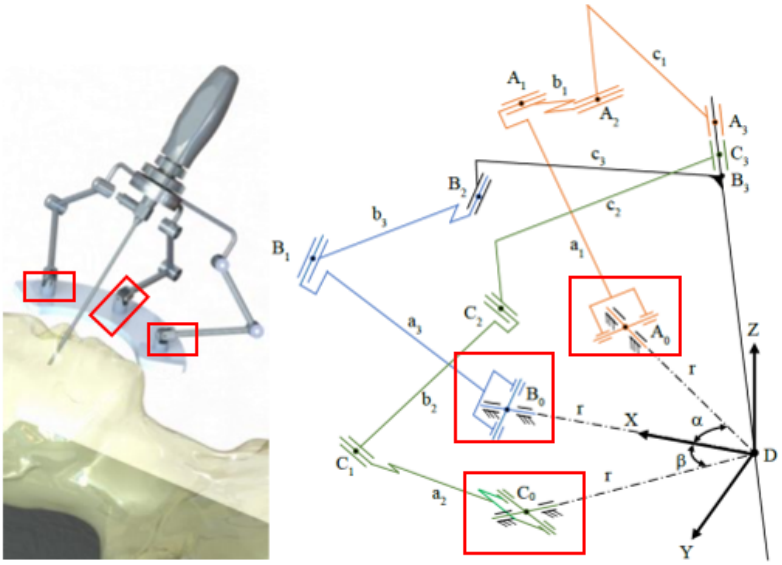

Figure 3.4. Kinematic Structure of the *Active Endoscope Holder*

Taniguchi et al. (2010) states that yaw, pitch, and insertion (surge) motions are the necessary and sufficient motions of an endoscope inside the surgical area. In order to control the robotic arm to move in these three DoFs, different approaches have been proposed in (Ates et al., 2018). Detailed information is given in section 5.2.

One of the most important points in this design is to adjust the precision and accuracy of the system in order not to cause undesirable consequences by damaging other tissues around. For that reason, motors with planetary gears that has 1:181 gear reduction ratio and a 1:5 capstan drives are used for the actuation of all 3 active revolute joints (denoted in Figure 3.4) to provide the system with finer motion.

3.1.3. Main Control Unit - AKS

Main Control Unit is the master part of the teleoperation scheme. It consists of two main hardwares: a ring-shaped remote control device which is worn by the doctor during the whole surgery in order to obtain the hand motions of him/her and a foot pedal triggering the initiation and termination of the teleoperation, and changing the active state type (detailed explanation is in Section 5.3).

Inside the ring, there is an IoT Sensor Development Kit from SmartBond company with a low-power Bluetooth Smart SoC (see Figure 3.5), 6-DoF IMU, 3-DoF geomagnetic field sensor and integrated environmental unit (for measuring pressure, temperature and

humidity) (DialogSemiconductor, 2018). It is stated as the lowest power wireless sensor in the world at the moment. Beside its low power, its small size (16 x 15 x 5 mm) is an advantage to be chosen for such an application (see Figure 3.6). The part stated as *breakable connection header* in Figure 3.6 is only used in the development process to embed the algorithm inside the chip. After the final algorithm is constructed, the program is embedded into the microprocessor and that part can be broken so that the overall hardware size gets smaller to be placed inside a ring.

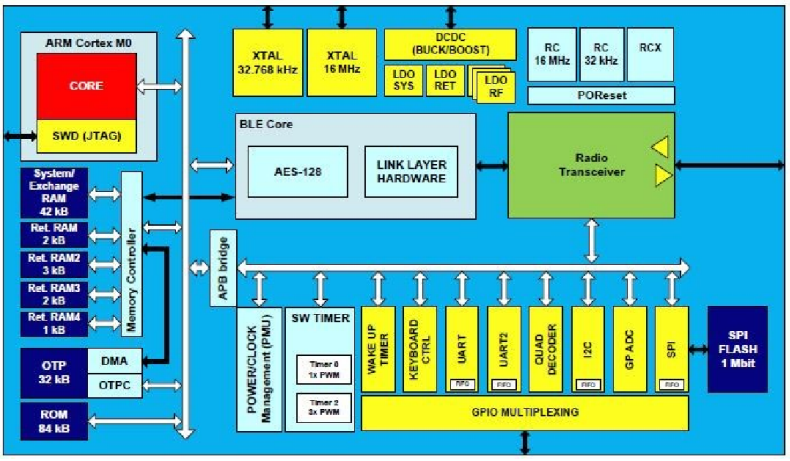

Figure 3.5. DA14583 hardware architecture
(Source: www.dialog-semiconductor.com)

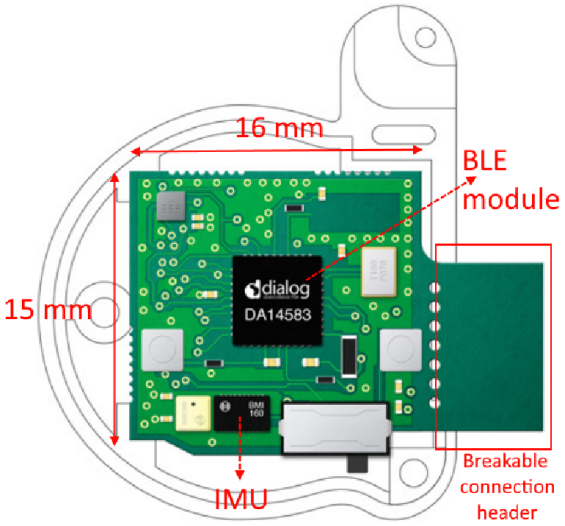

Figure 3.6. Smartbond Sensor Development Kit

Among available sensors on this kit, only 6-DoF from IMU is used within the scope of this thesis. Pressure, temperature and humidity information are not needed for

this application. Since the geomagnetic field sensor is affected by the magnetic noise from the other devices inside the surgery room, it is preferred not to be used in this application, as well.

Moreover, the foot pedal is connected directly to the microcontroller via cable. It triggers an ISR and eliminates all other low-priority processes to command a fast and reliable teleoperation between master and slave systems.

3.1.4. Communication System

Communication System is one of the three main subsystems in teleoperation aspect. It provides bilateral communication between the master and the slave. There are two different channels to deliver the necessary information: wired and wireless (see Figure 3.1)

Taking into account the communication types of the subsystems and their components, the communication path is summarized as shown in Appendix C. On the master side, as it is mentioned in Section 3.1.3, there are two components which are the ring and the foot pedal. Inside the ring, the microprocessor communicates with the IMU module via SPI protocol. The IMU updates the data at 100Hz. This frequency determines the overall teleoperation system speed at 100Hz, as well. The foot pedal is connected to the main processing unit, which is placed on the slave system, via a cable.

On the slave side, STBLE-RF (STBLE-RF, 2018) Bluetooth module from STMicroelectronics Co. receives the signals from the ring wirelessly and transmits them to the microprocessor STM32F407VG (STM32F407VG, 2018) via SPI protocol. Also, microprocessor is connected to the encoders chained via one SPI line (3 pins called MOSI, MISO and SCK) except for the one attached to *Surgeron Holds Endoscope Button* . The encoder used in *Surgeron Holds Endoscope Button* is connected to digital I/O port of the microprocessor and the signal is processed as a PWM input by interrupts. Moreover, force/torque sensors are connected to the microprocessor from an ADC module. Other user buttons are connected as GPIO inputs with ISR. More details about those components can be found in Section 3.2.

the chip-select pins (8 pins for each joint of the system in both KEY and PEK) for the encoders chained via one SPI line,

The microprocessor has many output connections: 1- motor drivers' input (total 9 pins for 3 motors; each has 2 inputs and 1 enable pins), 2- indicator lights (4 cables, 3 of them are for rising each LED respectively and one pin is for the common ground),

3- vibration element placed inside the quick release mechanism with the CEK to send haptic feedback to the surgeon and the laser pointers to assist in placing the pivot point of KEY manually positioning of the *Passive Balanced Arm* (total 2 pins, each has 1 pins for common rising and the common ground). 4- brakes...

The communication between them is regular digital I/O. Connections with microprocessors are GPIO outputs. Configuration of those pins can be found in Appendix A.

3.1.5. User Interface

User Interface is the user interface of the system to provide a visual feedback to the surgeon and receive the inputs to regulate the operation states from the surgeon. The inputs mentioned here are the user input buttons except for the foot pedal belong to the master system defined in Section 3.1.3. The outputs are provided by the visual feedback module.

3.1.5.1. User Input Buttons

There are xx buttons for different types of purposes and put the system into different teleoperation states (for more information about the states, please see section 5.3). These buttons have specific names and each is created from their Turkish translations. You may find how they stand for in Turkish under abbreviations section.

Following buttons have been ordered as their interrupt priorities of the system. When two buttons have been pressed at the same time, the teleoperation scheme would choose the whichever defined priorly in here. More details have been given in section 5.3 and in Appendix E.

- AGA: It is the key for the system to get power from the network. The power to go through the whole system is over this switch. Since all brakes will be de-energized when **AGA** is off, all joints are locked.

- ADD: It is designed to be a large button close to the working environment so that the surgeon can take over all control in a possible undesirable situation during operation. *ADD* is not connected to the main control unit. Contrarily, the main system and brakes are connected to this button on a relay system in order to eliminate any

extraordinary situations that may occur on the microprocessor. It is positioned close to the surgeon.

- ASB: This button is placed near to **ADD** and pressed only once at the beginning of each surgery to record the operation site. When this button is pressed, encoder values in passive joints will be stored in memory. Centering of *Active Endoscope Holder* will be done according to this position before switching from passive mode to active mode.

- CEK: It is a structure attached to quick-replace, between *Passive Balanced Arm* and *Active Endoscope Holder* with a spring. Its place should be easy-accessible since this button plays a critical role in overall teleoperation states.

  The main purpose of this button is to detach the endoscope from the system. Also assigning some tasks to this button, its made possible to drive the system manually without detaching the endoscope completely.

  When *CEK* is pressed, a vibrated element is actuated and give the information of the teleoperation state.

- MKB: It allows the system to be driven manually. When *MKB* is activated, then, 2 brakes on the wrist are released and 3 brakes on the arm are still locked in *Passive Balanced Arm* so that the surgeon can move the endoscope out of the system without removing it from the system. By that button, the system can be used as if it was a passive endoscope holder.

3.1.5.2. Visual Feedback Module

The visual feedback module has three different colored LEDs in order to give different information about the system. It is connected to the main system via cables as it is explained in Section 3.1.4. It is attached on top of the actual endoscope camera system's monitor in the surgery room. The main purpose of this module is to inform the surgeon about the states of the teleoperation system.

Apart from information about the states of the system, interaction information of the slave system is provided to the surgeon by visual feedback module. In many bilateral teleoperation schemes, the feedback signal is transmitted to the user as a haptic signal such as force feedback or vibration produced by the master device itself. However, it

is not possible to produce a reaction force since the ring does not attach to any fixed structure. Another solution to providing a haptic feedback is to use a vibration element inside the ring device. However, it is not safe to give a vibration to the surgeon's hand during the operation. Considering all these limitations, the feedback signal is determined to be a visual signal.

The color coding of the visual feedback module's LEDs are defined as follows:

- **Green light:**
  - Always on $\rightarrow$ *Active Endoscope Holder* is online but not active. It is ready to use as soon as the foot pedal is pressed.
  - Blinks at 4Hz $\rightarrow$ either *Active Endoscope Holder* is actively moving by the ring motions or homing process of KEY is being carried out.
- **Red light:**
  - Always on $\rightarrow$ *Active Endoscope Holder* is away from the home position and homing is necessary. However, the homing process cannot be executed since the endoscope is very close to the patient.
  - Blinks at 4Hz $\rightarrow$ ASB button has never been pressed.
- **Yellow light:** The slave system is applying excessive force/moment on the tissue.

3.2. Subsystem Components and Their Purposes

As the subsystems introduced formerly, components of these subsystems are explained in this section.

3.2.1. Main Processing Unit

The main processing unit is the *brain* of the system and attached to the robot manipulator. It initiates the teleoperation between master and slave, collects all the data from the sensors and encoders, processes the control algorithms and evaluates the necessary actions to be taken by the motors and the brakes. Since there are a number of different sensors with different types of communication interfaces, such a microprocessor

is required to contain multiple peripherals and to allow operating the system at very high frequencies. Moreover, a microprocessor that allows multiple peripheral options for the same pin is an advantage in order to broaden our freedom during the PCB design process. Moreover, there are different timing calculations for different purposes such as PWM inputs, integral calculations, double-click counting hence, the microprocessor should have many timers separately for such an application.

Considering all these reasons STM32F407VG ARM Cortex-M4 based 32-bit RISC core microcontroller allowing up to 168 MHz clock frequency is chosen. Additionally, it has a memory protection unit which enhances the application security.

Initially, during the test period of the microprocessor and sensors, an STM32F4 Discovery Development Board of STMicroelectronics is used. It allows the user to have a pin-to-pin connection to each microprocessor pin. It is a very commonly used development board to develop applications on an ARM Cortex-M4 based microprocessor. After all the tests are done, main processing unit's PCB board is developed with the assistance of CAROB company. The produced main processing unit is presented in Figure 3.7 by denoting the I/O modules and its components.

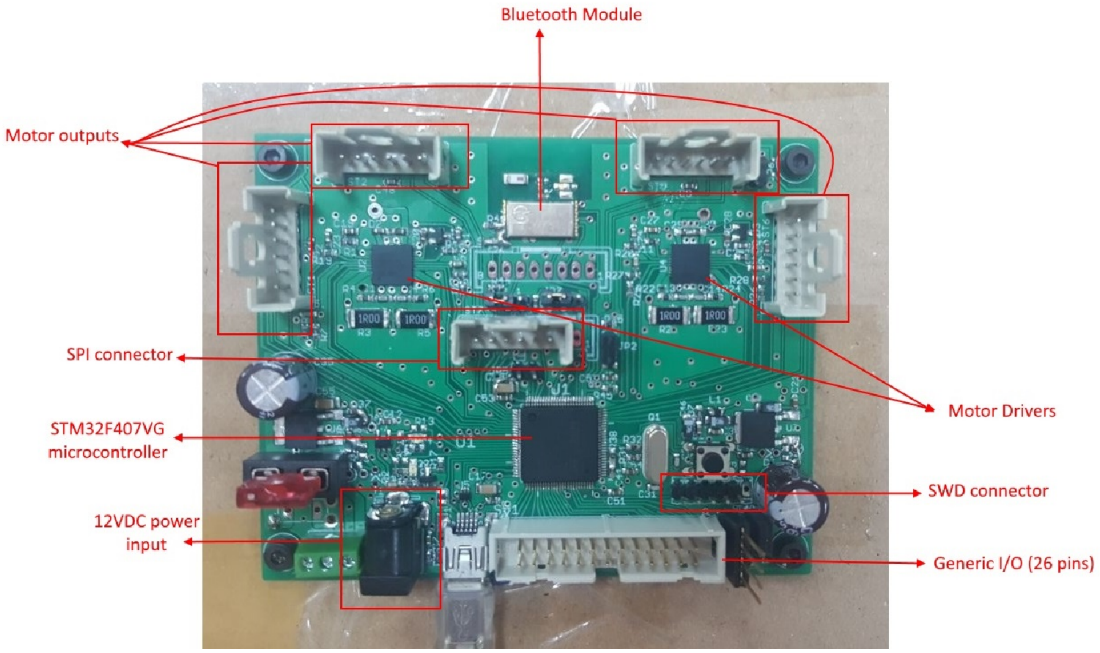

Figure 3.7. Main Processing Unit

3.2.2. Inertial Measurement Unit

One of the main components of the system is IMU which is a device composed of accelerometers (measuring the external acceleration), gyroscopes (measuring the angular velocity) and commonly magnetometers (measuring the magnetization information of the environment). Each information for each axis is defined as a degree of freedom of the sensor.

In this thesis, BMI160 6-DoF IMU from BOSCH company is chosen with a 3-DoF accelerometer and a 3-DoF gyroscope inside. It is already attached inside the Dialog IoT sensor development kit used in the ring device. The following subsections describe these IMU components.

3.2.2.1. Gyroscope

A gyroscope is a device that measures angular rate generally by a wheel or rotor spinning about its axes. They are mostly used in airplanes, space stations, any project in which the orientation is important.

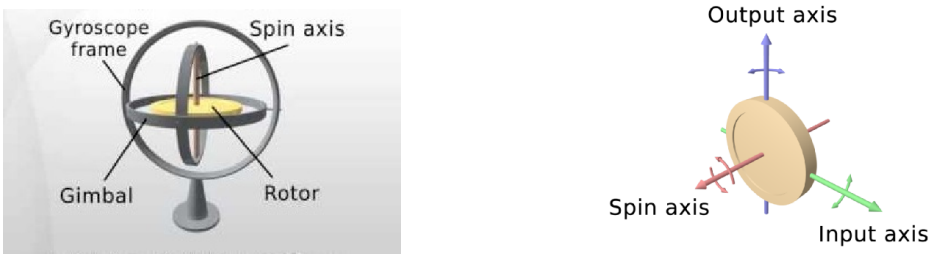

Figure 3.8. Gyroscope working principle
(Source: http://www.rfwireless-world.com/Terminology/MEMS-Gyroscope.html)

Basically, the spinning disk in the middle of gyroscope leads to resist forces applied to it about its spin axis. For that reason when you apply an input force, the gyroscope with a spinning disk would move as if that force were applied on the output axes in Figure 3.8 by the rule of gyroscopic effect.

In big devices, mechanical gyroscopes with a real spinning disk can be used easily. However, it is not possible to attach a spinning disk on small electronic circuits. The IC type gyroscopes uses MEMS technology. The main principle of this type of gyroscopes is when the system is rotated with an ω_r angular rate, it causes vibration on the drive and sense modes by Coriolis acceleration shown in Figure 3.9.

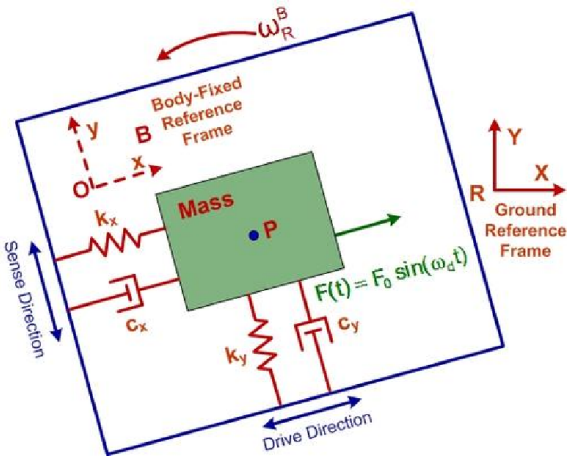

Figure 3.9. Working principle of MEMS gyroscopes
(Source: www.designnews.com/electronics-test/modeling-mems-gyroscope/187637938530637)

3.2.2.2. Accelerometer

An accelerometer is an electromechanical device which used to measure the acceleration forces. Such forces may be static, like the continuous force of gravity or, as is the case with many mobile devices, dynamic to sense the movement or vibrations. For example, when the system is stable of moving at a constant speed, the only acceleration force applied to the system is the gravitational force.

Accelerometers consist of many different parts and works in many ways. One of the most commonly used technologies of MEMS accelerometer is the capacitance effect. The sensor combines silicon and mechanical functions on the same micrometer silicon substrate. As the sensor accelerates or decelerates, the mass moves by the 2^{nd} law of Newton thanks to the springs as shown in Figure 3.10. This motion of the mass produces a capacitive effect in between the moving plate and the fixed plates.

3.2.3. Bluetooth Low Energy Module

In this section the BLE process which is as the communication protocol in wireless channel of this thesis.

In BLE, or another title as Bluetooth 4.0, the data is sent as notifications whereas in the previous versions of Bluetooth protocol the data was sent as *"data packages"*. It provides significantly lower power than classic Bluetooth.

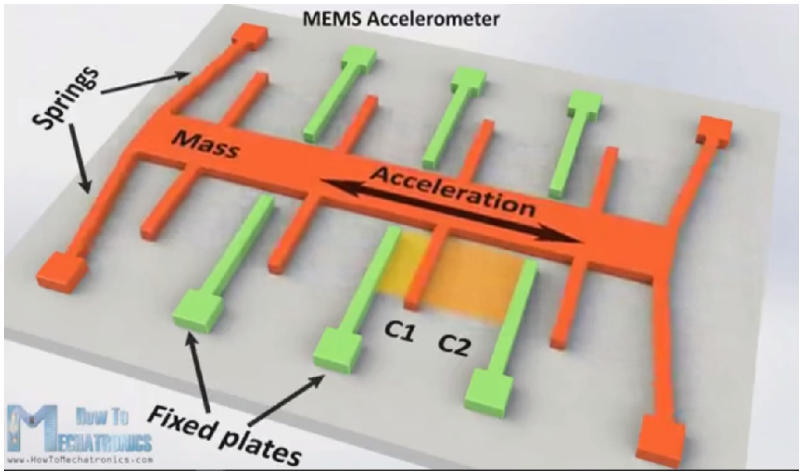

Figure 3.10. Working principle of MEMS accelerometer
(Source: www.HowToMechatronics.com)

Before starting how to implement BLE into systems, there are some terms and concepts needs to be explained. Although there are a bunch of criteria(Bluetooth(TM), 2001; Bluetooth, 2017) of designing a BLE system. In this section, most relevant of those are summarized and followed the implementation process following the procedures in Mourik (2005); Diagnostics (2006) for the STBLE-RF BLE module.

BLE has a constant rate of 1Mbps modulated by the radio signals. Indeed, it is the theoretical maximum rate and it reduces 5-10 KBps in practice depending on limitations of the BLE device that the one uses Bluetooth(TM) (2001). It can connect devices 30 meters away reliably in the line-of-sight distance. However, it needs to be considered that the higher range would consume more battery. Practically, the distance between master and slave devise is roughly 1-3 meters in this application explained in this thesis.

BLE has been organized as 3 major blocks:

- **Application:** Interfaces with the Bluetooth protocol stack. MCU runs the *application* block.
- **Host:** Upper layers of the stack. *Host* can communicate with the BLE module with HCI which is the interface between host and controller.
- **Controller:** Lower layers of the stack.

In BLE devices can be either *Central Device* or *Peripheral Device*. Central devices are generally chosen as the higher CPU processing power in the systems to process the data while peripheral devices are sensor type low power devices. In the proposed teleoperation scenario, since the ring controller has lower power, it is chosen as the peripheral

device and the MPU as the central device.

In network topology, peripheral devices send *Advertising Packages* constantly so that they can be seen by other devices. After the recognition is executed, the central device sends a *Scan Response Data* in order to request additional information such as sensor values etc.

There are two ways of communication in BLE protocol: *Broadcasting* and *Connections*. In broadcasting the data announced to all the listening devices. In such communication, devices can have two different roles: *Broadcaster* or *Observer*. On the other hand in connection way, there is an established permanent communication line between central device and the peripheral device and there is no possibility to transmit data to more than one peer at a time. After the central device initiates the connection line, the peripheral device stops sending connectable advertising packets and follows the central's timing and exchanges data regularly with it. While there is no exchanging, both devices go to sleep until the next connection event which provides the most power saving for the BLE protocol.

Figure 3.11 illustrates the relationship between each of the layers. *Application* interacts with each layer with the *Component*. Afterwards, the application is informed of the BLE events through the use of callback functions.

BLE Stack: A BLE stack is a precompiled library and it is embedded in BLE component. It implements all the mandatory and optional features of Low Energy Single-Mode BLE functionality as published in Bluetooth(TM) (2001).

Generic Access Profile (GAP): is a profile where the generic procedures of Bluetooth devices and link management are defined. Moreover, this profile includes common format requirements for parameters accessible on the user interface level. Choosing a role for the device as an observer or broadcaster and peripheral or central is implemented in this interface level.

Generic Attribute Profile (GATT): is a generic service framework is defined using the ATT protocol layer. This framework defines the procedures and formats of services and their Characteristics. It defines the procedures for Service, Characteristic, and Descriptor discovery, reading, writing, notifying, and indicating Characteristics, as well as configuring the broadcast of *Characteristics*. A device can have two roles in GATT; either *GATT Server* or *GATT Client*.

The roles of each device in our system are shown in Figure 3.13. It is a simplified version of the proposed system just to show the BLE roles.

Security Manager Protocol (SMP): defines the procedures and behavior to man-

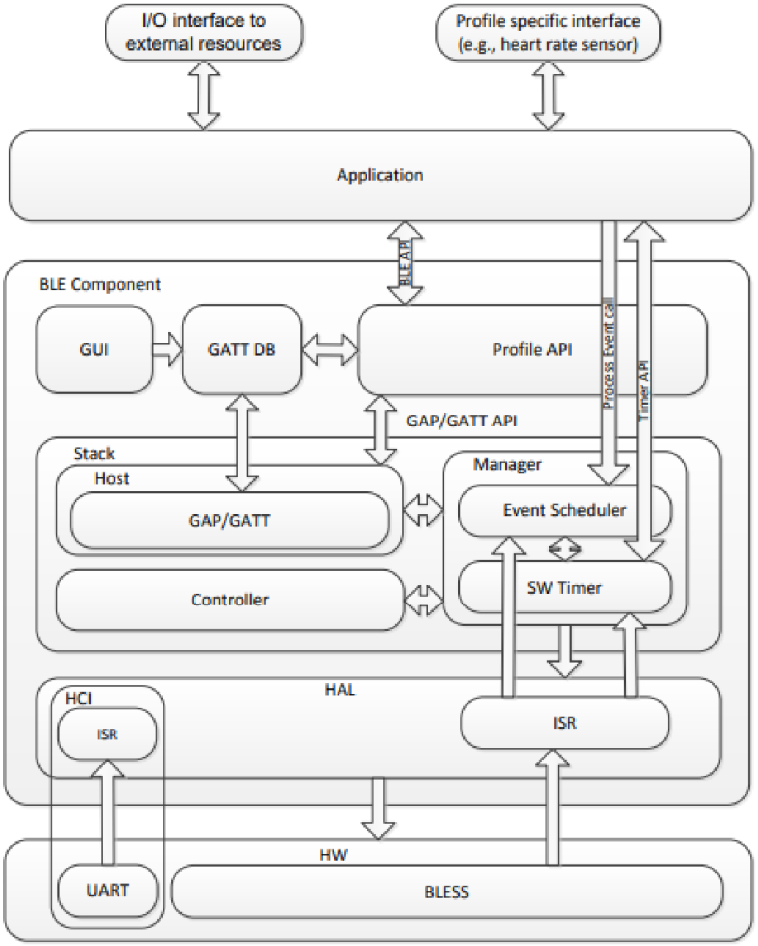

Figure 3.11. High-level BLE Component Architecture
(Source: Cypress (2015))

age pairing, authentication, and encryption between the devices.

Logical Link Control Adaptation Protocol (L2CAP): provides a connectionless data channel with channel multiplexing, segmentation of BLE Controller to manage the maximum packet size and connection-oriented channel over a specific application register.

Host Controller Interface (HCI): layer implements a command, event, and data interface to allow link layer access from upper layers such as GAP, L2CAP, and SMP.

Link Layer (LL): manages the physical BLE connections between devices. It supports all LL states such as Advertising, Scanning, Initiating, and Connecting (Master and Slave).

These layers have been implemented our built-in BLE module into our system according to (Mourik, 2005; Diagnostics, 2006).

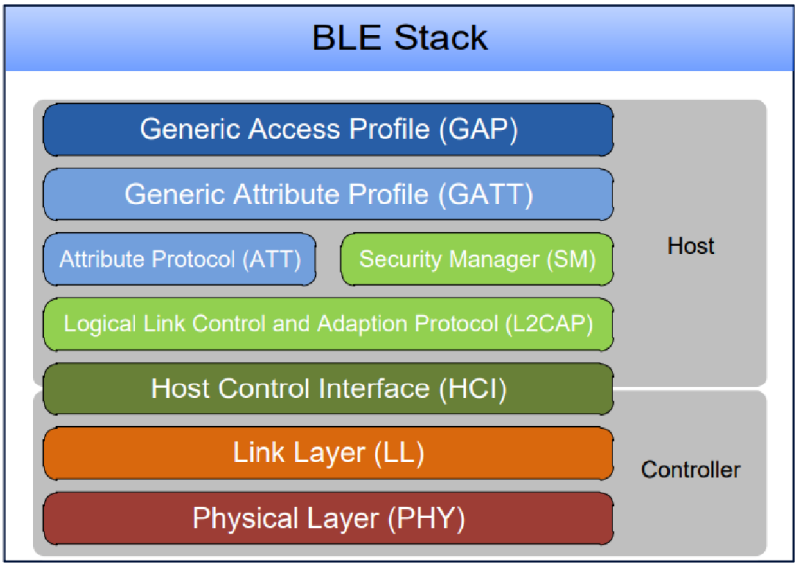

Figure 3.12. Layered architecture of the BLE protocol stack
(Source: Cypress (2015))

3.2.4. Encoder

Encoders are the electromechanical components allow measuring the amount of rotation of the rotor by being attached on the stator. They are used to generate digital position and motion information. Depending on the output type, there are two different encoders which are incremental or absolute. Incremental encoders are preferred when the relative position is needed and resolution is defined as counts per turn. Each time the encoder is powered on it starts counting from zero, regardless of where the shaft is or its previous position. It is necessary for incremental encoders to re-home upon the reference point when powered down. They are preferred for simple pulse counting or frequency monitoring applications such as speed, direction, and position monitoring.

An incremental encoder can have 1 output signal named “A” or typically 2 output signals, called “A” and “B”. There is a 90° phase difference in order to detect the encoder’s rotation. In clockwise rotation, the “A” pulse rises 90° ahead of the “B” pulse and clockwise rotation, the “B” pulse rises 90° ahead of the “A” pulse. Additionally, some incremental encoders provide one more output signal called “Z” in order to identify the homing point with much higher precision.

It is possible to calculate absolute position by incremental encoders and the calculated value can be reserved in the non-volatile memory of the system. However, it causes more computational load and for some applications, it is unnecessarily hassling.

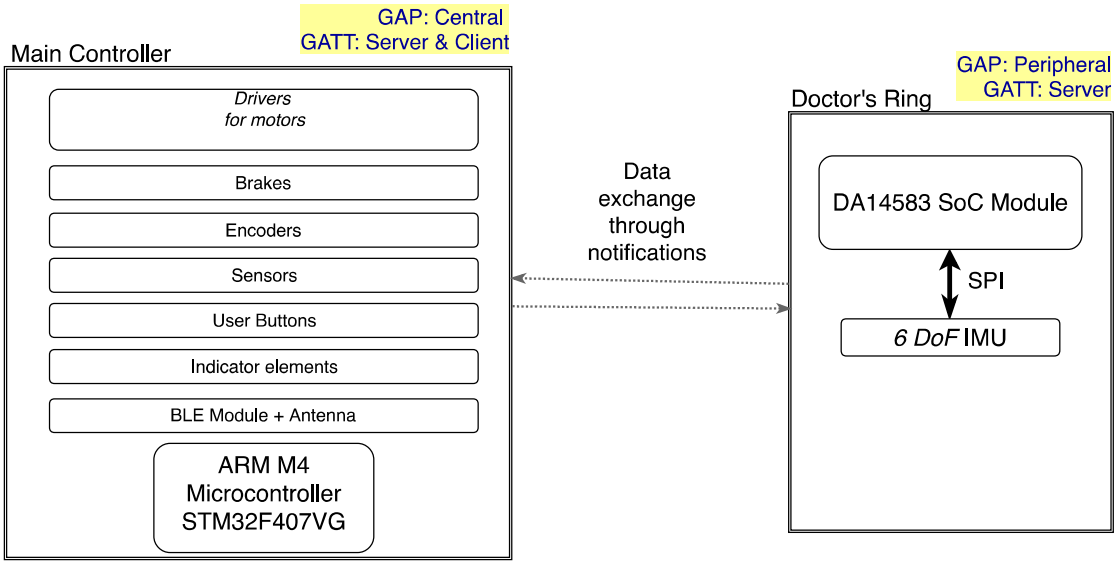

Figure 3.13. BLE roles of the system on simplified scheme

Contrary to incremental encoders, absolute encoders give a different binary output at each position. Therefore the shaft position is absolutely determined. This type of encoder is preferred when the absolute position of the rotor according to the stator is necessary.

There are different absolute encoder types in the markets, most commonly optical encoders, and magnetic encoders. The ones which were used in this thesis is the magnetic ones. They produce digital outputs by the rotation of the magnet attached to the rotor. Suitable magnet type can vary from one magnetic encoder to another and it affects the resolution. In this thesis, the diametrically magnetized magnets are used with MA702 magnetic encoders. It has 12-bit resolution and provides either absolute output via SPI interface or PWM signal with a varying duty cycle according to the measured angle, or incremental output via regular A, B, Z signals. For measuring the joint angles, SPI interface is used as the communication interface between the encoders and the microcontroller.

Also, for the ease of mounting the endoscope, NeuRoboScope project's mechanical team designed a quick-replace between endoscope and *Active Endoscope Holder* as seen in Figure 3.15. According to the holding type of this quick-replace, there the operation states of the overall system changes system (see section 5.3). In order to measure how much the surgeon pressed to the button shown in Figure 3.15.b, a magnetic encoder is used so that it can detect the rotation while the button is pressed.

In this mechanism, the same magnetic encoder is used instead of classical potentiometer type buttons due to mechanical design limitations. In order to measure how much

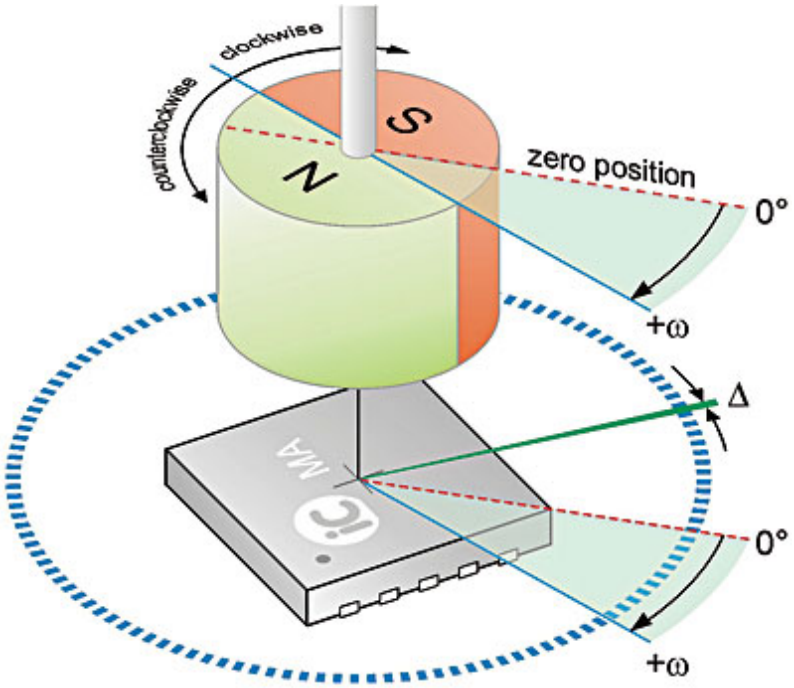

Figure 3.14. Magnetic encoder working principle
(Source: archives.sensorsmag.com/articles/1105/15/main.shtml)

the button is pressed as in Figure 3.15 one magnet is attached to the pin of the button and the encoder is attached to the shaft of the system.

Contrary to the measuring process on the encoders attached to the joints, PWM output interface of MA702 magnetic encoders is preferred for the quick-replace mechanism. The reason for using different interfaces is the mechanical constraints on the quick-replace mechanism for placing the cables connecting the encoder with the microcontroller. As it was stated before, the number of required pins for SPI interface is 4 contrary to the PWM output interface's 3 cables.

Furthermore, the reason why only the encoder attached on quick-replace was chosen to be read on PWM output of the encoder whereas all of the other identical encoders were read on SPI output is the following: In order to read PWM signals on the microprocessor with high precision, each PWM input pin needs to be defined as an external interrupt. However, in the main code, it is preferred as less as ISR requests to be executed. Since the highest priority IRQ is the SPI interrupt of the Bluetooth module so that the communication can start immediately, it can interrupt any other IRQ. This is not a problem for many IRQs executed in the main code but it can cause wrong values for IRQs which process time-based measurements such as PWM duty cycle calculations. Also, the computational cost of reading a PWM signal with interrupts is higher than reading a

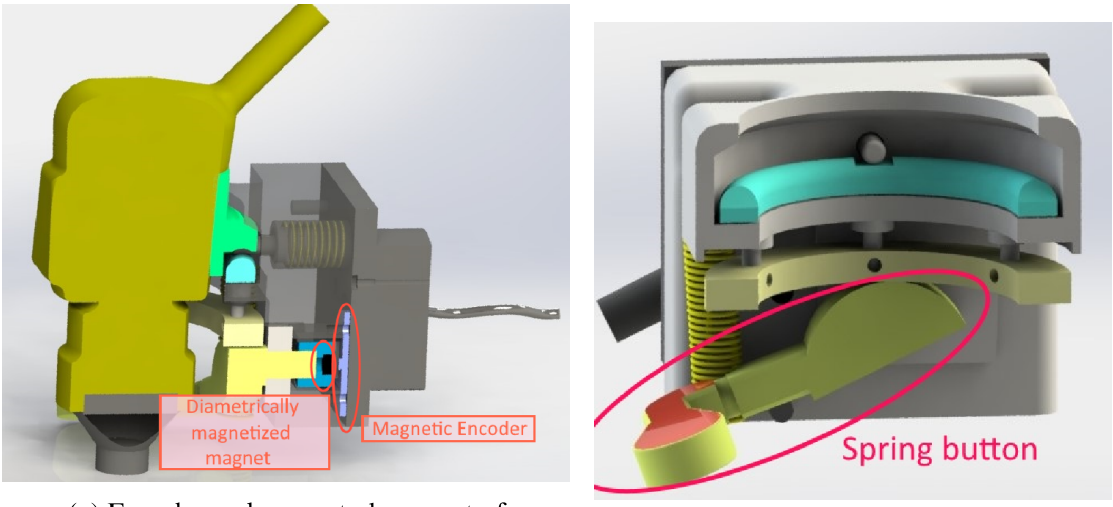

(a) Encoder and magnet placement of quick-replace mechanism

(b) Button mechanism of quick-replace

Figure 3.15. Renderred image of quick-replace mechanism

sensor data via SPI protocol by using the DMA stream for such an application.

3.2.5. Force-Torque Sensor

The slave system operates inside the skull full of various tissues and bones. In order not to damage any part of the skull, it is important to inform the surgeon about the slave environment. The way of performing this is measuring the forces and torques exerted on the endoscope when it touches anything inside the skull and returns this information to the master side via visual feedback module.

In order to provide the interaction information of the slave robot with the tissue or bone, one solution is to use an F/T sensor. As the name implies, an F/T sensor is a device that measures force and torque applied on each axis of the sensor. Its types vary depending on the mechanism used inside the sensor.

The F/T sensor which is used in this thesis is Mini45 by ATI Industrial Automation. Mini45 is a compact, low-profile device that can measure up to 5100 N force and 110 Nm torque on x and y-axes, increasing up to 10000N force and 140 Nm torque on z-axis as the axes are shown in Figure 3.16.

The sensor has twelve silicon strain gauges as located in Figure 3.17. Strain gauges change resistance as the applied force elongates or shortens the gauge. A change in resistance can be read as a voltage change. Therefore, force and torque values on each

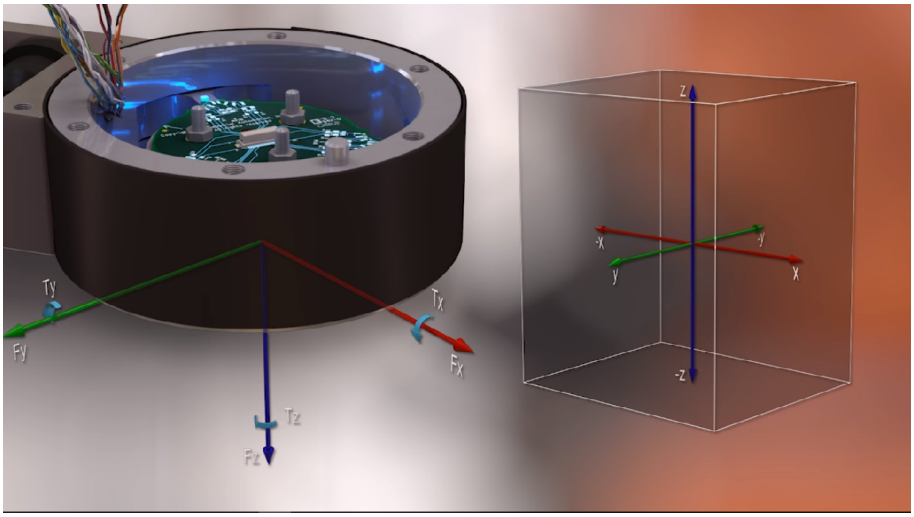

Figure 3.16. Axes of ATI Force/Torque sensors
(Source: ATI Industrial Automation, (2015, Feb 18)*Why ATI Force/Torque Sensors? URL: youtu.be/b4nz_hAh7qs*)

axis can be calculated separately by taking position and orientation of all gauges into account.

Figure 3.17. Strain gauge placements of ATI Force/Torque sensors
(Source: ATI Industrial Automation, (2015, Feb 18)*Why ATI Force/Torque Sensors? URL: youtu.be/b4nz_hAh7qs*)

Importantly, strain gauges are very sensitive elements to the temperature changes. For that reason, Mini45 F/T sensor outputs the signal as a combination of two strain gauges. Electrical equivalent schematic of the transducer is shown in Figure 3.18. Thanks to this method, the effect of the temperature changes are minimized since both strain gauges on the same line would be affected similarly. Therefore, twelve strain gauges compose six half-bridge strain gauges and each pair works together as a voltage divider to produce a signal representing the pair's load.

Each strain gauge pair is excited from SG_{HI} pin for the upper excitation voltage

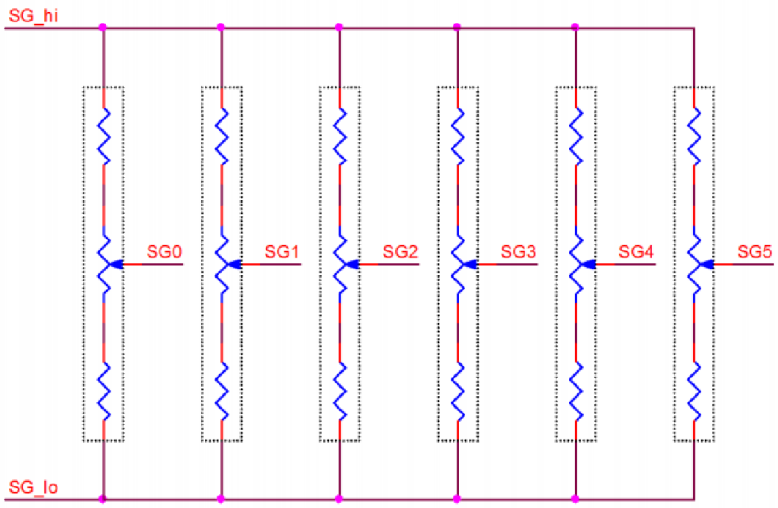

Figure 3.18. Strain gauge ourputs of Mini45 F/T sensor
(Source: ATI Industrial Automation F/T Transducer without Electronics (TWE) Manual (ATI, 2018))

and SG_{LO} pin for the lower excitation voltage as shown in Figure 3.18. The nominal unloaded output of each of the half-bridges is the voltage halfway between SG_{HI} and SG_{LO}. These excitation voltages can be chosen by the designer depending on the desired output voltage of the half-bridges. However, since the calibration spreadsheet recommends 5VDC for SG_{HI} and 0VDC for SG_{LO}, these values are used in the application explained in this thesis.

Although the expected unloaded output is the arithmetic mean of SG_{HI} and SG_{LO}, some offset bias voltage presents in practice. Therefore this half-bridge is biased by another half-bridge circuit as shown in Figure 3.19 and both of those half-bridges compose a Wheatstone bridge. A multi-turn potentiometer is placed in order to calibrate it precisely. For the calibration, the output signal of the second half-bridge is set exactly the same value as the strain gauge pairs' when there is no force applied to the sensor.

Figure 3.19. Bias Reference Voltage Circuit
(Source: ATI Industrial Automation F/T Transducer without Electronics (TWE) Manual)

Two outputs of the Wheatstone bridge is connected to the OPAMP circuit demonstrated in Appendix D. Eventually, the output of the OPAMP circuit is connected to the microcontroller's ADC inputs.

3.2.6. Actuation System

As it was previously mentioned *Active Endoscope Holder* has three motors on it and positions the endoscope by the actuation of these motors. Since the surgical area involves several vital parts of the human body such as the brain and arteries, it is very important to have a precise actuation system. As it is mentioned in Section 3.1.2 motors with planetary gears that has 1:181 gear reduction ratio and a 1:5 capstan drives are used for the actuation of all 3 active revolute joints to provide the system with finer motion. In addition to increasing the precision of the motors by gearbox and capstan drives, it is also important to design a precise driving circuit.

Maxon Motor companies 339150 part number brushed DC motors (MaxonMotor, 2018b) are chosen for this application. The nominal torque that a single motor can apply is 27.5mNm with 2.45A continuous current under 12VDC supply.

The motors attached on KEY are driven by two different motor drivers on main processing unit given in Section 3.2.1. The driver regulates the signals provided by the microcontroller and provides necessary type of signal outputs for the motors. In other words, the driver provides sufficient power to drive them by an external power source.

In this thesis, L6207Q DMOS dual full bridge driver by STMicroelectronics company is used. It can drive two motors simultaneously within the operating range of 8 V to 52 V and can supply up to 2.5 A current to each motor continuously, but capable of reaching as high as 5.6 A. The motors are current-controlled according to PWM signal inputs to Vref pins. The directions of the motors are determined with the logic inputs to IN1 and IN2 pins of each motor channel. Positive direction is achieved by supplying HIGH and LOW logic signal to IN1 and IN2 pins, respectively and vice versa for negative direction.

In the main processing unit introduced in Section 3.2.1, there are two L6207Q DMOS dual full bridge drivers allowing to drive up to four motors at the same time. However, within the scope of this thesis, only three motors are driven at a time. The driver is supplied by 12 VDC external power source.

3.2.7. Brake System

Even though *Passive Balanced Arm* system is weight balanced and *Active Endoscope Holder* has motors on its joints, in order to increase the safety of the overall system, each 8 joint on both PEK and KEY have their own brakes.

Brakes are controlled by a MOSFET system whose gates are connected to the microcontroller. According to working principle of the brakes which are used in this thesis, they are released when a voltage difference is applied and they are locked if there is no voltage difference in between two inputs. For precaution, the brakes are chosen not to work when there is no power so that it cannot move in case of an electricity cut circumstance.

According to the proposed teleoperation scheme and the mechanical structure of *PEK* and *KEY*, some of the brakes are locked and released as a group. More clearly there are three sets of brakes; on the *KEY*, on the wrist of the *PEK* and on the arm of the *PEK*. Therefore, it does not need to control each motor separately but it is necessary to control each brake set.

In order to control these brake sets, three different MOSFETs are connected between the microcontroller and brakes as demonstrated in Appendix D.

EMF Elektromanyatik Fren ve Kavrama Sistemleri company's spring weighed type of brakes with part number ASEM-1 and ASEM-2, which are custom production, are used on PEK. ASEM-1 has lower power and the nominal torque of it is 2.5Nm. It requires 24VDC supply and it releases the springs at 0.3A. Three of them are attached to the structure where two of them are on the wrist structure and one of them is on the arm structure PEK. ASEM-2 has higher power and the nominal torque of it is 7Nm. It requires 24VDC supply and it releases the springs at 0.7A. Two of them are attached to the wrist structure of PEK.

Maxon Motor companies 228384 part number brakes (MaxonMotor, 2018a) are chosen for KEY. The nominal torque of a single brake is 400mNm. It requires 24VDC supply and it releases itself at 0.2A. Three of them are attached on KEY.

CHAPTER 4

WORKSPACE ANALYSIS

The proposed teleoperation scheme is categorized under limited-workspace teleoperated systems. This limitation of the workspace is especially important in NeuRoboSope project since the surgical area involves several vital parts of the human body such as the brain and arteries. The surgical area mentioned here is the critical area where the tumor resection takes place which is just after sella turcica. Therefore, a proper calculation of the workspace is necessary for the design of KEY. It is also necessary to understand the key properties of the workspace. One important aspect is the location of the pivot point with respect to the surgical area. The other important aspect of the workspace is the area to be visualized during the tumor resection process beyond the sella turcica.

For the calculations of the limits of the surgical area, two different measurement methods that complement each other are employed. First of all, the total rotational motion that the surgeon can do during surgery inside the surgical area is measured by using an IMU placed on the endoscope. In the second method, radiologic data from the patients are collected and computations of the location of the pivot point and surgical area to be viewed are carried out in a statistical study in Hacettepe University Neurosurgery Department. In this section, the measurement processes are explained and the results of both methods are combined to provide a statistical data for the workspace limits.

4.1. Workspace Analysis Using Inertial Measurement Unit

The purpose of this study is to examine the workspace limits of the surgical area during a surgery. The shape of the workspace is more likely to be measured as a circular or elliptic area since the measurements are carried out by performing rotations about two axes about the pivot point. Therefore, the maximum angles about these two axes that a surgeon can do during the surgery are investigated. These measurements were performed by two surgeons on an ex-vivo subject[1]. 22 different types of motions are recorded.

[1] According to the national legislation in Turkey, studies involving human cadavers are exempt from ethics approval. Besides, all cadaveric samples used in our study have been purchased from a qualified cadaver bank in the USA in compliance with national and international trade regulations. Therefore, we

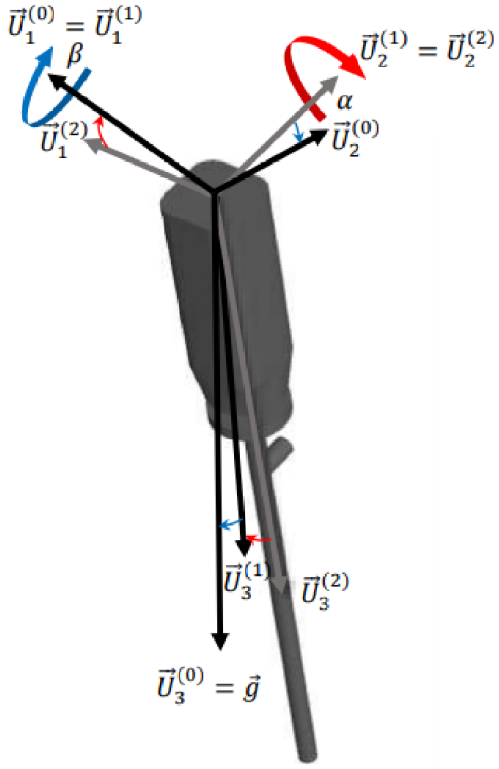

Figure 4.1. Euler axes on endoscope

In the experimental setup, one 3-axis accelerometer that is embedded in an IMU, which is attached to the endoscope used in the surgery, is used. The reason for using the accelerometer as an inclinometer is to eliminate drifting errors when integrating the gyroscope values. Since only absolute angular positions (α and β in Figure 4.1) about two axes are investigated, 3-DoF vectorial acceleration information can provide absolute 2-DoF angular position information by the approach in figure 4.1. Since relatively slow motions are performed during the surgery inside the surgical area, the inertial acceleration effects are neglected. Therefore, the only acceleration measured by the sensor is assumed to be gravitational acceleration $\overrightarrow{g}$. The principle of calculation of the absolute orientation of the endoscope in two axes is expressing the measured $\overrightarrow{g}$ in body-fixed frame F_2 with respect to the inertial frame F_0 in which $\overrightarrow{g}$ is always along $\overrightarrow{u_3^{(0)}}$.

The Euler sequence selected to represent the 3D rotation of the endoscope presented in Figure 4.2 is expressed as in equation 4.1

have not sought an ethics review for the study.

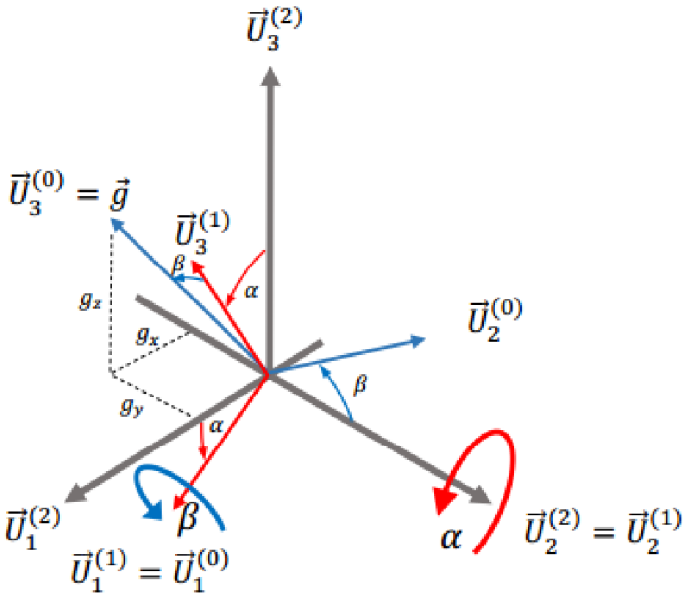

Figure 4.2. Demonstration of chosen Euler sequence in coordinate systems.

$$F_2 \xrightarrow[(\vec{u}_2^2)]{\alpha} F_1 \xrightarrow[(\vec{u}_1^1)]{\beta} F_0 \tag{4.1}$$

The gravity vector $\overrightarrow{g}$ that is resolved in F_0 is presented in F_2 in matrix form as follows:

$$\overline{g}^{(2)} = \hat{C}^{(2,0)}\overline{g}^{(0)}. \tag{4.2}$$

The transformation matrix $\hat{C}$ defined between F_2 and F_0 is calculated by the selected Euler-(21) Rotating Frame-Based sequence and presented in the following equation.

$$\hat{C}^{(2,0)} = \hat{C}^{(2,1)}\hat{C}^{(1,0)} = \begin{bmatrix} cos\alpha & 0 & sin\alpha \\ 0 & 1 & 0 \\ -sin\alpha & 0 & cos\alpha \end{bmatrix} \cdot \begin{bmatrix} 1 & 0 & 0 \\ 0 & cos\beta & -sin\beta \\ 0 & sin\beta & cos\beta \end{bmatrix}$$

$$= \begin{bmatrix} cos\alpha & sin\alpha sin\beta & sin\alpha cos\beta \\ 0 & cos\beta & -sin\beta \\ -sin\alpha & cos\alpha sin\beta & cos\alpha cos\beta \end{bmatrix} \tag{4.3}$$

When equation 4.3 is substituted into 4.2:

$$\overline{g}^{(2)} = \frac{1}{9.81}\begin{bmatrix} g_x \\ g_y \\ g_z \end{bmatrix} = \begin{bmatrix} cos\beta sin\alpha \\ -sin\beta \\ cos\alpha cos\beta \end{bmatrix} \tag{4.4}$$

The Euler angles, which provide the absolute orientation information of the endoscope, are calculated by using the measured $\overline{g}^{(2)}$ information and using its components in equations 4.5 and 4.6.

$$\beta = \begin{Bmatrix} sin^{-1} - g_y/9.81 & cos\beta > 0 \\ \pi - sin^{-1} - g_y/9.81 & cos\beta < 0 \end{Bmatrix} \tag{4.5}$$

and If $cos\beta \neq 0$, α angle is calculated as

$$\alpha = atan2(\sigma g_x, \sigma g_y) \tag{4.6}$$

where $\sigma = sgn(cos\beta)$. If $cos\beta = 0$ that means $\beta = \pm\frac{\pi}{2}$ then, α angle becomes indeterminate.

According to these evaluation steps, each measured acceleration value acquired during the surgery is transformed into α and β angles so that the absolute orientation of the endoscope about two axes can be found. In order to cover the maximum range of the workspace, it is requested from doctors to perform "2-full-rotations" inside the allowed workspace within the surgical area. It should be noted that the surgeons do not perform such large motions during a standard surgery. This 2-full-rotations motion data provided us a larger workspace than actually used one nevertheless, a safety factor has been introduced to the kinematic design of *Active Endoscope Holder* .

Finally, 22 different motion types from 2 different doctors during a surgery are analyzed and it is calculated that α angle varies in between $12° - 45°$ and β angle varies in between $1° - 22°$. These values may differ from one patient to another, therefore, a statistical data of the workspace variations is computed by using radiologic data, which is explained in the next section.

4.2. Workspace Analysis Using Radiologic Measuring

In order to verify the workspace analysis performed by IMU and extend this data to a larger population's data, radiologic measurements are carried out in Hacettepe University Neurosurgery Department (Dede et al., 2018). These tests are performed on 28 patients (11 men, 17 women and ages 45.9 ± 16.5) who were diagnosed with a pituitary tumor in 2017.

The distances defined as A, B, C and D letters are indicating:

- **Distance between *nostril* and *sella*:** It is the distance on the middle sagittal plane, between the pivot point (on the nostril) where the endoscope is stabilized and sella

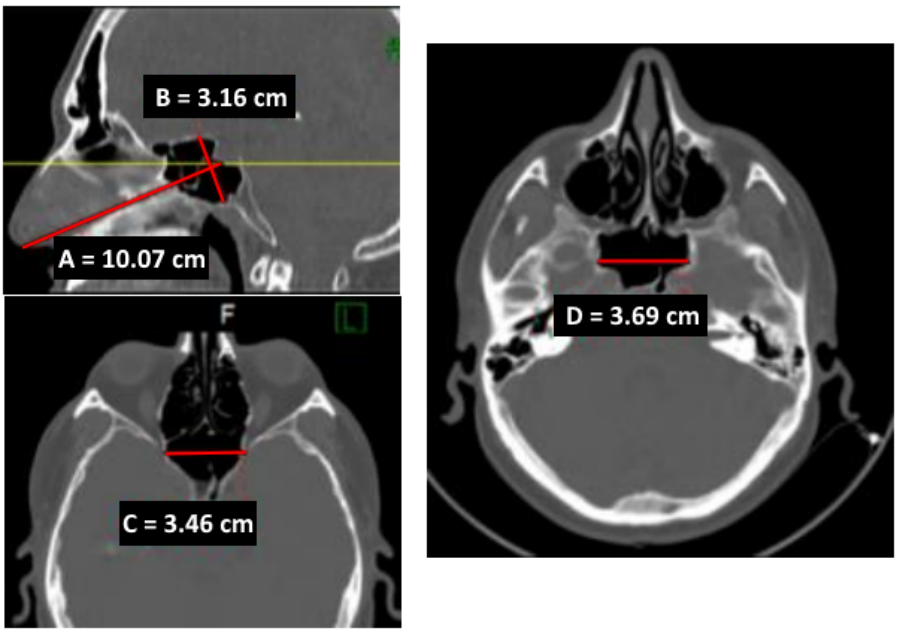

Figure 4.3. Tomograpy results

turcica where the pituitary gland is located. This distance represents the dolly motion (zoom in and out) of the endoscope.

- **Distance between *planum* and clivus:** It is the distance on the axis perpendicular to the depth axis, from the furthest point on this perpendicular axis (sella base) and upper base of the sphenoid sinus (planum sphenoidale) sella turcica where the pituitary gland is located. This distance represents the dolly motion (zoom in and out) of the endoscope.

Results of the measurements and standard deviations are shown in Table 4.1. All units are in cm.

Table 4.1. Radiologic results and standard deviations
(Source: Dede et al. (2018))

Measurement	Average ±Standard Deviation(SD)	95% confidence interval (Avg+2SD)	99.7% confidence interval (Avg+3SD)
A - Depth of Workspace	9.5±0.5	$8.5 - 10.5$	$8 - 11$
B - Height of Workspace	2.±0.5	$1.7 - 3.7$	$1.2 - 4.2$
C - Middle weight of Workspace	3.0±0.5	$2.2 - 3.8$	$1.8 - 4.2$
D - Maximum weight of Workspace	3.4±0.5	$2.4 - 4.4$	$1.9 - 4.9$

4.3. Discussion

Two different types of measurement methods are used to assess the workspace inside the skull. One is performed measuring the endoscope motions during a surgery via an IMU and second type of measurements is carried out by investigating the tomography results of a population suffering from a pituitary tumor. These two types of measurements are combined in order to extend the endoscope motion data received in the first type of measurements to a wider range of the population. In order to combine these results, a relation between the endoscope motion and tomography results should be established.

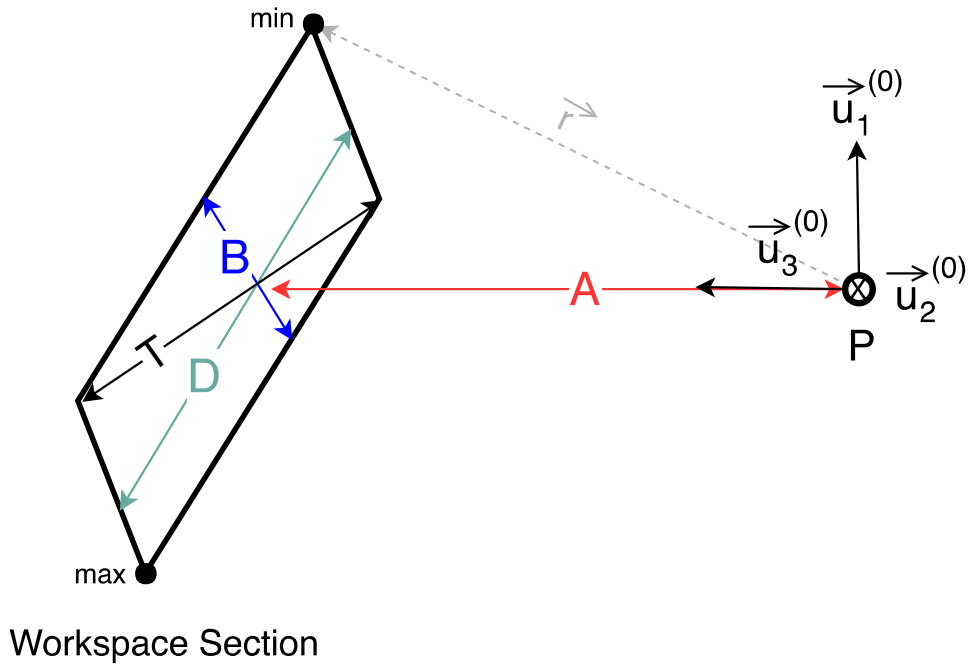

Figure 4.4. Workspace section

Figure 4.4 indicates the relation between the endoscope motion and the surgical area (workspace section) measured from tomography results. This relation enables the calculation of the workspace section covered by the tip point of the endoscope due to α and β rotations obtained in section 4.1 or vice-versa. The distance definitions denoted in the Workspace Analysis Using Radiologic Measuring Section are used for consistency. However, since D length is larger than C length to identify the workspace section, in order to insert a safety factor in the calculations, D length is used to define the workspace section.

The position vector of the endoscope tip point from pivot point is denoted as $\overrightarrow{r} =$

$r\overrightarrow{u}_3^{(2)}$. It is defined in the Earth (inertial) frame as

$$\overline{r}^{(2/0)} = \hat{C}^{(0,2)}\overline{r} \tag{4.7}$$

where $\hat{C}^{(0,2)}$ is the inverse of the rotation matrix calculated in Section 4.1 and column representation of the position vector in Earth frame is defined below.

$$\overline{r}^{(2/0)} = \begin{bmatrix} r_1 \\ r_2 \\ r_3 \end{bmatrix} \tag{4.8}$$

When equation 4.8 is substituted into equation 4.7, the following results are obtained, where T is the diagonal length of the workspace section.

$$r_1 = -\frac{B}{2} = Asin\frac{\alpha}{2}$$

$$r_2 = -\frac{D}{2} = -Asin\frac{\beta}{2}cos\frac{\alpha}{2} \tag{4.9}$$

$$T = \sqrt{B^2 + D^2}$$

On the other hand, instead of using the absolute values of the angles that determine the workspace as defined in section 4.1, the mean of the α and β angles are moved to zero. α and β angles' range is taken as the largest motion that any one of the doctors has performed to construct the largest possible workspace. Otherwise, since the absolute limit angle values denoted in Section 4.1 are the combination of both doctors and it depends on the gripping style of the doctor and thus, using combined maximum ranges of motion would not be reliable.

According to IMU measurements, the maximum range of α angle is 22° and β angle is 12°. As the mean of the ranges of angles are moved to zero since the designed KEY starts motion from its home position without any offset, α is designated to vary in between $(-11^\circ, 11^\circ)$ and β is designated to vary in between $(-6^\circ, 6^\circ)$.

Assuming the patients on which the IMU measurements were performed has nominal skull sizes, the average value of A parameter is used in equation 4.9. Also, resetting the ranges of α and β, the maximum ranges of these angles are substituted into equation 4.9 and a nominal T' is calculated using the IMU measurements as $T' = 4.12cm$. However, T' value calculated from the IMU measurements is different from the average T value calculated from the radiological data. The ratio between the average value, T_{ratio}, is denoted below.

T_{ratio} provides information about the ratio between the viewable workspace section and the required endoscope motion to view this section. Figure 4.5 presents the surgical area versus the actual workspace of the endoscope by denoting the average calculated values of both workspaces diagonal length.

$$T_{ratio} = \frac{T'}{T} = \frac{4.12}{4.34} = 0.95 \tag{4.10}$$

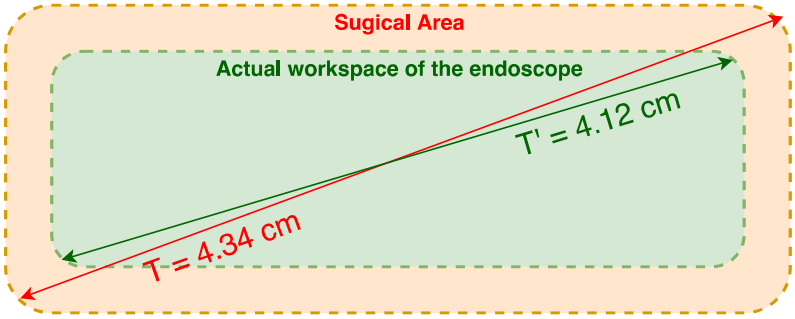

Figure 4.5. Actual workspace of the endoscope in surgical area

In order to extrapolate the IMU measurements to a wider population, 99.7% confidence interval is chosen. Accordingly, the maximum workspace parameters are identified as follows:

$$\begin{aligned} D'_{99.7\%} &= T_{ratio} * D_{99.7\%} = 4.66cm \\ B'_{99.7\%} &= T_{ratio} * B_{99.7\%} = 3.99cm \\ T'_{99.7\%} &= T_{ratio} * T_{99.7\%} = 6.12cm \end{aligned} \tag{4.11}$$

Equation 4.9 is reorganized to calculate the maximum range of the endoscope motion in two axes as follows:

$$\begin{aligned} \alpha &= -2asin(\frac{B}{2A}) \\ \beta &= 2asin(\frac{D}{2Acos\frac{\alpha}{2}}) \end{aligned} \tag{4.12}$$

where α and β are the total rotation when the calculated maximum ranges of α and β are distributed about null position, the ranges are described as $(-\frac{\alpha}{2}, \frac{\alpha}{2})$ & $(-\frac{\beta}{2}, \frac{\beta}{2})$.

Substituting $D'_{99.7\%}$ and $B'_{99.7\%}$ values into equation 4.12, the maximum range of motions of the endoscope about two axes are calculated as $\alpha_{99.7\%} = 33.86$ and $\beta_{99.7\%} = 36.68$. These results indicate that *Active Endoscope Holder* limits should be within this range in order to be in $99,7\%$ confidence interval.

CHAPTER 5

SYSTEM OPERATION MODES

In the first section of this chapter, two different processing methods of the doctor's hand motion demands are explained under teleoperation information flow alternatives category (Dede et al., 2017). Among these two methods, the one that requires the least effort by the surgeon is to be determined via user evaluation tests.

In Section 5.2, two usage mode of the master system is introduced under master system's command computation alternatives (Ates et al., 2018). These two modes allow the doctors to choose the most feasible use of the master system in order to generate commands.

The experimental procedure and test results of these two sections are not covered in this chapter but explained in Chapter 6.

In Section 5.3, the operation states of the robotic system are covered from the initiation process to termination of the whole system operation when the surgery finishes. Each state is explained in details by denoting in which combination of the user buttons make the system work in the represented state and what outputs the system issues according to its current state via visual feedback panel of *User Interface* .

5.1. Teleoperation Information Flow Alternatives

The gyroscope in the master system measures angular rate and this information is used to compute the driving commands of endoscope robot. Two different approaches are formulated by processing this angular velocity information using two different methodologies as stated in Dede et al. (2017). Both of these methods start by integrating the angular velocity measured by the gyroscope as soon as the foot pedal is pressed (formerly, a push button attached on the replica of a surgical tool. See Section 6.1.1) in order to eliminate the drift problem in the discrete integration process. Otherwise, in longer durations of the integration process, drift occurs due to discrete integration.

In the first method namely displacement-to-displacement method, doctors need to move their hand until the endoscope tip point reaches the desired position. In this scenario, doctor's hand is required to cover wider workspace. On the other hand, in the

second method namely displacement-to-velocity method, doctors do not need to keep moving their hands during the whole motion of the endoscope. Since the endoscope keeps moving at a constant speed when the doctors hold their hand stable after giving an initial orientation, the workspace covered by the doctor's hand is relatively smaller than the previous method.

5.1.1. Displacement-to-displacement method

In this method, integrated angular velocity is processed as the **POSITION** demand of the slave system. The process is triggered by pressing the foot pedal and the position of the endoscope tip point changes according to the doctor's hand orientation directly until the foot pedal is released. As soon as the pedal is pressed again, the integration process is initiated by taking the initial position of the ring as zero. As a result of this, relative position information can be forwarded to KEY.

This method can be understood easier if the working principle of the mouse on a screen is considered. As the mouse is moved, the cursor on the screen is moved proportionally. Similarly, if the mouse is stopped, then the cursor stops moving. Then, during the re-initiation of the process, if the mouse position has reached the boundary of the user's workspace, it can be picked up and placed in the middle of the workspace and transmit the relative motion information with respect to this new initiation location. Nevertheless, the violation of the workspace can be avoided by increasing the sensitivity of the mouse which calls for a more precise operation by the user for keeping the same precision in operating the mouse.

The similar working principle applied to this method. The amount of the relative position change of the endoscope tip point is directly proportional to the orientation change of the surgeon's hand. This proportional relationship is adjusted by gains which also results in changing the sensitivity of the operation. Equation set 5.1 explains the working principle of this method.

$$\begin{aligned} S_i &= sat(K_s \int R_r dt + Si - 1); i = 0, 1, 2, ... \\ Y_i &= sat(K_y \int Y_r dt + Yi - 1); i = 0, 1, 2, ... \\ P_i &= sat(K_p \int P_r dt + Pi - 1); i = 0, 1, 2, ... \end{aligned} \tag{5.1}$$

Each time the pedal is pressed, real-time gyroscope measurements are sent to the slave system and also pressing the pedal increases the *i* count by 1 in Equation set 5.1. In the initial conditions, S_0, Y_0 and P_0 values are set to zero and the S_1, Y_1 and P_1 values

are updated as long as the pedal is pressed. After the pedal is released S_1, Y_1 and P_1 values are stored for the next time the pedal will be pressed. S_i, Y_i and P_i are the i^{th} displacement demand along surge (dolly) axis, i^{th} angular displacement demands about the yaw and pitch axes, respectively. R_r, Y_r and P_r are the angular rates measured from the gyroscope about the roll, pitch, and yaw axes. Finally, K_s, K_y and K_p are the gains used to scale the workspaces of the main control unit attached surgical tool and the slave robot handling the endoscope. If these gains are selected to be larger, then with a smaller motion of the main control unit attached surgical tool, a larger displacement demand for the slave robot will be issued.

5.1.2. Displacement-to-velocity method

In this method, the integrated angular velocity information received from the ring is processed as the **VELOCITY** demand of the slave system (KEY). This process is triggered by pressing the foot pedal and the velocity of the endoscope tip point changes according to the doctor's hand orientation until the foot pedal is released again. As soon as the pedal is pressed again, the integration process is initiated by taking the initial position of the ring as zero which results in a zero initial speed command to KEY.

In this method, contrary to the displacement-to-displacement method, the endoscope is not stopped when the doctor stops moving his/her hand. In this case, the endoscope stops accelerating but keep on moving with the same speed which is directly proportional to the stationary orientation of the doctor's hand. As soon as the pedal is released, the endoscope motion stops, the angular position of the ring is set as zero and the integration process stops.

Equation set 5.2 explains the working principle of this method.

$$\begin{aligned} S_i &= sat[(K_s.\sigma \int R_r dt + Si - 1)]; i = 0, 1, 2, ... \\ Y_i &= sat[(K_y.\sigma \int Y_r dt + Yi - 1)]; i = 0, 1, 2, ... \\ P_i &= sat[(K_p.\sigma \int P_r dt + Pi - 1)]; i = 0, 1, 2, ... \end{aligned} \tag{5.2}$$

The parameters, initial conditions and the applications of the formulas for this method are almost the same as the previous method. The only difference is that in the first integrations, a reset signal is utilized to reset the result of the first integration in Equation set 5.2 to zero whenever the pedal in the master side is released. Therefore, whenever the pedal is not pressed σ values in Equation set 5.2 becomes equal to 0 and otherwise it is equal to 1. In this way, it is guaranteed that the control demand in terms of

velocity sent to the slave system is a zero command and the slave robot does not operate until the pedal is pressed.

5.2. Master System's Command Computation Alternatives

The proposed teleoperation system (shown in Figure 5.1) allows the surgeons to remotely control an endoscope using their hand within a constrained environment (such as holding a tool that is partially inside a patient's nose) (Ates et al., 2018). Teleoperation schemes differ depending on masters system's command computation methods.

Evaluations of the operation modes introduced in this section are explained and the results are discussed by comparing the operation modes in terms of usability, learning curve and the user effort in Section 6.2.

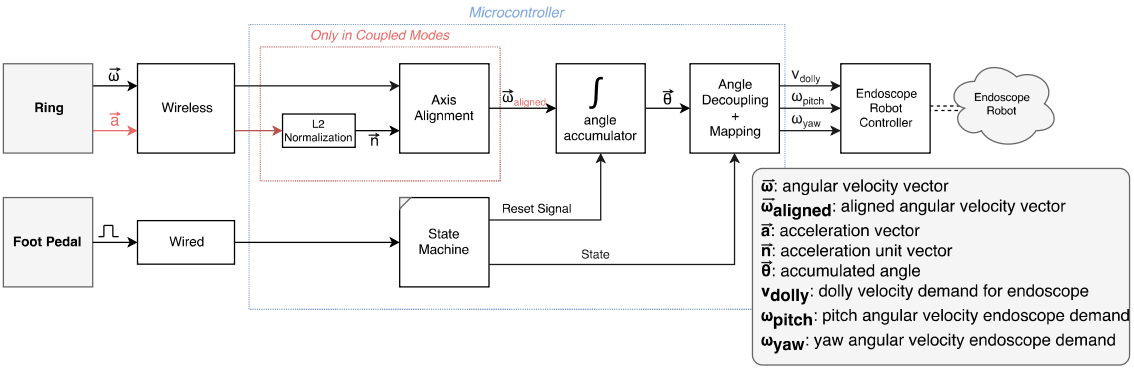

Figure 5.1. An overview of the teleoperation schemes.

The teleoperation system presented in this section allows the surgeons to control an endoscope remotely using their hand within a constrained environment (i.e. holding a tool that is partially inside a person's nose). This system is composed of three parts as; master, slave and communication channels which are depicted priorly in Figure 3.1. The master consists of 2 parts:

- A ring that embeds a 6 DoF (Degree of Freedom) IMU (Inertial Measurement Unit) and Bluetooth module and is worn on the surgeon's index finger of the hand that will hold the non critical tools during the surgery. It transmits the angular velocity and acceleration of the surgeon's hand motions at a rate of 100 Hz.
- A foot pedal that triggers the teleoperation scheme and sets the operation mode.

The slave consists of 3 parts:

- A microcontroller that implements the teleoperation scheme's algorithm described in Appendix B, in order to generate a set of velocity demands for the endoscope robot controller.
- Endoscope Robot Controller: a microcontroller that processes the generated endoscope velocity demands and utilizes motor drivers and signal processing to control the endoscope robot accordingly.
- Endoscope Robot: a manipulator with its joint actuators and sensors that handles an endoscope. This robot has 2 rotational DoF (pitch and yaw) and 1 translational DoF (dolly) around a remote center of motion (Yaşır and Kiper, 2018).

There are two communication channels:

- Wireless: transmits the angular velocity and acceleration vectors measured by the ring to the microcontroller.
- Wired: transmits the pedal state to the microcontroller.

The teleoperation schemes render hand motions by integrating the angular velocity that the ring transmits, calculating the angular position difference since the foot pedal was pressed, and then maps these angles to a proportional velocity demand for the endoscope as shown in figure 5.2. The accumulated angle is reset to zero when the pedal is released. This is also known as the displacement to velocity teleoperation scheme as described in Dede et al. (2017).

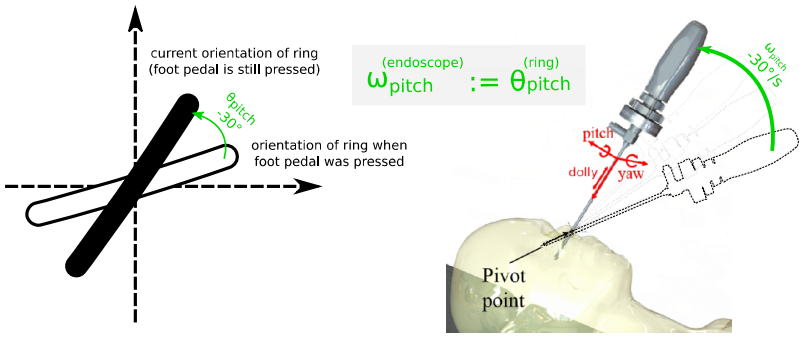

Figure 5.2. Representation of angle accumulation and its mapping to a velocity demand

There are 3 system states:

- **OFF:** when the teleoperation system is inactive and the angle accumulator is reset since the foot pedal is not pressed.

- **ROTATION:** when the foot pedal is pressed and held down. In this mode, only motions of the ring mapped to the rotational motions of the endoscope are processed.
- **DOLLY:** activated when the foot pedal is pressed 2 consecutive times (a double click) and held down. In this mode, only the motion of the ring mapped to the dolly motion of the endoscope is processed.

The reason why ROTATION and DOLLY motions are separated into two different state is while the surgeon means to execute one motion (especially in dolly motion), he/she orients their hands about other axes, as well (translational axes). This causes undemanding motions of the slave system.

- **Coupled 3D mode:** when the system is in the DOLLY state, the ring's roll motion is mapped to the endoscope's dolly motion.
- **Coupled 2D mode:** when the system is in the DOLLY state, the ring's pitch motion is mapped to the endoscope's dolly motion, which means 3 DoF Robot is controlled by only 2 DoF motion of the hand.

5.2.1. Uncoupled Mode

In this mode, no axis alignment is performed, meaning that the surgeon depends on their index finger's motions to control the endoscope. Orientations are rendered in the ring's own frame, they are not assigned into Earth's frame. Intuitively, the surgeon would be holding a tool with their hand except for the index finger which would be free to move when the surgeon wishes to control the endoscope. Also due to the physical difficulty of performing roll motion while the surgeon's hand is gripping a tool, the pitch motion of the ring is mapped to the dolly motion of the endoscope when the system is in the DOLLY state. The mapping of the ring's motions to the endoscope's motions are described in Table 5.1.

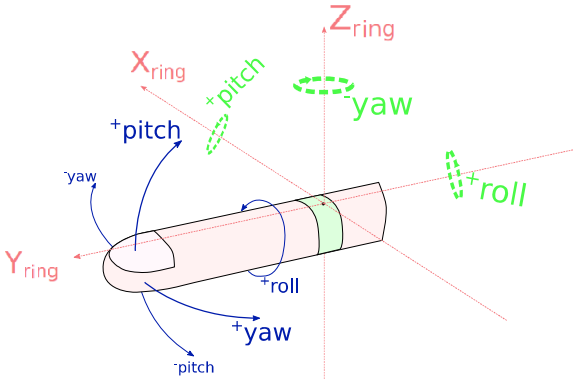

Figure 5.3. Uncoupled mode pose

Table 5.1. Axes map of uncoupled mode

mode	ring motion	endoscope motion
ROTATION	pitch	pitch
	yaw	yaw
	0	dolly
DOLLY	0	pitch
	0	yaw
	pitch	dolly

5.2.2. Coupled Mode

In this mode, the surgeon is able to control the endoscope while maintaining their full grip around the tool. The hand motions are performed with the tool as a guide. The ring's motions are performed by rotating the tool while keeping its tip stable, giving the feeling the rotations are performed with the tool's tip as the pivot. The location of the pivot point can also be chosen by the surgeon. The motions are mapped in such a way that tool rotates proportional to the endoscope's desired rotation. To allow for such motions, axis alignment is performed to compensate for the hand's orientation while holding the tool. Axis alignment will reorient the angular velocities measured in the ring frame to the Earth's inertial frame of reference.

Two variations of tool pose are defined differing only in the mapping of the endoscope's DOLLY motion:

- coupled 3D mode: when the system is in the DOLLY state, the ring's roll motion is mapped to the endoscope's dolly motion.
- coupled 2D mode: when the system is in the DOLLY state, the ring's pitch motion is mapped to the endoscope's dolly motion, meaning we controlling a 3 DoF Robot using only 2 DoF motion.

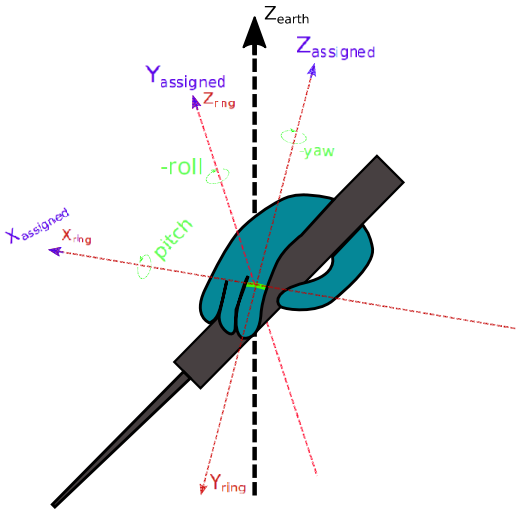

Figure 5.4. Coupled modes pose

Table 5.2. Axes map of coupled 2D

mode	ring motion	endoscope motion
ROTATION	pitch	pitch
	roll	yaw
	0	dolly
DOLLY	0	pitch
	0	yaw
	yaw	dolly

Table 5.3. Axes map of coupled 3D

mode	ring motion	endoscope motion
ROTATION	pitch	pitch
	roll	yaw
	0	dolly
DOLLY	0	pitch
	0	yaw
	pitch	dolly

5.2.2.1. Axis Alignment

The misalignment of the ring's vertical axis with the Earth frame's vertical axis (given by the unit vector of the ring's accelerometer data) is compensated transforming to the gyroscope angular velocity vector data transmitted by the ring to render them in the Earth's frame of reference by using Euler rotation sequence.

The first step of axis alignment is to assign raw gyroscope angles ω_x, ω_y, ω_z to their corresponding rotational motion *yaw*, *pitch*, *roll* by deciding which of the ring's accelerometer axes is closest to the z-axis of the Earth frame when the button was *pressed*. (Currently, this is done manually based on which orientation the surgeon is assumed to hold a tool with, but there are plans for automating the vertical axis selecting in the future). Then the unit vector of the accelerometer data $\overrightarrow{a}$ is used to determine the orientation of the gyroscope axes and to select which of the axes should be considered as the vertical roll axis.

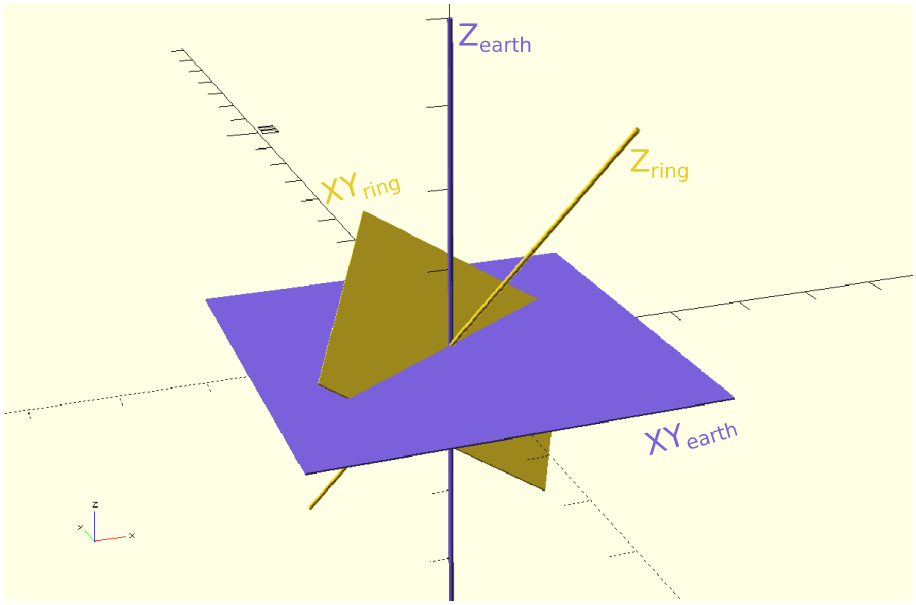

Figure 5.5. Visualization of the misalignment between the ring and Earth's axes.

Then, the unit vector that defines the gravity direction in ring-fixed frame is calculated as:

$$\overrightarrow{n} = \frac{\overrightarrow{a}}{\| \overrightarrow{a} \|} = n_x \overrightarrow{u_x}^{(r)} + n_y \overrightarrow{u_y}^{(r)} + n_z \overrightarrow{u_z}^{(r)} \tag{5.3}$$

This unit vector $\overrightarrow{n}$ is used in order to determine how much the ring is rotated with respect to the Earth's frame. Since the gravity vector is defined as $\overrightarrow{g} = g.\overrightarrow{u_z}^{(e)}$ in Earth's frame, the orientation about $\overrightarrow{u_z}^{(e)}$ cannot be determined. Assuming the ring is oriented with a Euler Y-X sequence by α and β amount of rotations respectively, the transformation matrix $\widehat{C}^{(e,r)}$ from Earth's frame to ring's frame is evaluated as follows:

$$\widehat{C}^{(e,r)} = e^{\tilde{u}_y \alpha} e^{\tilde{u}_x \beta} \tag{5.4}$$

where, its α and β values can be determined by solving the following equation:

$$\overline{n}^{(r)} = \widehat{C}^{(r,e)} \overline{u}_z \tag{5.5}$$

Given the raw gyroscope data of angular velocity in the ring-fixed frame, $\overrightarrow{\omega}$ which is the input to the accumulator node in the Coupled Modes, is calculated with the following formula:

$$\{\overrightarrow{\omega}_{aligned}\}\Big|_{\mathcal{F}_e} \triangleq \overline{\omega}^{(e)} = \hat{C}^{(e,r)} \cdot \overline{\omega}^{(r)} \tag{5.6}$$

5.2.2.2. Angle Accumulator

The angle accumulator converts the raw IMU gyroscope data (angular velocity $\overrightarrow{\omega}$) to the angular displacement which will be processed to be a velocity demand as proposed in Dede et al. (2017). It is active and accumulating when the teleoperation scheme is active and is reset and stopped when the teleoperation scheme is deactivated. The angle accumulator is mathematically modeled in (5.7), with K_i being the scaling constants, and σ being the activation value and it is set to 1 when the teleoperation scheme is active, and 0 otherwise.

$$\theta_i = sat\left[K_i \cdot \sigma \int \omega_i^{(j)}\, dt\right]; \quad i = pitch, yaw, roll; \quad j = \begin{cases} r & \text{in Uncoupled Mode} \\ e & \text{in Coupled Modes} \end{cases} \tag{5.7}$$

5.2.2.3. State Machine for the Foot Pedal

The state machine is responsible for managing the system state and its transitions based on the foot pedal press states. The transition of the system's states are shown in Figure 5.7 and Figure 5.6, and described as follows:

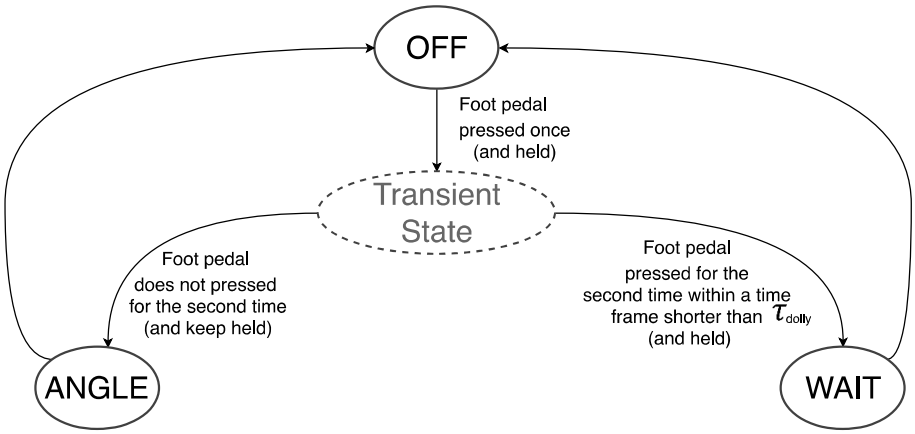

Figure 5.6. State machine for the foot pedal

The transient state is not an actual state of the system. The system state stays in OFF state, however it checks whether the foot pedal is pressed consecutive times.

- *OFF*: set when the pedal is released. The angle accumulator is reset and stopped, and the teleoperation scheme is inactive.
- *ROTATION*: set when the foot pedal is pressed and held down longer than a predefined time called the *double click tolerance* τ_{dolly}. Only motions of the ring mapped to the rotational motions of the endoscope are processed.
- *DOLLY*: set when the foot pedal is pressed 2 consecutive times and it is held down longer than τ_{dolly} in the second time, where the time elapsed between the two pedal presses is τ_{dolly}. Only the motion of the ring mapped to the dolly motion of the endoscope is processed.

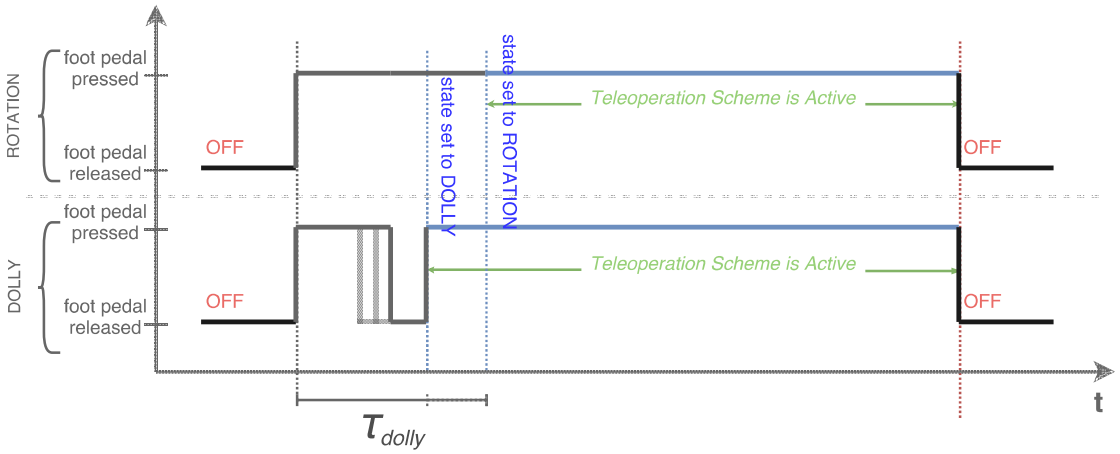

Figure 5.7. Visualization of system state transitions.

5.2.2.4. Decoupling and Mapping

The final step of the scheme is converting and mapping the accumulated angle displacement to appropriate velocity demands for the endoscope robot controller according to the current system state. The mapping is fully dependent on the mode of operation and is described in their relevant subsections (5.2.2 and 5.2.1).

5.3. Overall System's Operation States

During the surgery, the system should operate in different states under different scenarios according to sensor readings or surgeon's inputs to the system by different buttons (see section 3.1.5.1). Actually, these states can be summarized into following sections starting from the setup of the system until the shut down it when the operation finishes. See Appendix E for summarized chart.

- **SHUT DOWN STATE :**
  - *Main Power Button* is in OFF state and there is no power in the system.
  - *Passive Balanced Arm* and *Active Endoscope Holder* are locked from their all joints.
  - *Main Control Unit* , *Communication System* and *User Interface* is in OFF state.
  - Before the surgery starts and when the surgery ends, the medical team should leave the system in this state.
- **EMERGENCY STATE :**
  - As soon as *Emergency Button* is pressed, the system starts operating in this mode.
  - The power of the microcontroller is cut.
  - This is the mode in which the system is able to be driven manually by the relay system connected to the brakes on the arm structure of PEK even though the power of the microcontroller is cut.
  - All brakes on *Active Endoscope Holder* are locked.
  - 3 brakes of *Passive Balanced Arm* on its arm are open whereas 2 brakes on the wrist are locked so that the surgeon can back-drive the system by positioning the system along these 3-DoF.
- **MANUAL STATE :**
  - As soon as *Manual Control Button* is pressed, the system starts operating in this mode.
  - This is the mode in which the system is able to be driven manually

- All brakes on *Active Endoscope Holder* are locked.
- 3 brakes of *Passive Balanced Arm* on its arm are open whereas 2 brakes on the wrist are locked so that the surgeon can back-drive the system by positioning the system along these 3-DoF.

• **PASSIVE STATE :**

- Triggering *Surgeron Holds Endoscope Button* enables this state.
- There are two sub-states according to pressing type of *Surgeron Holds Endoscope Button* :

  ENDOSCOPE IS HELD:

  * In this mode, the surgeon takes out the system from surgery zone without detaching the endoscope.
  * *Surgeron Holds Endoscope Button* is half-pressed and tiny vibration motor on hot-plug is vibrating for haptic feedback in order to issue a feedback starting that this type of pressing is sufficient to back-drive the system.
  * All brakes on *Active Endoscope Holder* are locked.
  * All brakes of *Passive Balanced Arm* are free, however, the very first linear joint's brake is locked since it is only changed by the beginning of the surgery to arrange the overall system's height.
  * In order to leave this state, the surgeon releases *Surgeron Holds Endoscope Button* in a close neighborhood of the surgery zone. After a short wait (1sec), the system centers *Active Endoscope Holder* and enters WAIT STATE.
  * If surgeon releases *Surgeron Holds Endoscope Button* inside the surgery zone and if *Active Endoscope Holder* needs to be centralized than the system would not take any action and gives visual feedback on *User Interface* that it needs to be centralized. In this case, the surgeon should reposition the system away from surgery zone and let the system centralize itself. Then, it enters WAIT STATE.

  ENDOSCOPE IS DETACHED :

  * In this mode, the surgeon takes out the system from surgery zone by detaching the endoscope.

* All brakes on *Active Endoscope Holder* and *Passive Balanced Arm* are locked.
* When surgeon re-attaches the endoscope to the system, s/he is supposed to press *Surgeron Holds Endoscope Button* half so that the system can be manually driven again by releasing the brakes of *Passive Balanced Arm* .

- **WAIT STATE :**
  - This state is the one that the system stays most of the time.
  - After any passive states explained above, the system enters WAIT STATE unless *Main Power Button* , *Emergency Button* or *Surgeron Holds Endoscope Button* is triggered. Before entering this state, *Surgery Zone Button* check process is performed as explained in Appendix E.
  - All brakes on *Active Endoscope Holder* and *Passive Balanced Arm* are locked.
  - Surgeon knows the system is ready to enter the ACTIVE MODE by triggering *Master-Unit-is-Active Switch* (in other words, the foot pedal).
  - In any case of leaving this state except for entering the ACTIVE MODE, the system needs to check if centering is needed for *Active Endoscope Holder* . This is crucial for especially if *Active Endoscope Holder* is within limits from the previous state.

- **ACTIVE STATE :**
  - It is the state when *Master-Unit-is-Active Switch* is triggered in WAIT STATE.
  - There are two sub-states according to the pressing type of *Master-Unit-is-Active Switch* :

    ROTATION STATE :

    * The system enters this mode when *Master-Unit-is-Active Switch* is pressed only once (and held down). Yaw and pitch motions of the ring are mapped as yaw and pitch motions of the endoscope.
    * All brakes on *Active Endoscope Holder* are free and all brakes on *Passive Balanced Arm* are locked.

    DOLLY STATE :

    * The system enters this mode when *Master-Unit-is-Active Switch* is pressed twice (and held down). Roll motion of the ring is mapped as dolly motion of the endoscope if the system was chosen to operate in the coupled

mode with 3-DoF control commands. Pitch motion of the ring is mapped as dolly motion of the endoscope if the system was chosen to operate in either coupled mode with 2-DoF control commands or uncoupled mode.

* All brakes on *Active Endoscope Holder* are free and all brakes on *Passive Balanced Arm* are locked.

5.4. Discussion

In this chapter, operation modes of the system are explained. Firstly, teleoperation information flow alternatives are discussed. These alternatives are proposed as displacement-to-displacement control or displacement-to-velocity control of the slave robot by the master (ring). Secondly, three master system's command computation alternatives are proposed in order to give an easier and more intuitive controlling option to the doctors. Finally, the operation states of the overall system are introduced.

CHAPTER 6

USER EVALUATION EXPERIMENTS

Three different experiments are executed for testing two proposed operation modes explained in Chapter 5. The first experimental procedure is performed in order to determine the type of teleoperation information flow. The second experimental procedure is performed in order to determine and improve the usability of the ring device. Under this process, two different procedure is performed: optimal scaling determination between master and slave, and tests for determining command computation types.

6.1. Tests for Determining the Type of Teleoperation Information Flow

As it is mentioned in Section 5.2, that there are two different processing methods of the doctor's hand motion demands which are displacement-to-displacement and displacement-to-velocity. This section explains the experimental procedure of choosing the one that requires less effort by the surgeon.

6.1.1. Experimental Setup

The experimental setup is composed of a replica of a surgical tool (represents the ring controller) with an embedded gyroscope with an attached push-button (represents the foot pedal) to be used as the master system and a virtual 3-DoF spherical arm robot representation of the slave robot. Since at the beginning phase of this thesis, the proposed master system was an attachable device on any surgical tool, the master system of this experimental setup is not a ring but an IMU attached to the replica of a surgical tool. The slave system is a virtual spherical arm robot and a camera viewpoint placed at the tip point of this robot arm. The surgeon handling the master system is shown in Figure 6.1. While the surgeon uses the replica of the surgical tool, he/she can prefer viewing the surgical area from the computer screen as shown in Figure 6.2 for more intuitive usage. This view is generated by the virtual camera placed at the tip of the slave robot. As the robot is

moved by the processed control demands, the view of the virtual surgical area changes accordingly. This provides the sense that the surgeon is controlling a real endoscope robot which is handling the camera during a surgery. The surgeon constantly looks at the endoscope image presented on a screen.

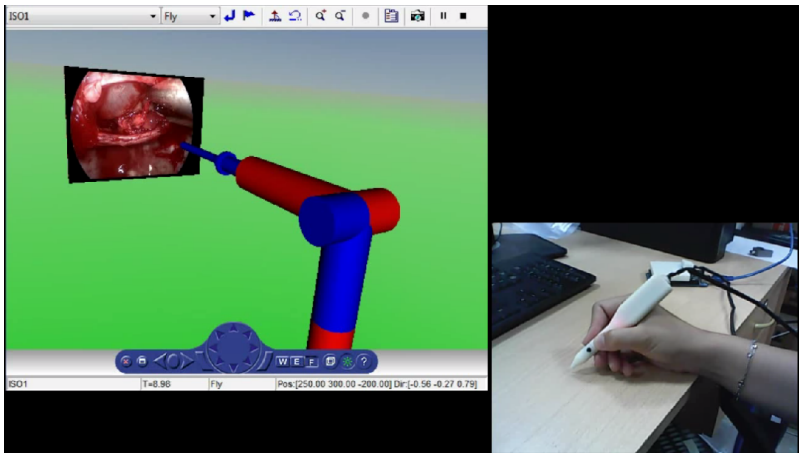

Figure 6.1. Master-slave system of the test setup for determining the type of teleoperation information flow

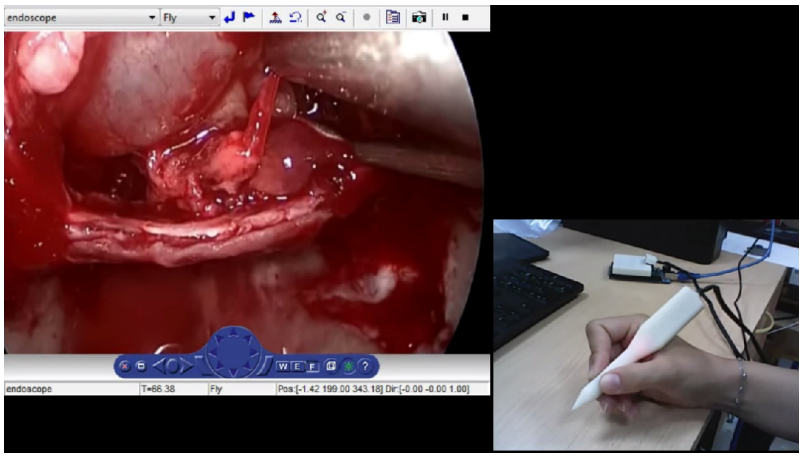

Figure 6.2. Actual surgical view on the endoscope monitoring screen

The replica of the surgical tool, which is produced by using an additive manufacturing system, is shown in Figure 6.1 and 6.2. The main control unit on this tool is composed of a gyroscope unit and a push-button.

In the experimental setup, the gyroscope of the inertial measurement unit (IMU) named GY-88 MPU-6050 by MotionTracking Devices is used. This sensor offers four different sensitivity measures. In the scope of this work, the resolution is relatively more

important than full-scale range; therefore, $FS_SEL = 0$ setting is selected to set the range as ±250 °/sec and sensitivity as 131 LSB/(°/sec). In order to receive and process the measurements obtained from the gyroscope, Arduino Mega 2560 board is used. I2C protocol is used for the communication between microprocessor and gyroscope in order to have a noise-free acquisition of the sensor measurements. The processed sensor measurements are forwarded to Matlab via the serial port as control demands for the slave robot in real time by using Real-Time Windows Target at a sampling frequency of 50 Hz. This rate is enough for visualization of the surgical area. The connection details of the gyroscope and the push-button are shown in Figure 6.3. LED is placed to warn the surgeon that the push-button is pressed and the data is being transferred to the slave system.

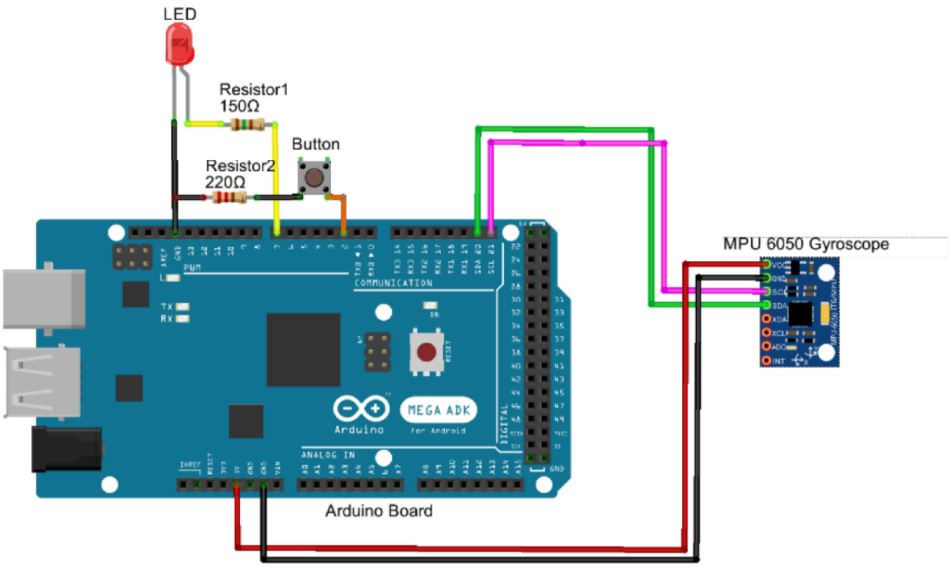

Figure 6.3. Connection of the gyroscope and the push button with the microcontroller

The flowchart of the main control unit is shown in Figure 6.4. It is observed from the figure that the system initiates as soon as it is connected to the power. In the first step, I2C and serial communication protocols should be declared since all the wiring between the gyroscope and the Arduino board should be known by the microprocessor before receiving any signal. Then, the baud rate of serial communication is specified. After these, identification starts and gyroscope measurements are acquired and kept in predefined variables. This process repeats in each loop.

The push-button is used to either allow or prevent the data flow from the Arduino board to Matlab. The state of the button is checked continuously and if the button is pressed, data flow is allowed and the speed information is sent to Matlab. Otherwise, only

"zero" value is sent through the serial port.

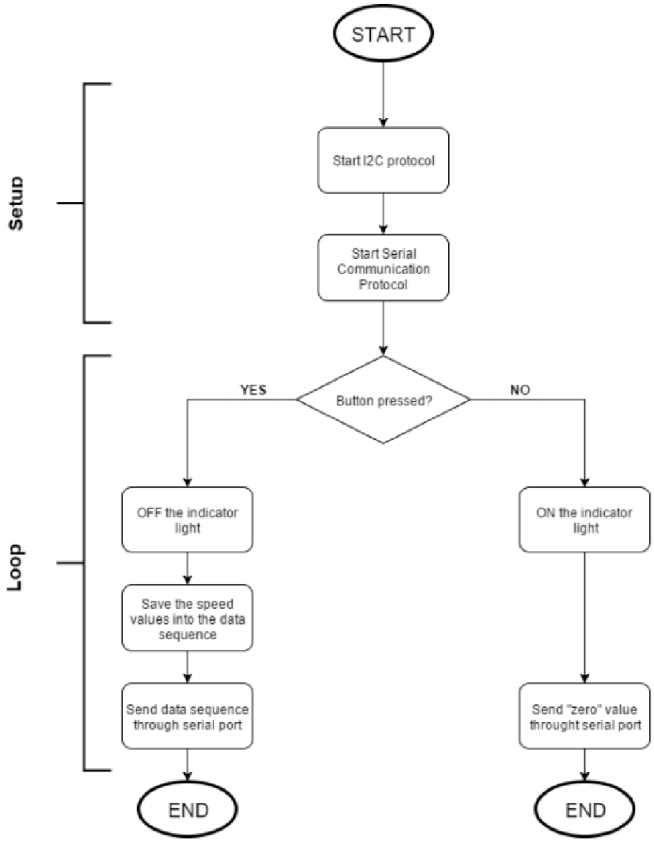

Figure 6.4. Flowchart of the implemented algorithm on Arduino board

In the main control unit, there is also an indicator light (LED) to indicate the data flow condition. If the light is on, it means that the system is ready for the data to be sent but currently there is no data being sent. If the light is off, that means there is a loaded data flow over the serial link. The state of this light is dependent on the condition of the push-button. The program is terminated stopping the hardware-in-the-loop simulation built in Matlab Simulink.

6.1.2. Test Results

This work is dedicated to investigating the most suitable way of control demand acquisition from the surgeon in order to control an endoscope robot during the endoscopic pituitary surgery. Even before constructing the robot to control the endoscope, a simulation of the surgery is developed only to evaluate the ease of sending control demands

to the slave robot, which is also called the endoscope robot in this work. The experimental setup is devised as a hardware-in-the-loop simulation in which the control signals are acquired from a gyroscope and processed to drive a virtual slave robot with a camera that can replicate the visual information in the related surgery. In this study, there is no haptic feedback and the virtual robot is directed by only motion demands in a kinematics mode simulation environment. Two different methods to drive the endoscope robot have been developed and the neurosurgeons from Hacettepe University tested the system with these methods. The first method is very similar to moving the cursor with the mouse on a screen. Although the workspace scaling ratios are increased, it was found to be requiring too much motion during a surgery. It should be recalled that the main controller with the gyroscope is mounted on the replica of a tool and this tool is inside the surgical area during the control of the endoscope robot. The displacement-to-velocity method is evaluated to be much easier to be operated with minimal effort especially when the workspace scaling ratio is increased. In this method, although the surgeon moves the replica of the tool in the required direction by a minimal amount and just stops there while pressing the push-button, the slave robot still continues to move the endoscope in the required direction. As a result of these evaluations, the displacement-to-velocity method was found to be the most convenient way of sending control demands to the endoscope robot.

6.2. Tests for Usability of Master System

For determining the master system's command computation, the slave system is simulated in two different software environments. One environment named CHAI3D (Chai3d, 2018) provides 3D visualization for the doctors while the second environment is a script evaluates the learning curve and effort in use.

This 3D simulation environment is designed to give a more realistic feeling for the doctors as if they were in the surgery room. Tests are executed for determining the most intuitive and comfortable usage of the ring to control the slave system.

6.2.1. Optimal Scaling Determination Between Master and Slave

In order to determine the most convenient scaling factors between the motions of the ring and the motion of the endoscope positioned by *Active Endoscope Holder* , optimal scaling determination test is performed in CHAI3D environment.

CHAI3D (Computer Haptics and Active Interface) is an open source set of C++ libraries for computer haptics, visualization, and interactive real-time simulation. It was designed to make it easier and more intuitive for developers to create applications that combine 3D modeling with force-feedback rendering capabilities.

Additionally, since all quantities are expressed in IUS (metric) unit in CHAI3D environment, this framework is convenient to perform optimal scaling determination tests.

6.2.1.1. Experimental Setup

As a master, Dialog Semiconducters Company's DA14583 IoT sensor development kit (DialogSemiconductor, 2018) is used. A ring-shaped outer case is produced by additive manufacturing as seen in Figure 6.5

For this test setup, only gyroscope values are processed to create velocity demand of the slave. The maximum angular rate is adjusted as $250\,\mathrm{deg}/sec$ where $\pm 250\,\mathrm{deg}/sec$ is the lowest range that BMI160 IMU sensor inside the IoT sensor development kit provides. By choosing this rate, the ring device captures the hand's rotational speed at the highest precision. The ring information is transmitted as a raw data via Bluetooth to the slave.

Afterwards, the slave controller's microprocessor sends the processed data to the simulation environment, which is CHAI3D platform, via UART in a wired medium as the velocity demand of the slave.

As the microcontroller on the slave, STM32F401 Nucleo Development Board (STM32F401RE, 2018) is used as shown in Figure 6.5. Its main purpose is to establish a wireless (in Bluetooth Low Energy protocol) communication with the master device, get the angular velocity information through that communication line, filter this information and integrate it to obtain a reliable angle information in order to calculate the hand's orientation, and transmit it as a velocity demand of the slave to PC via USART. The Bluetooth module used in the slave controller is STBLE-RF Bluetooth Low-Energy module (STBLE-RF, 2018).

The slave system is a virtual endoscope that is able to move in 3D space in CHAI3D environment. In order to introduce the slave controller to the CHAI3D environment, a custom driver is written in C++ since CHAI3D environment only supports C++ language. The driver gets the integrated hand's orientation by setting up a serial communication line, and processes this data into the virtual endoscope position on the screen. Additionally, the slave environment provides two different views as shown in

Figure 6.5: the whole world of the virtual endoscope in its workspace on the left and the camera view of the endoscope on the right.

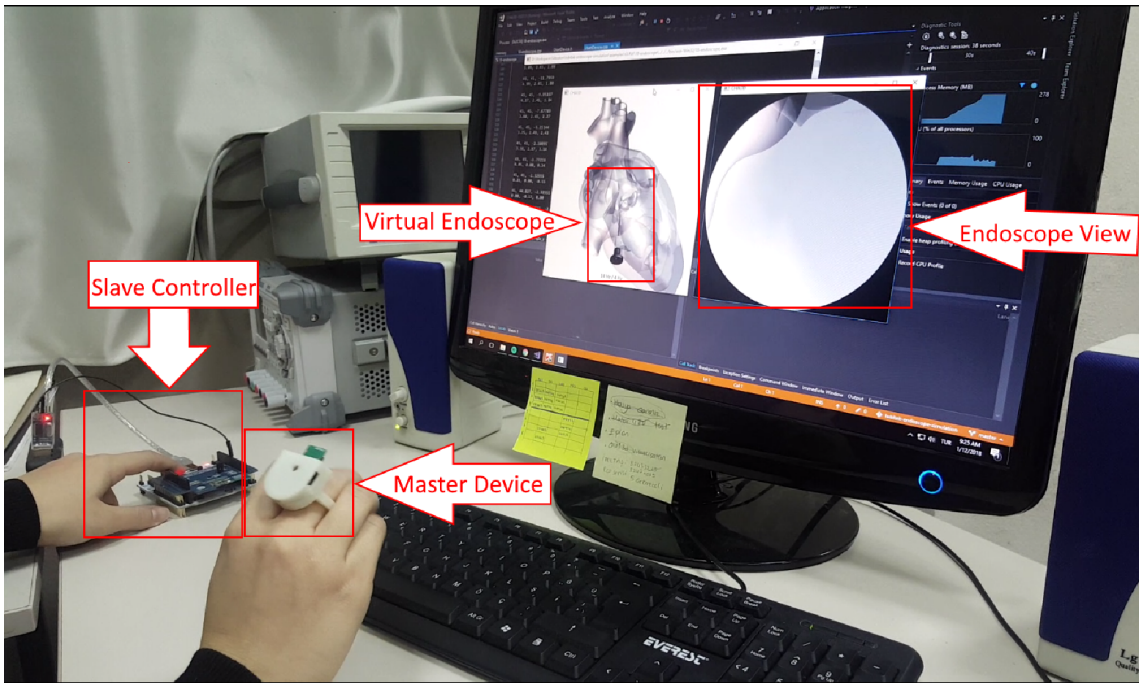

Figure 6.5. Experimental setup for optimal scaling tests

The ring provides 3-DoF angular velocity information with the trigger of foot pedal as described in Figure 6.6.

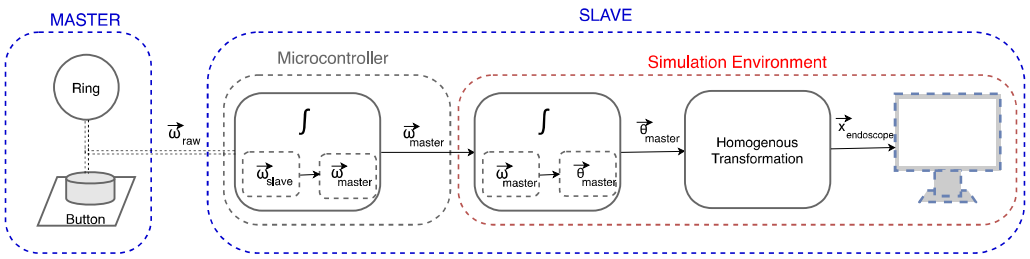

Figure 6.6. Information flow in the test setup of optimal scaling determination between master and slave

In the surgery, the endoscope is leaned on the nose tissue as a support and oriented as if this contact point was a pivot point. In order to import this usage into the visual environment, the following homogenous transformation matrix (4x4) in equation 6.6 is formed.

The rotation matrix is formed by using Euler angles such that:

$$R_{(3x3)} = e^{\tilde{u}_z\theta_2}e^{\tilde{u}_y\theta_1} = \begin{bmatrix} cos\theta_1 cos\theta_2 & -sin\theta_2 & cos\theta_2 sin\theta_1 \\ cos\theta_1 sin\theta_2 & cos\theta_2 & sin\theta_1 sin\theta_2 \\ -sin\theta_1 & 0 & cos\theta_1 \end{bmatrix} \tag{6.1}$$

which can be transformed into HTM without any translation:

$$H_{(4x4)} = \begin{bmatrix} cos\theta_1 cos\theta_2 & -sin\theta_2 & cos\theta_2 sin\theta_1 & 0 \\ cos\theta_1 sin\theta_2 & cos\theta_2 & sin\theta_1 sin\theta_2 & 0 \\ -sin\theta_1 & 0 & cos\theta_1 & 0 \\ 0 & 0 & 0 & 1 \end{bmatrix} \tag{6.2}$$

On the other hand in translation column vector can be evaluated as:

$$T^t = \begin{bmatrix} s_3 & 0 & 0 \end{bmatrix} \tag{6.3}$$

where $s_3 = pivotOffset + \theta_3$. $pivotOffset$ is the distance between the tip point of the endoscope and the pivot point. This column vector can be transformed into HTM without any rotation:

$$H_{(4x4)} = \begin{bmatrix} 1 & 0 & 0 & s_3 \\ 0 & 1 & 0 & 0 \\ 0 & 0 & 1 & 0 \\ 0 & 0 & 0 & 1 \end{bmatrix} \tag{6.4}$$

and,

$$H^{-1}_{(4x4)} = \begin{bmatrix} 1 & 0 & 0 & -s_3 \\ 0 & 1 & 0 & 0 \\ 0 & 0 & 1 & 0 \\ 0 & 0 & 0 & 1 \end{bmatrix} \tag{6.5}$$

Hence, the homogenous transformation matrix representing rotation about a given point is calculated as in the equation 6.6 where the point is the pivot point which is s_3 cm is away from the endoscope tip point and the θ_1 and θ_2 angles are rotation angles around $\overrightarrow{u}_y$ and $\overrightarrow{u}_z$ respectively.

$$H = T^{-1}RT = \begin{bmatrix} cos\theta_1 cos\theta_2 & -sin\theta_2 & cos\theta_2 sin\theta_1 & s_3 \\ cos\theta_1 sin\theta_2 & cos\theta_2 & sin\theta_1 sin\theta_2 & 0 \\ -sin\theta_1 & 0 & cos\theta_1 & 0 \\ 0 & 0 & 0 & 1 \end{bmatrix} \tag{6.6}$$

Eventually, tip point of the endoscope on the screen is:

$$\begin{bmatrix} x_t \\ y_t \\ z_t \end{bmatrix} = \begin{bmatrix} cos\theta_1 cos\theta_2 & -sin\theta_2 & cos\theta_2 sin\theta_1 & s_3 \\ cos\theta_1 sin\theta_2 & cos\theta_2 & sin\theta_1 sin\theta_2 & 0 \\ -sin\theta_1 & 0 & cos\theta_1 & 0 \\ 0 & 0 & 0 & 1 \end{bmatrix} \begin{bmatrix} x_{t-1} \\ y_{t-1} \\ z_{t-1} \end{bmatrix} \tag{6.7}$$

$$\overrightarrow{x}_{endoscope} = \begin{bmatrix} x_{endoscope} \\ y_{endoscope} \\ z_{endoscope} \end{bmatrix} = K * \begin{bmatrix} x_t \\ y_t \\ z_t \end{bmatrix} \tag{6.8}$$

In the simulation environment, the position of the endoscope tip point $\overrightarrow{x}_{endoscope}$ is in the scaled form by factor K, which was evaluated by the doctors. This scaling process is a vital step since the small hand motions should make the slave system smaller motions. Doctors should not lose the control of the system in any level or angular velocity of their hands. On the other hand, too high scaling factors cause logginess in the system which is a negative effect for the whole surgery time.

6.2.1.2. Test Results

Eventually, taken the $pivotOffset = 13cm$, scaling factors $scaling_{tra} = -40$ for translation and $scaling_{ori} = 8$ for the zoom. The minus sign in translational scaling reverses the motion of the hand for providing more intuitive usage. In other words, while doctors are moving their hands upwards, the endoscope moves downwards or vice versa so that it can give the feeling as if the doctor is holding the endoscope by his/her own hands.

Additionally, in order to simulate the kinematic limits of the *Active Endoscope Holder* zoom and orientation limits were applied. They were chosen as $\pm 45\,\mathrm{deg}$ for orientation and $20cm$ for zoom considering results obtained in Chapter 4 by giving extra spaces so that surgeons can try each motion more freely.

6.3. Tests for Determining Command Computation Types

To measure, assess, by compare the feasibility of the proposed schemes, a training simulation is developed by Ates et al. (2018). The simulation is comprised of a 2D workspace, with a set of specified circles at various coordinates with varying radii, and a special circle that can be controlled which is called the ”tool”.

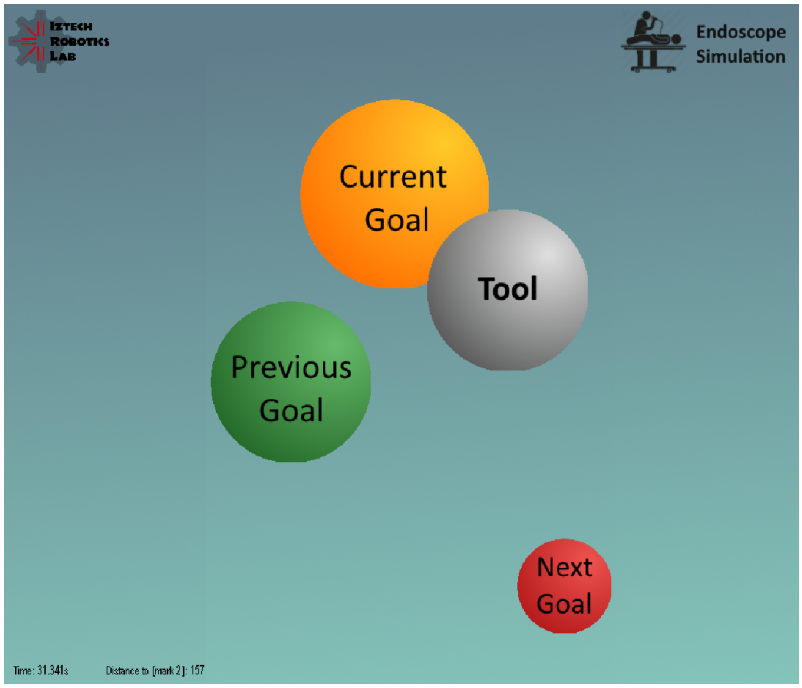

Figure 6.7. Training simulator screen shot

6.3.1. Experimental Setup

For this setup, the same hardware components and slave controller algorithm are used as described in Section 6.2.1.1. On the other hand, the slave system is a 2D platform which is written in Python language. The simulator is designate to count the number of pedal presses and calculates the simulation time on the background.

The goal of the simulation is to manipulate the *tool* to overlap the specified circles one at a time as directed by the simulation program (see figure 6.7). The grey circle named as ”tool” is the one that the user control by the ring. The green one called ”previous goal” is the target which has been passed. In other words, the ”tool” was matched with the ”previous goal” both in location and the size. Following, the yellow circle called ”current goal” is the one that user needs to match the tool. Finally, the red circle named ”next goal” is the target that user needs to match after matching the tool with the ”current goal”. As soon as all the targets are matched one by one in an order, the simulation time stops and records the overall performance into a log file.

This is made possible by connecting the microcontroller of the previously described system to a computer running the simulation software (emulating the endoscope holder). Pitch and yaw motions of the endoscope are mapped to the vertical and hor-

izontal translation of the *tool* respectively. The dolly endoscope motion is mapped to increase/decrease the radius of the *tool*.

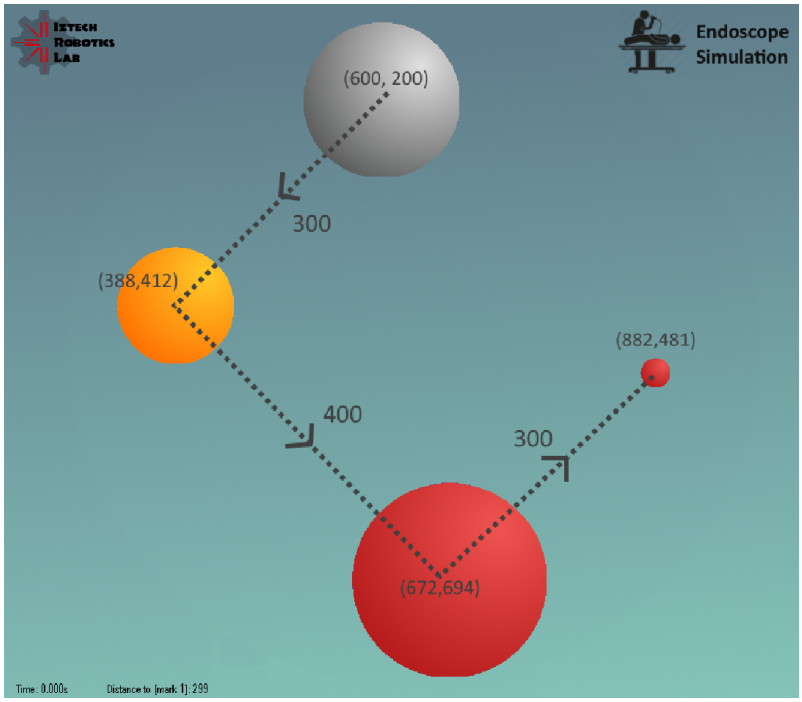

Figure 6.8. Example simulator map

In Figure 6.8, one simulation scenario is shown as an example. The numbers in parenthesis indicate the coordinates and numbers near to their respective dotted lines indicate the distances. The overall path is 1000 pixel in each map. The rest of scenarios have the same overall distance, however, each target has different coordinates and sizes. This arrangement makes sure the duration of each scenario does not depend on the total displacement but only on the learning to control the ”tool”.

The following metrics are used to measure the overall ”performance” of the proposed system:

- **Training time:** the time it took to complete a whole run of the simulation
- **Number of pedal presses:** the number of times the foot pedal was pressed during a run of the simulation

In the experimental procedure, 10 different subjects run 5 different scenarios two times for each mode described in section 5.2. All subjects performed their test on the same scenarios in the same order. This enables to plot the average improvement in performance in time, and visualize a learning curve of the system. Also, the correlation between the

time it took users to complete the simulation and the number of times they pressed the foot pedal is studied.

These measurements are performed on a limited workspace which is inside a 3D-printed skull as shown in Figure 6.9 provided by Hacettepe University Neurosurgery Department. The skull itself is made from a hard material to mimic the bones and it has a soft outer skin to provide the elastic feeling of the nose where the pivot point is located.

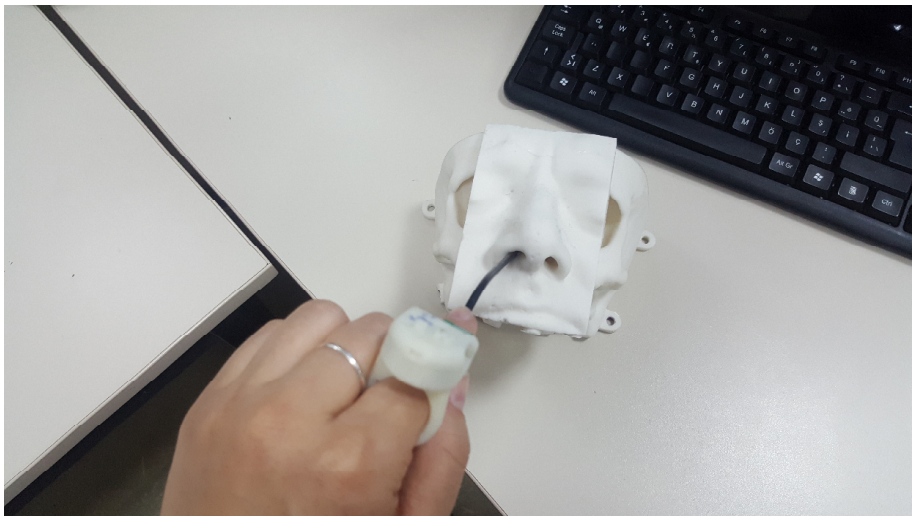

Figure 6.9. Constrained workspace in 3D printed skull

6.3.1.1. Test Results

The final evaluation shows that the three operation modes of the proposed teleoperation scheme have similar exponential curvature, although the two coupled modes have a steeper learning curve. In the initial trials (the first 5 trials), coupled mode 2D resulted in slightly shorter completion durations ($\sim$ 63 s average) over 3D ($\sim$ 73 s average) which are longer than the uncoupled mode's ($\sim$ 39 s average) (see figure 6.10). Moreover, the two coupled modes show almost the same longer learning curves compared to the uncoupled mode: their completion durations drop to 40 s limit in the 5^{th} trial whereas the uncoupled mode results drop to 40 s limit in the 2^{nd} trial. Similar to the decrease in completion durations for each consecutive trial, the average pedal press count shows a decreasing trend in all modes. In the 10^{th} trials, all modes' completion duration converge to $25 \sim 30$ and pedal press counts converge to $25 \sim 30$ counts.

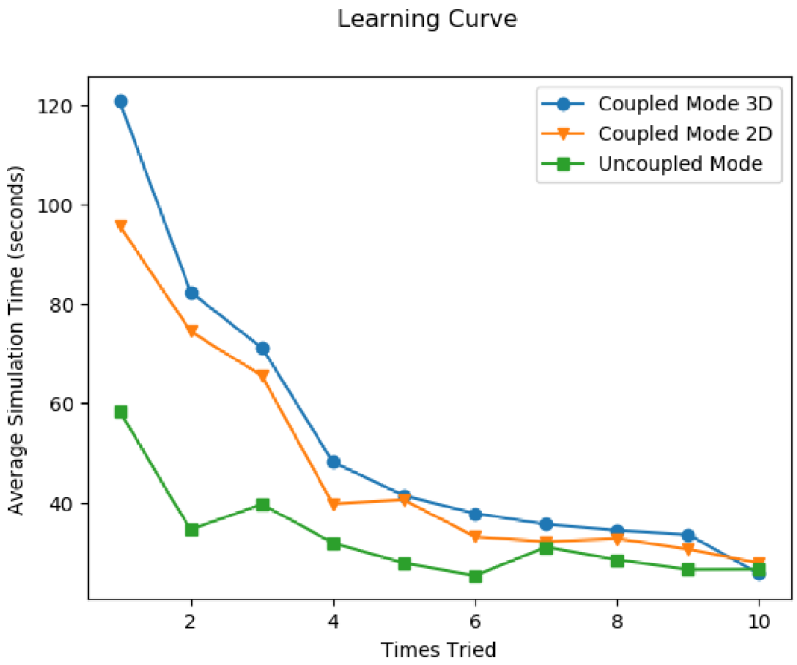

Figure 6.10. Plot of average time versus number of trials.

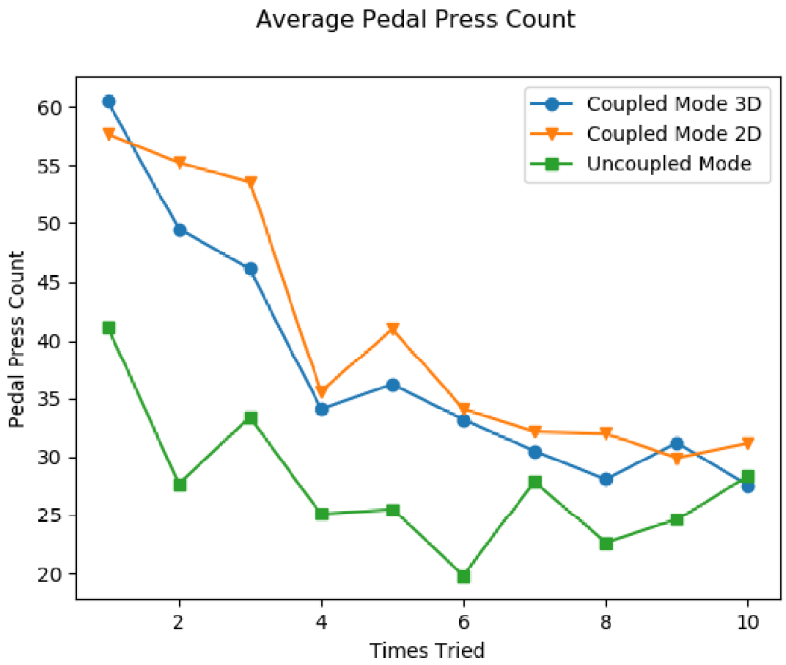

Figure 6.11. Plot of average pedal presses per trial.

6.4. Discussion

In the first test setup, the teleoperation system's information flow method was investigated and displacement-to-velocity method was chosen as easier to use by the doctors in Hacettepe University Neurosurgery Department.

Afterwards, two different tests were performed in order to enhance the usability of the master system. The first usability test was performed in order to determine the optimal scaling factors between the motion of the master and the slave. These parameters are selected as $scaling_{tra} = -40$ for translation and $scaling_{ori} = 8$ for the zoom by the same doctors. The second accessibility test was performed on a custom training simulator in order to assess the learning curve and the effort in use. Three different master usage modes are experienced on the simulator. The final evaluation showed that the three operation modes of the proposed teleoperation scheme have similar exponential curvature, although the two coupled modes have a steeper learning curve.

CHAPTER 7

CONCLUSION

A novel teleoperation system architecture is developed within the scope of this thesis. This study involves the teleoperation system design in both electronic and software aspects, and feasibility studies of this system for the use in the endoscopic pituitary surgery.

The operation scenario of this robotic endoscopic pituitary surgery system is developed within the scope of this thesis. In order to accomplish this, all the possible operation modes were identified from the initiation until the termination of the operation in order to efficiently and safely conduct the surgery.

In the proposed teleoperation system, the ring-shaped master controller captures the hand gestures of the surgeon using an IMU (Inertial Measurement Unit) and transmits this information wirelessly (via Bluetooth Low Energy). This transmitted information is later processed on the slave side as a velocity or position demand of the active endoscope holder. In other words, this active endoscope holder is positioned during the surgery according to surgeon's online demands issued by the master controller. As a response from the slave system, the interaction force level is sent back to the master side and displayed on an LED panel. Additionally other informative visual feedbacks are provided to facilitate the process.

The subsystems of the proposed teleoperation system are introduced by describing their purposes and components respectively in Chapter 3. The experimentations that are carried out to determine the required workspace of the active endoscope holder are described and their results are discussed in Chapter 4.

Moreover, in Chapter 5, system operation modes are explained in three sections; teleoperation information flow alternatives, master system's command computation alternatives and overall system's operation states. Finally, user evaluation experiments are described and their results are shared in Chapter 6.

The surgical team in Hacettepe University found the proposed teleoperation system architecture to be convenient for use in endoscopic pituitary surgeries. Additionally, other subjects who performed experiments to evaluate the usability of the system stated that the master system is easy to operate with and it is found to be relatively easy to learn how to use the device.

As a future study, the proposed teleoperation scheme is going to be tested and evaluated by a surgical team in the laboratory environment and in ex-vivo tests on a cadaver.

REFERENCES

Almeida, J., L. A. De, M. F. Dal, M. Sampaio, R. Medina, M. Chacon, and J. Gondim (2015). Endoscopic skull base surgery: evaluation of current clinical outcomes. *Journal of neurosurgical sciences*.

Ates, G., R. Majani, and C. Dede (2018). Design of Teleoperation Scheme with a Wearable Master for Minimally Invasive Surgery. Cassino. Springer US.

ATI, I. A. ([Online; accessed 20-May-2018]). `http://www.ati-ia.com/app\_content/documents/9620-05-TWE.pdf`.

Austin, Edmund; Fong, C. P. (1987). Teleoperated Position Control of a PUMA Robot. In *Teleoperated Position Control of a PUMA Robot*, pp. 19.

Ballantyne, G. H. (2002). Robotic surgery, telerobotic surgery, telepresence, and telementoring: Review of early clinical results. *Surgical Endoscopy and Other Interventional Techniques 16*(10), 1389–1402.

Beasley, R. A. (2012). Medical robots: current systems and research directions. *Journal of Robotics 2012*.

Berker, M., I. Işikay, D. Berker, M. Bayraktar, and A. Gürlek (2013, nov). Early promising results for the endoscopic surgical treatment of cushing's disease. *Neurosurgical Review 37*(1), 105–114.

Berker, M., I. Işikay, D. Berker, M. Bayraktar, and A. Gürlek (2014). Early promising results for the endoscopic surgical treatment of cushing's disease. *Neurosurgical review 37*(1), 105–114.

Bluetooth, U. (2017). BlueNRG-MS Upgradable Bluetooth ® low energy network processor. (January).

Bluetooth(TM) (2001). *Bluetooth Specification*, Volume 1.

Bowersox, J. C., A. Shah, J. Jensen, J. Hill, P. R. Cordts, and P. S. Green (1996, feb). Vascular applications of telepresence surgery: Initial feasibility studies in swine. *Journal of Vascular Surgery 23*(2), 281–287.

Casals, A., J. Amat, and E. Laporte (1996, Apr). Automatic guidance of an assistant robot in laparoscopic surgery. In *Proceedings of IEEE International Conference on Robotics and Automation*, Volume 1, pp. 895–900 vol.1.

Chai3d ([Online; accessed 20-May-2018]). `www.chai3d.org`.

Cypress (2015). PSoC ® Creator™ Component Datasheet Generic Attribute Profile (GATT) Features GATT Client and Server General Description SIG adopted Pro-

files and Services Comprehensive APIs. pp. 408–943.

Davies, B. L., R. D. Hibberd, W. S. Ng, A. G. Timoney, and J. E. A. Wickham (1991, mar). The development of a surgeon robot for prostatectomies. *Proceedings of the Institution of Mechanical Engineers, Part H: Journal of Engineering in Medicine 205*(1), 35–38.

Dede, M. (2007). Adaptive Fault-Tolerant Teleoperation. *FIU Electronic Theses and Dissertations*, 308.

Dede, M. İ. C., G. Kiper, T. Ayav, E. Tatlıcıoğlu, B. Özdemirel, O. W. Maaroof, G. Ateş, M. Berker, İ. Işıkay, and Ş. Hanalioğlu (2018, april). Cerrahın anlık yönlendirilebildiği robot yardımlı endoskop kontrol sistemi mimarisi - neuroboscope. In *Türkiye Robotbilim Konferansıs*, pp. 1–5.

Dede, M. İ. C., O. W. Maaroof, G. Ateş, M. Berker, İ. Işıkay, and Ş. Hanalioğlu (2017, jul). Unilateral teleoperation design for a robotic endoscopic pituitary surgery system. In *New Trends in Medical and Service Robots*, pp. 101–115. Springer International Publishing.

Devol, J. G. C. (1954-12-10). *PROGRAMMED ARTICLE TRANSFER*. US2988237A.

Diagnostics, A. C. (2006). User Manual. (June), 1–36.

DialogSemiconductor ([Online; accessed 20-May-2018]). `https://www.dialog-semiconductor.com/iotsensor`.

Ezzat, S., S. L. Asa, W. T. Couldwell, C. E. Barr, W. E. Dodge, M. L. Vance, and I. E. McCutcheon (2004, jul). The prevalence of pituitary adenomas. *Cancer 101*(3), 613–619.

Finlay, P. A. (1989). Medical robotics—why, what and when. *Industrial Robot: An International Journal 16*(1), 37–39.

Fong, T. and C. Thorpe (2001). Vehicle teleoperation interfaces. *Autonomous robots 11*(1), 9–18.

FreeHandSurgeon (2010 [Online; accessed 20-May-2018]). `http://freehandsurgeon.com/`.

Glauser, D., H. Fankhauser, M. Epitaux, J.-L. Hefti, and A. Jaccottet (1995a). Neurosurgical robot minerva: first results and current developments. *Journal of Image Guided Surgery 1*(5), 266–272.

Glauser, D., H. Fankhauser, M. Epitaux, J.-L. Hefti, and A. Jaccottet (1995b). Neurosurgical robot minerva: First results and current developments. *Journal of Image Guided Surgery 1*(5), 266–272. PMID: 9080346.

Hamed, A., S. Tang, H. Ren, A. Squires, C. Payne, K. Masamune, G. Tang, J. Moham-

madpour Velni, and Z. Tse (2012, 12). Advances in haptics, tactile sensing, and manipulation for robot-assisted minimally invasive surgery, noninvasive surgery, and diagnosis. *2012*, 14.

Harris, S. J., F. Arambula-Cosio, Q. Mei, R. D. Hibberd, B. L. Davies, J. E. A. Wickham, M. S. Nathan, and B. Kundu (1997, apr). The probot—an active robot for prostate resection. *Proceedings of the Institution of Mechanical Engineers, Part H: Journal of Engineering in Medicine 211*(4), 317–325.

Hernandez-Vaquero, D., M. Fernandez-Fairen, A. Torres-Perez, and A. Santamaria (2012). Minimally invasive surgery versus conventional surgery. A review of the scientific evidence. *Revista Espanola de Cirugia Ortopedica y Traumatologia (English Edition) 56*(6), 444–458.

Ho, G., W. Ng, M. Teo, C. Kwoh, and W. Cheng (2001). Computer-assisted transurethral laser resection of the prostate (CALRP): theoretical and experimental motion plan. *IEEE Transactions on Biomedical Engineering 48*(10), 1125–1133.

IntuitiveSurgical (2000 [Online; accessed 20-May-2018]). *The da Vinci Surgical System*. `www.davincisurgery.com`.

Jakopec, M., S. J. Harris, F. R. y Baena, P. Gomes, and B. L. Davies (2002). Acrobot: a "hands-on" robot for total knee replacement surgery. In *7th International Workshop on Advanced Motion Control. Proceedings (Cat. No.02TH8623)*, pp. 116–120.

Jane, J. A., L. D. Sulton, and E. R. Laws (2005, nov). Surgery for primary brain tumors at united states academic training centers: results from the residency review committee for neurological surgery. *Journal of Neurosurgery 103*(5), 789–793.

Kapoor, A., R. Kumar, and R. H. Taylor (2003). Simple biomanipulation tasks with "steady hand" cooperative manipulator. In R. E. Ellis and T. M. Peters (Eds.), *Medical Image Computing and Computer-Assisted Intervention - MICCAI 2003*, Berlin, Heidelberg, pp. 141–148. Springer Berlin Heidelberg.

Kim, K. C. (Ed.) (2014). *Robotics in General Surgery*. Springer New York.

Kockerling, F. (2014). Robotic vs. standard laparoscopic technique What is Better? *Frontiers in Surgery 1*(May), 10–13.

Komotar, R. J., R. M. Starke, D. M. S. Raper, V. K. Anand, and T. H. Schwartz (2011, oct). Endoscopic endonasal compared with microscopic transsphenoidal and open transcranial resection of giant pituitary adenomas. *Pituitary 15*(2), 150–159.

Kubo, R., N. Iiyama, K. Natori, K. Ohnishi, and H. Furukawa (2007, 01). Performance analysis of a three-channel control architecture for bilateral teleoperation with time delay. *127*, 1224–1230.

Kwoh, Y., J. Hou, E. Jonckheere, and S. Hayati (1988). A robot with improved absolute positioning accuracy for CT guided stereotactic brain surgery. *IEEE Transactions*

on Biomedical Engineering 35(2), 153–160.

Lanfranco, A. R., A. E. Castellanos, J. P. Desai, and W. C. Meyers (2004). Robotic Surgery. *Annals of Surgery 239*(1), 14–21.

MaxonMotor ([Online; accessed 20-May-2018]a). *228384 part number brakes*. www.maxonmotor.com/maxon/view/product/accessory/brake/228384.

MaxonMotor ([Online; accessed 20-May-2018]b). *339150 part number brushes DC motors*. www.maxonmotor.com/maxon/view/product/motor/dcmotor/re/re25/339150.

Mohammad, S. (2013, jan). Robotic surgery. *Journal of Oral Biology and Craniofacial Research 3*(1), 2.

Mourik, T. V. (2005). Programming Manual. (December), 1–99.

Moustris, G. P., S. C. Hiridis, K. Deliparaschos, and K. Konstantinidis (2011). Evolution of autnomous and semi-autnomous robotic surgical systems: a review of the literature. *The international journal of medical robotics + computer assisted surgery : MRCAS 7*(April), 375–392.

Nathan, C.-A., V. Chakradeo, K. Malhotra, H. D'Agostino, and R. Patwardhan (2006, may). The voice-controlled robotic assist scope holder AESOP for the endoscopic approach to the sella. *Skull Base 16*(03), 123–131.

Petermann, J., R. Kober, R. Heinze, J. J. Frölich, P. F. Heeckt, and L. Gotzen (2000). Computer-assisted planning and robot-assisted surgery in anterior cruciate ligament reconstruction. *Operative Techniques in Orthopaedics 10*(1), 50 – 55.

Pisaneschi, M. and G. Kapoor (2005, feb). Imaging the sella and parasellar region. *Neuroimaging Clinics of North America 15*(1), 203–219.

Polet, R. and J. Donnez (2008). Using a laparoscope manipulator (LAPMAN) in laparoscopic gynecological surgery. *Surgical technology international 17*, 187–91.

Primus, F. J., M. D. Goldenberg, and S. Hills (1991). United States Patent (19). (19).

Rosheim, M. E. (1994). *Robot evolution: the development of anthrobotics*. John Wiley & Sons.

STBLE-RF, S. ([Online; accessed 20-May-2018]). www.st.com/en/wireless-connectivity/spbtle-rf.html.

Steinhart, H., K. Bumm, J. Wurm, and H. Iro (2015). Surgical Application of a New Robotic System for Paranasal Sinus Surgery - Steinhart 2004.pdf. pp. 303–309.

STM32F401RE, S. ([Online; accessed 20-May-2018]). www.st.com/en/evaluation-tools/nucleo-f401re.html.

STM32F407VG, S. ([Online; accessed 20-May-2018]). www.st.com/en/microcontrollers/stm32f407vg.html.

Takahashi, M., M. Takahashi, N. Nishinari, H. Matsuya, T. Tosha, Y. Minagawa, O. Shimooki, and T. Abe (2017, Feb). Clinical evaluation of complete solo surgery with the "viky®" robotic laparoscope manipulator. *Surgical Endoscopy 31*(2), 981–986.

Taniguchi, K., A. Nishikawa, and M. Sekimoto (2010). Classification, design and evaluation of endoscope robots. *Robot Surgery 1*(January), 172.

Taylor, R., P. Jensen, L. Whitcomb, A. Barnes, R. Kumar, D. Stoianovici, P. Gupta, Z. Wang, E. DeJuan, and L. Kavoussi (1999, 12). Steady-hand robotic system for microsurgical augmentation. *International Journal of Robotics Research 18*(12), 1201–1210.

ThinkSurgical (1986 [Online; accessed 20-May-2018]). *ROBODOC Surgical System*. https://www.thinksurgical.com/company/history.

TitanMedical (2009 [Online; accessed 20-May-2018]). titanmedicalinc.com/technology.

Vertut, J. and P. Coiffet (1986). *Teleoperation and robotics: evolution and development*. Teleoperation and Robotics. Kogan Page.

Voros, S., G.-P. Haber, J.-F. Menudet, J.-A. Long, and P. Cinquin (2010, dec). ViKY robotic scope holder: Initial clinical experience and preliminary results using instrument tracking. *IEEE/ASME Transactions on Mechatronics*.

Wei, G.-q., K. Arbter, G. Hirzinger, W. Guo-Qing, K. Arbter, G. Hirzinger, G.-q. Wei, K. Arbter, and G. Hirzinger (1997). Real-time visual servoing for laparoscopic surgery. Controlling robot motion with color image segmentation. *Engineering in Medicine and Biology Magazine, IEEE 16*(1), 40–45.

Wen, J. T. (2001). EndoBot: a robotic assistant in minimally invasive surgeries. *Proceedings 2001 ICRA. IEEE International Conference on Robotics and Automation (Cat. No.01CH37164) 2*(June 2014), 2031–2036.

Yaşır, A. and G. Kiper (2018). Structural synthesis of 2R1T type mechanisms for minimally invasive surgery applications. *Mechanisms and Machine Science 52*, 31–38.

Yip, M. and N. Das (2017). Robot Autonomy for Surgery. pp. 1–33.

Yoshino, I., T. Yasunaga, M. Hashizume, and Y. Maehara (2005). A novel endoscope manipulator, naviot, enables solo-surgery to be performed during video-assisted thoracic surgery. *Interactive CardioVascular and Thoracic Surgery 4*(5), 404–405.

APPENDIX A

PERIPHERAL CONFIGURATIONS

Implementation of the proposed teleoperation scheme has been started on STM32CubeMX environment. This tool allows the users to initialize their C code for STM32 microcontroller series. The following implementation named as *All_in_One* includes every buttons and sensors mentioned in section 3 by explaining peripheral setups and pin connections as well as the clock configurations of the overall microcontroller. The following report has been generated by the CubeMX tool itself.

First of all MCU selection was made as described in table A.1

Table A.1. MCU selection of the implemented algorithm

MCU Series	STM32F4
MCU Line	STM32F407/417
MCU name	STM32F407VGTx
MCU Package	LQFP100
MCU Pin number	100

Before presenting the report, it is important to clarify the pin labels. Please take references from the abbreviation section while reading the Table A.2

Table A.2. Clarification of pin labels assigned on MCU

Label	Explanation
Ux**y**_IN**z**	Input pin **z** of motor **y** connected to U**x** driver
Ux**y**_EN**z**	Enable pin **z** of motor **y** connected to U**x** driver
Ux**y**_PWM**z**_T**a**C**b**	Reference voltage pin for PWM current control **z** of motor **y** connected to U**x** driver on the channel **b** of the timer **a**
FT_SG**x**	$\mathbf{x}^{th}$ strain gauge output of the force/torque sensor
BLE_CS	Chip Select pin of the Bluetooth module
BLE_CLK	Clock pin of the Bluetooth module
BLE_MOSI	Master-out-slave-in pin of the Bluetooth module
BLE_MISO	Master-in-slave-out pin of the Bluetooth module
BLE_RESET	Hard reset pin of the Bluetooth module
BLE_IRQ	Interrupt input of the Bluetooth module
ENC_CS_PAS**x**	Chip Select pin of the encoder attached to the $\mathbf{x}^{th}$ joint of the **PEK**
ENC_CS_U**xy**	Chip Select pin of the encoder attached onto the motor **y** connected to U**x** driver
ENC_CLK	Clock pin of the encoder chain
ENC_MOSI	Master-out-slave-in pin of the encoder chain
ENC_MISO	Master-in-slave-out pin of the encoder chain
BRAKE_ACTIVE	Pin for triggering the MOSFET which controls the 3-brakes on the **KEY**
BRAKE_PASSIVE1	Pin for triggering the MOSFET which controls the 2-brakes on the arm of the **PEK**
BRAKE_PASSIVE2	Pin for triggering the MOSFET which controls the 3-brakes on the wrist of the **PEK**
CEK_T8CH1	PWM input of CEK (Surgeon Holds Endoscope) switch on the channel-1 of the timer-8
PEDAL_IRQ	Interrupt input pin of the **KBE**
MKB_IRQ	Interrupt input pin of the **MKB**
ASB_IRQ	Interrupt input pin of the **ASB**
LASER_OUT	Pin for triggering the laser pointer

2. Pinout Configuration

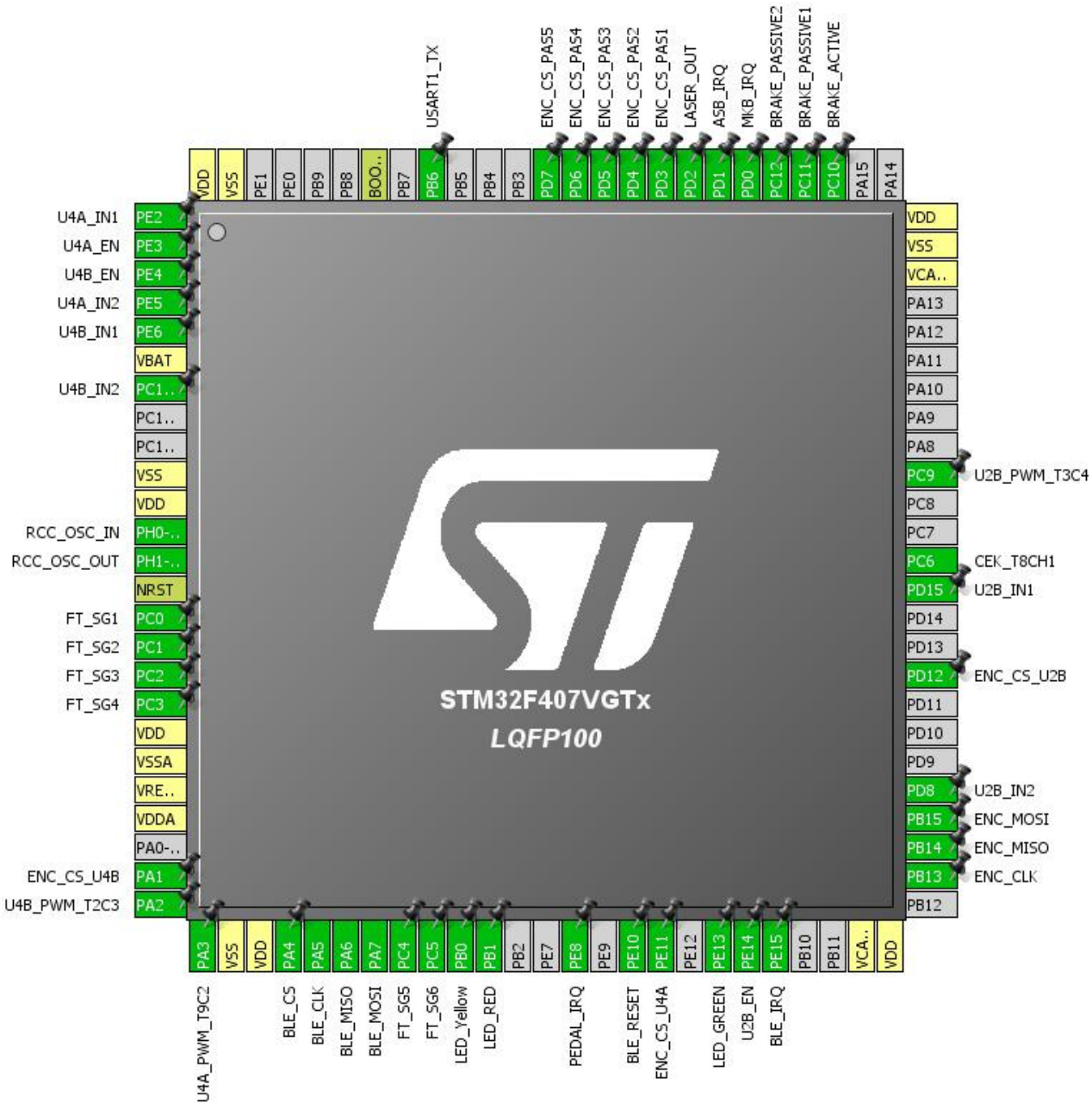

3. Pins Configuration

Pin Number LQFP100	Pin Name (function after reset)	Pin Type	Alternate Function(s)	Label
1	PE2 *	I/O	GPIO_Output	U4A_IN1
2	PE3 *	I/O	GPIO_Output	U4A_EN
3	PE4 *	I/O	GPIO_Output	U4B_EN
4	PE5 *	I/O	GPIO_Output	U4A_IN2
5	PE6 *	I/O	GPIO_Output	U4B_IN1
6	VBAT	Power		
7	PC13-ANTI_TAMP *	I/O	GPIO_Output	U4B_IN2
10	VSS	Power		
11	VDD	Power		
12	PH0-OSC_IN	I/O	RCC_OSC_IN	
13	PH1-OSC_OUT	I/O	RCC_OSC_OUT	
14	NRST	Reset		
15	PC0	I/O	ADC1_IN10	FT_SG1
16	PC1	I/O	ADC1_IN11	FT_SG2
17	PC2	I/O	ADC1_IN12	FT_SG3
18	PC3	I/O	ADC1_IN13	FT_SG4
19	VDD	Power		
20	VSSA	Power		
21	VREF+	Power		
22	VDDA	Power		
24	PA1 *	I/O	GPIO_Output	ENC_CS_U4B
25	PA2	I/O	TIM2_CH3	U4B_PWM_T2C3
26	PA3	I/O	TIM9_CH2	U4A_PWM_T9C2
27	VSS	Power		
28	VDD	Power		
29	PA4 *	I/O	GPIO_Output	BLE_CS
30	PA5	I/O	SPI1_SCK	BLE_CLK
31	PA6	I/O	SPI1_MISO	BLE_MISO
32	PA7	I/O	SPI1_MOSI	BLE_MOSI
33	PC4	I/O	ADC1_IN14	FT_SG5
34	PC5	I/O	ADC1_IN15	FT_SG6
35	PB0 *	I/O	GPIO_Output	LED_Yellow
36	PB1 *	I/O	GPIO_Output	LED_RED
39	PE8	I/O	GPIO_EXTI8	PEDAL_IRQ
41	PE10 *	I/O	GPIO_Output	BLE_RESET
42	PE11 *	I/O	GPIO_Output	ENC_CS_U4A

Pin Number LQFP100	Pin Name (function after reset)	Pin Type	Alternate Function(s)	Label
44	PE13 *	I/O	GPIO_Output	LED_GREEN
45	PE14 *	I/O	GPIO_Output	U2B_EN
46	PE15	I/O	GPIO_EXTI15	BLE_IRQ
49	VCAP_1	Power		
50	VDD	Power		
52	PB13	I/O	SPI2_SCK	ENC_CLK
53	PB14	I/O	SPI2_MISO	ENC_MISO
54	PB15	I/O	SPI2_MOSI	ENC_MOSI
55	PD8 *	I/O	GPIO_Output	U2B_IN2
59	PD12 *	I/O	GPIO_Output	ENC_CS_U2B
62	PD15 *	I/O	GPIO_Output	U2B_IN1
63	PC6	I/O	TIM8_CH1	CEK_T8CH1
66	PC9	I/O	TIM3_CH4	U2B_PWM_T3C4
73	VCAP_2	Power		
74	VSS	Power		
75	VDD	Power		
78	PC10 *	I/O	GPIO_Output	BRAKE_ACTIVE
79	PC11 *	I/O	GPIO_Output	BRAKE_PASSIVE1
80	PC12 *	I/O	GPIO_Output	BRAKE_PASSIVE2
81	PD0	I/O	GPIO_EXTI0	MKB_IRQ
82	PD1	I/O	GPIO_EXTI1	ASB_IRQ
83	PD2 *	I/O	GPIO_Output	LASER_OUT
84	PD3 *	I/O	GPIO_Output	ENC_CS_PAS1
85	PD4 *	I/O	GPIO_Output	ENC_CS_PAS2
86	PD5 *	I/O	GPIO_Output	ENC_CS_PAS3
87	PD6 *	I/O	GPIO_Output	ENC_CS_PAS4
88	PD7 *	I/O	GPIO_Output	ENC_CS_PAS5
92	PB6	I/O	USART1_TX	
94	BOOT0	Boot		
99	VSS	Power		
100	VDD	Power		

* The pin is affected with an I/O function

4. Clock Tree Configuration

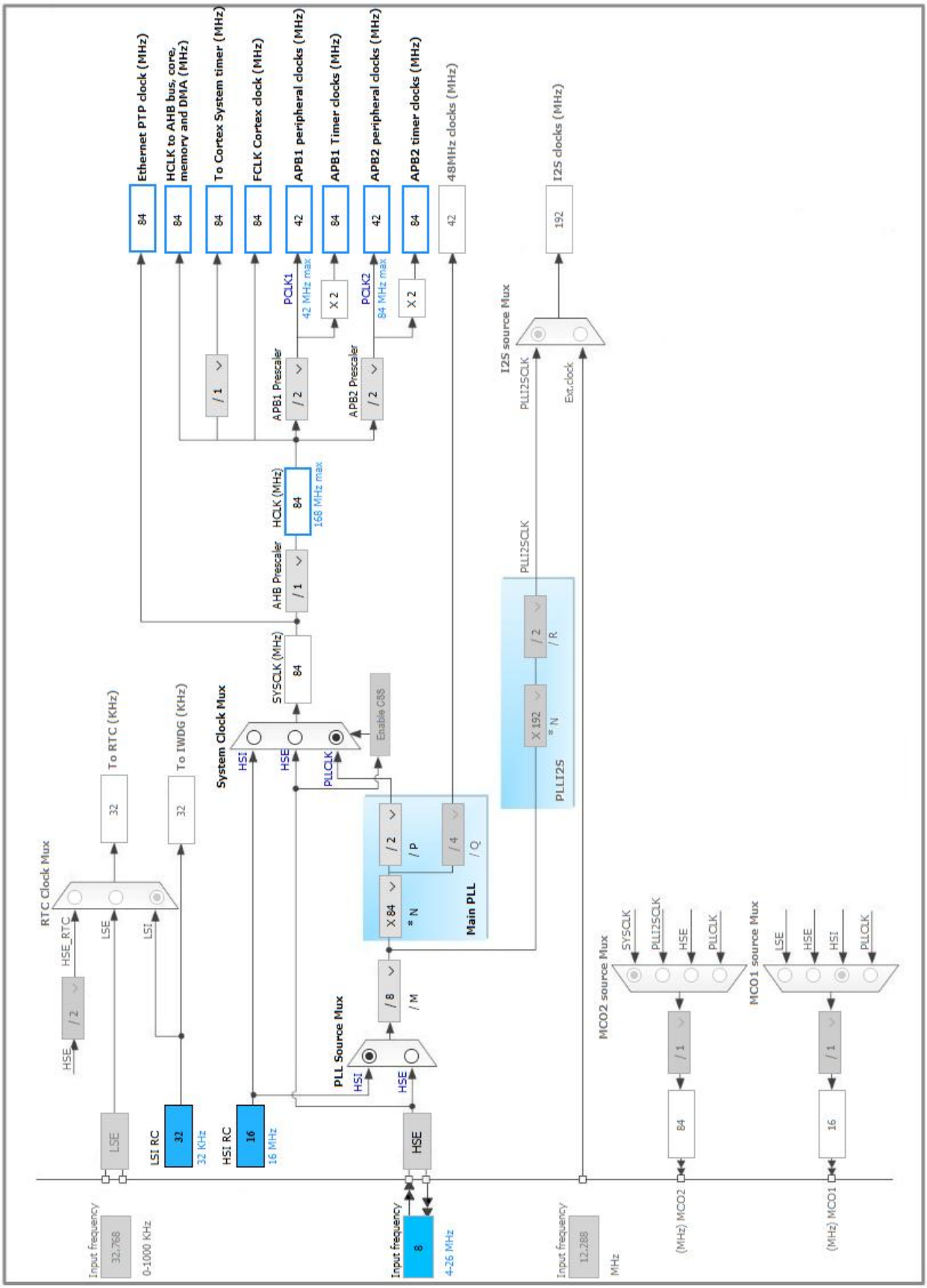

5. IPs and Middleware Configuration

5.1. ADC1

mode: IN10
mode: IN11
mode: IN12
mode: IN13
mode: IN14
mode: IN15

5.1.1. Parameter Settings:

ADCs_Common_Settings:	
Mode	Independent mode
ADC_Settings:	
Clock Prescaler	**PCLK2 divided by 4 ***
Resolution	**8 bits (11 ADC Clock cycles) ***
Data Alignment	Right alignment
Scan Conversion Mode	**Enabled ***
Continuous Conversion Mode	**Enabled ***
Discontinuous Conversion Mode	Disabled
DMA Continuous Requests	**Enabled ***
End Of Conversion Selection	EOC flag at the end of single channel conversion
ADC_Regular_ConversionMode:	
Number Of Conversion	**6 ***
External Trigger Conversion Source	Regular Conversion launched by software
External Trigger Conversion Edge	None
Rank	1
Channel	Channel 10
Sampling Time	3 Cycles
Rank	**2 ***
Channel	**Channel 11 ***
Sampling Time	3 Cycles
Rank	**3 ***
Channel	**Channel 12 ***
Sampling Time	3 Cycles
Rank	

	4 *
Channel	**Channel 13 ***
Sampling Time	3 Cycles
Rank	**5 ***
Channel	**Channel 14 ***
Sampling Time	3 Cycles
Rank	**6 ***
Channel	**Channel 15 ***
Sampling Time	3 Cycles
ADC_Injected_ConversionMode:	
Number Of Conversions	0
WatchDog:	
Enable Analog WatchDog Mode	false

5.2. RCC

High Speed Clock (HSE): Crystal/Ceramic Resonator

5.2.1. Parameter Settings:

System Parameters:	
VDD voltage (V)	3.3
Instruction Cache	Enabled
Prefetch Buffer	Enabled
Data Cache	Enabled
Flash Latency(WS)	2 WS (3 CPU cycle)
RCC Parameters:	
HSI Calibration Value	16
HSE Startup Timout Value (ms)	100
LSE Startup Timout Value (ms)	5000
Power Parameters:	
Power Regulatror Voltage Scale	Power Regulator Voltage Scale 1

5.3. SPI1

Mode: Full-Duplex Master

5.3.1. Parameter Settings:

Basic Parameters:

Frame Format	Motorola
Data Size	8 Bits
First Bit	MSB First

Clock Parameters:

Prescaler (for Baud Rate)	**4 ***
Baud Rate	**10.5 MBits/s ***
Clock Polarity (CPOL)	Low
Clock Phase (CPHA)	1 Edge

Advanced Parameters:

CRC Calculation	Disabled
NSS Signal Type	Software

5.4. SPI2

Mode: Full-Duplex Master

5.4.1. Parameter Settings:

Basic Parameters:

Frame Format	Motorola
Data Size	**16 Bits ***
First Bit	MSB First

Clock Parameters:

Prescaler (for Baud Rate)	**4 ***
Baud Rate	**10.5 MBits/s ***
Clock Polarity (CPOL)	**High ***
Clock Phase (CPHA)	**2 Edge ***

Advanced Parameters:

CRC Calculation	Disabled
NSS Signal Type	Software

5.5. SYS

Timebase Source: SysTick

5.6. TIM2

Channel3: PWM Generation CH3

5.6.1. Parameter Settings:

Counter Settings:

Prescaler (PSC - 16 bits value)	**41 ***
Counter Mode	Up
Counter Period (AutoReload Register - 32 bits value)	**99 ***
Internal Clock Division (CKD)	No Division

Trigger Output (TRGO) Parameters:

Master/Slave Mode (MSM bit)	Disable (Trigger input effect not delayed)
Trigger Event Selection	Reset (UG bit from TIMx_EGR)

PWM Generation Channel 3:

Mode	PWM mode 1
Pulse (32 bits value)	**50 ***
Fast Mode	Disable
CH Polarity	High

5.7. TIM3

Channel4: PWM Generation CH4

5.7.1. Parameter Settings:

Counter Settings:

Prescaler (PSC - 16 bits value)	**41 ***
Counter Mode	Up
Counter Period (AutoReload Register - 16 bits value)	**99 ***
Internal Clock Division (CKD)	No Division

Trigger Output (TRGO) Parameters:

Master/Slave Mode (MSM bit)	Disable (Trigger input effect not delayed)
Trigger Event Selection	Reset (UG bit from TIMx_EGR)

PWM Generation Channel 4:

Mode	PWM mode 1
Pulse (16 bits value)	

	50 *
Fast Mode	Disable
CH Polarity	High

5.8. TIM4

Channel2: Output Compare No Output

5.8.1. Parameter Settings:

Counter Settings:

Prescaler (PSC - 16 bits value)	**83 ***
Counter Mode	Up
Counter Period (AutoReload Register - 16 bits value)	**1999 ***
Internal Clock Division (CKD)	No Division

Trigger Output (TRGO) Parameters:

Master/Slave Mode (MSM bit)	Disable (Trigger input effect not delayed)
Trigger Event Selection	Reset (UG bit from TIMx_EGR)

Output Compare No Output Channel 2:

Mode	Frozen (used for Timing base)
Pulse (16 bits value)	0
CH Polarity	High

5.9. TIM5

Channel1: Output Compare No Output

5.9.1. Parameter Settings:

Counter Settings:

Prescaler (PSC - 16 bits value)	**83 ***
Counter Mode	Up
Counter Period (AutoReload Register - 32 bits value)	**249999 ***
Internal Clock Division (CKD)	No Division

Trigger Output (TRGO) Parameters:

Master/Slave Mode (MSM bit)	Disable (Trigger input effect not delayed)
Trigger Event Selection	Reset (UG bit from TIMx_EGR)

Output Compare No Output Channel 1:

Mode	Frozen (used for Timing base)
Pulse (32 bits value)	0
CH Polarity	High

5.10. TIM8

Combined Channels: PWM Input on CH1

5.10.1. Parameter Settings:

Counter Settings:

Prescaler (PSC - 16 bits value)	**20 ***
Counter Mode	Up
Counter Period (AutoReload Register - 16 bits value)	**65535 ***
Internal Clock Division (CKD)	No Division
Repetition Counter (RCR - 8 bits value)	0

Trigger Output (TRGO) Parameters:

Master/Slave Mode (MSM bit)	Disable (Trigger input effect not delayed)
Trigger Event Selection	Reset (UG bit from TIMx_EGR)

PWM Input CH1 :

Input Trigger	TI1FP1
Slave Mode Controller	Reset Mode
____ Parameters for Channel 1 ____	
Polarity Selection	Rising Edge
IC Selection	Direct
Prescaler Division Ratio	No division
Input Filter (4 bits value)	0
____ Parameters for Channel 2 ____	
Polarity Selection (opposite CH1)	Falling Edge
IC Selection	Indirect
Prescaler Division Ratio	No division
Input Filter (4 bits value)	0

5.11. TIM9

Channel2: PWM Generation CH2

5.11.1. Parameter Settings:

Counter Settings:

Prescaler (PSC - 16 bits value)	**41 ***
Counter Mode	Up
Counter Period (AutoReload Register - 16 bits value)	**99 ***
Internal Clock Division (CKD)	No Division

PWM Generation Channel 2:

Mode	PWM mode 1
Pulse (16 bits value)	**50 ***
Fast Mode	Disable
CH Polarity	High

5.12. USART1

Mode: Single Wire (Half-Duplex)

5.12.1. Parameter Settings:

Basic Parameters:

Baud Rate	**57600 ***
Word Length	8 Bits (including Parity)
Parity	None
Stop Bits	1

Advanced Parameters:

Data Direction	Receive and Transmit
Over Sampling	16 Samples

*** User modified value**

6. System Configuration

6.1. GPIO configuration

IP	Pin	Signal	GPIO mode	GPIO pull/up pull down	Max Speed	User Label
ADC1	PC0	ADC1_IN10	Analog mode	No pull-up and no pull-down	n/a	FT_SG1
	PC1	ADC1_IN11	Analog mode	No pull-up and no pull-down	n/a	FT_SG2
	PC2	ADC1_IN12	Analog mode	No pull-up and no pull-down	n/a	FT_SG3
	PC3	ADC1_IN13	Analog mode	No pull-up and no pull-down	n/a	FT_SG4
	PC4	ADC1_IN14	Analog mode	No pull-up and no pull-down	n/a	FT_SG5
	PC5	ADC1_IN15	Analog mode	No pull-up and no pull-down	n/a	FT_SG6
RCC	PH0-OSC_IN	RCC_OSC_IN	n/a	n/a	n/a	
	PH1-OSC_OUT	RCC_OSC_OUT	n/a	n/a	n/a	
SPI1	PA5	SPI1_SCK	Alternate Function Push Pull	No pull-up and no pull-down	**Very High ***	BLE_CLK
	PA6	SPI1_MISO	Alternate Function Push Pull	No pull-up and no pull-down	**Very High ***	BLE_MISO
	PA7	SPI1_MOSI	Alternate Function Push Pull	No pull-up and no pull-down	**Very High ***	BLE_MOSI
SPI2	PB13	SPI2_SCK	Alternate Function Push Pull	No pull-up and no pull-down	**Very High ***	ENC_CLK
	PB14	SPI2_MISO	Alternate Function Push Pull	No pull-up and no pull-down	**Very High ***	ENC_MISO
	PB15	SPI2_MOSI	Alternate Function Push Pull	No pull-up and no pull-down	**Very High ***	ENC_MOSI
TIM2	PA2	TIM2_CH3	Alternate Function Push Pull	No pull-up and no pull-down	Low	U4B_PWM_T2C3
TIM3	PC9	TIM3_CH4	Alternate Function Push Pull	No pull-up and no pull-down	Low	U2B_PWM_T3C4
TIM8	PC6	TIM8_CH1	Alternate Function Push Pull	No pull-up and no pull-down	Low	CEK_T8CH1
TIM9	PA3	TIM9_CH2	Alternate Function Push Pull	No pull-up and no pull-down	Low	U4A_PWM_T9C2
USART1	PB6	USART1_TX	Alternate Function Open Drain	Pull-up	**Very High ***	
GPIO	PE2	GPIO_Output	Output Push Pull	No pull-up and no pull-down	Low	U4A_IN1
	PE3	GPIO_Output	Output Push Pull	No pull-up and no pull-down	Low	U4A_EN
	PE4	GPIO_Output	Output Push Pull	No pull-up and no pull-down	Low	U4B_EN
	PE5	GPIO_Output	Output Push Pull	No pull-up and no pull-down	Low	U4A_IN2
	PE6	GPIO_Output	Output Push Pull	No pull-up and no pull-down	Low	U4B_IN1

IP	Pin	Signal	GPIO mode	GPIO pull/up pull down	Max Speed	User Label
	PC13-ANTI_TAMP	GPIO_Output	Output Push Pull	No pull-up and no pull-down	Low	U4B_IN2
	PA1	GPIO_Output	Output Push Pull	No pull-up and no pull-down	**High ***	ENC_CS_U4B
	PA4	GPIO_Output	Output Push Pull	No pull-up and no pull-down	**Very High ***	BLE_CS
	PB0	GPIO_Output	Output Push Pull	No pull-up and no pull-down	Low	LED_Yellow
	PB1	GPIO_Output	Output Push Pull	No pull-up and no pull-down	Low	LED_RED
	PE8	GPIO_EXTI8	**External Interrupt Mode with Rising/Falling edge**	No pull-up and no pull-down	n/a	PEDAL_IRQ
	PE10	GPIO_Output	Output Push Pull	No pull-up and no pull-down	Low	BLE_RESET
	PE11	GPIO_Output	Output Push Pull	No pull-up and no pull-down	**High ***	ENC_CS_U4A
	PE13	GPIO_Output	Output Push Pull	No pull-up and no pull-down	Low	LED_GREEN
	PE14	GPIO_Output	Output Push Pull	No pull-up and no pull-down	Low	U2B_EN
	PE15	GPIO_EXTI15	External Interrupt Mode with Rising edge trigger detection	**Pull-down ***	n/a	BLE_IRQ
	PD8	GPIO_Output	Output Push Pull	No pull-up and no pull-down	Low	U2B_IN2
	PD12	GPIO_Output	Output Push Pull	No pull-up and no pull-down	**High ***	ENC_CS_U2B
	PD15	GPIO_Output	Output Push Pull	No pull-up and no pull-down	Low	U2B_IN1
	PC10	GPIO_Output	Output Push Pull	No pull-up and no pull-down	**Very High ***	BRAKE_ACTIVE
	PC11	GPIO_Output	Output Push Pull	No pull-up and no pull-down	**Very High ***	BRAKE_PASSIVE1
	PC12	GPIO_Output	Output Push Pull	No pull-up and no pull-down	**Very High ***	BRAKE_PASSIVE2
	PD0	GPIO_EXTI0	**External Interrupt Mode with Rising/Falling edge**	No pull-up and no pull-down	**n/a**	MKB_IRQ
	PD1	GPIO_EXTI1	External Interrupt Mode with Rising edge trigger detection	No pull-up and no pull-down	**n/a**	ASB_IRQ
	PD2	GPIO_Output	Output Push Pull	No pull-up and no pull-down	Low	LASER_OUT
	PD3	GPIO_Output	Output Push Pull	No pull-up and no pull-down	**High ***	ENC_CS_PAS1
	PD4	GPIO_Output	Output Push Pull	No pull-up and no pull-down	**High ***	ENC_CS_PAS2
	PD5	GPIO_Output	Output Push Pull	No pull-up and no pull-down	**High ***	ENC_CS_PAS3
	PD6	GPIO_Output	Output Push Pull	No pull-up and no pull-down	**High ***	ENC_CS_PAS4
	PD7	GPIO_Output	Output Push Pull	No pull-up and no pull-down	**High ***	ENC_CS_PAS5

6.2. DMA configuration

DMA request	Stream	Direction	Priority
ADC1	DMA2_Stream0	Peripheral To Memory	Low
SPI2_RX	DMA1_Stream3	Peripheral To Memory	Low
SPI2_TX	DMA1_Stream4	Memory To Peripheral	Low

ADC1: DMA2_Stream0 DMA request Settings:

Mode:	**Circular ***
Use fifo:	Disable
Peripheral Increment:	Disable
Memory Increment:	**Enable ***
Peripheral Data Width:	**Byte ***
Memory Data Width:	**Byte ***

SPI2_RX: DMA1_Stream3 DMA request Settings:

Mode:	Normal
Use fifo:	Disable
Peripheral Increment:	Disable
Memory Increment:	**Enable ***
Peripheral Data Width:	Half Word
Memory Data Width:	Half Word

SPI2_TX: DMA1_Stream4 DMA request Settings:

Mode:	Normal
Use fifo:	Disable
Peripheral Increment:	Disable
Memory Increment:	**Enable ***
Peripheral Data Width:	Half Word
Memory Data Width:	Half Word

6.3. NVIC configuration

Interrupt Table	Enable	Preenmption Priority	SubPriority
Non maskable interrupt	true	0	0
Hard fault interrupt	true	0	0
Memory management fault	true	0	0
Pre-fetch fault, memory access fault	true	0	0
Undefined instruction or illegal state	true	0	0
System service call via SWI instruction	true	0	0
Debug monitor	true	0	0
Pendable request for system service	true	0	0
System tick timer	true	0	0
EXTI line0 interrupt	true	2	0
EXTI line1 interrupt	true	1	1
DMA1 stream3 global interrupt	true	0	0
DMA1 stream4 global interrupt	true	0	0
EXTI line[9:5] interrupts	true	5	0
TIM4 global interrupt	true	5	0
SPI2 global interrupt	true	4	0
EXTI line[15:10] interrupts	true	1	0
TIM5 global interrupt	true	0	0
DMA2 stream0 global interrupt	true	0	0
PVD interrupt through EXTI line 16	unused		
Flash global interrupt	unused		
RCC global interrupt	unused		
ADC1, ADC2 and ADC3 global interrupts	unused		
TIM1 break interrupt and TIM9 global interrupt	unused		
TIM2 global interrupt	unused		
TIM3 global interrupt	unused		
SPI1 global interrupt	unused		
USART1 global interrupt	unused		
TIM8 break interrupt and TIM12 global interrupt	unused		
TIM8 update interrupt and TIM13 global interrupt	unused		
TIM8 trigger and commutation interrupts and TIM14 global interrupt	unused		
TIM8 capture compare interrupt	unused		
FPU global interrupt	unused		

*** User modified value**

APPENDIX B

IMPLEMENTED ALGORITHM

Since the code implemented on the microprocessor is overlong, the following flow chart explains the algorithm.

Start
System starts by activating AGA and ADD buttons.
Initialize HAL_Libraries
SystemClock Configuration
Initialize GPIO,DMA,ADC,SPIs,Timers and USART
All brakes are locked,
All LEDs are OFF.
Initialize Sensors, Motor drivers and Bluetooth Module
All motors' speed are set zero,
All encoder chip selects are high,
Bluetooth module is ready to connection.
Empty the HCI queue (BLE notification queue)
Initalize HCI (Preparing BLE Module for connection)
Enable MKB and ASB interrupts
Connect to the ring
Get the necessary handles
The primary service handle,
Gyroscope Report handle,
Configuration Report handle.
Enable the accelerometer and gyroscope notifications
Check the system state:
MKB interrupt (rising/falling edges)
Enable manual mode
case: MANUAL MODE
Error handler jump
If any disconnection occurs while the system operates
Disable manual mode
case: OPERATION MODE
Disable pedal interrupt
the timer which is being used to detect double click
Stop pedal's double click timer
Release passive arm brakes
Lock passive wrist brakes
Stop all the motors
Lock active brakes
Green LED OFF
Enable the laser pointer and vibration element on CEK
Set operation flag = 0
Disable sending notification of the ring
Lock passive arm brakes
Lock passive wrist brakes
Lock active wrist brakes
Disable the laser pointer and vibration element on CEK
Set operation flag = 1
ASB interrupt (falling edge)
Get SPI readings of encoders
Set ASB workspace
END
Enable operation mode
Start ASB check:
Has the ASB button ever pressed?
NO
Start red LED blinking
YES
Check CEK state:
FULL PRESSED
Set CEK state: ENDOSCOPE DETACHED
Disable pedal interrupt
Stop pedal's double click timer
Green LED OFF
Lock passive wrist brakes
Lock active brakes
Disable all motors
Enable the laser pointer and vibration element on CEK
Disable sending notification of the ring
Is CEK state == FULL PRESSED
NO
YES
HALF PRESSED
Set CEK state: ENDOSCOPE FLOATING
Disable MKB interrupt
Disable pedal interrupt
Stop pedal's double click timer
Green LED OFF
Release passive arm brakes
Release passive wrist brakes
Lock active brakes
Disable all motors
Enable laser pointer and vibration element on CEK
Disable sending notification of the ring
Is CEK state == HALF PRESSED
NO
YES
RELEASED
BREAK
Check MKB state:
HIGH
Set system state: MANUAL
Enable manual mode
LOW
BREAK
Does AKS need centering?
NO
YES
Is the system in ASB? OR CEK State == RELEASED
NO
Start green LED blinking
Wait 1 second
Do centering
Red LED OFF
YES
Red LED ON
Start pedal's double click timer
Enable pedal interrupt
Enable sending notification of the ring
Enable MKB interrupt
NO
YES
Is the system in operation state?
Disable the laser pointer and vibration element on CEK
NO
YES
Disable the laser pointer and vibration element on CEK
lock passive wrist brakes
lock passive arm brakes
START MAIN LOOP:
Is the CEK state RELEASED?
NO
YES
Start HCI Process
Is the operation flag == 1
NO
YES
Start operation mode
Start operation mode
Disable MKB interrupt
Lock passive arm brakes
Lock passive wrist brakes
Start HCI Process
Is the teleoperation state == OFF
YES
Green LED ON
Disable all motors
Lock active brakes
Enable MKB interrupt
NO
Pedal Interrupt (rising/falling edges)
Is the Pedal pin == HIGH
YES
teleoperation state = OFF
NO
Is double click counter < treshold
YES
teleoperation state = DOLLY
NO
teleoperation state = ANGLE
reset double click counter
reset angle accumulator
Is coupled mode enabled?
YES
Align gyroscope data to the earth frame
Is coupled mode in 3D?
YES
NO
COUPLED 3D
Is the teleoperation state == ANGLE
YES
Update angle accumulator such that:
angle->x += gyroscope_value->x;
angle->y += gyroscope_value->y;
angle->z += 0.0;
NO
Update angle accumulator such that:
angle->x += 0.0;
angle->y += 0.0;
angle->z += gyroscope_value->z;
COUPLED 2D
Is the teleoperation state == ANGLE
YES
Update angle accumulator such that:
angle->x += gyroscope_value->x;
angle->y += gyroscope_value->y;
angle->z += 0.0;
NO
Update angle accumulator such that:
angle->x += 0.0;
angle->y += 0.0;
angle->z += gyroscope_value->x;
NO
Is the teleoperation state == ANGLE
YES
UNCOUPLED 2D
Update angle accumulator such that:
angle->x += 0.0;
angle->y += gyroscope_value->x;
angle->z += 0.0;
Update angle accumulator such that:
angle->x += gyroscope_value->x;
angle->y += 0.0;
angle->z += gyroscope_value->z;
Apply control algorithms:
Read FT sensor values by ADC
Read encoder values by SPI
Kinematic calculations
Generate motor velocity demand
Is the force limit exceeded?
YES
Yellow LED ON
NO
Yellow LED OFF
Disable active brakes
Enable motors with the speed calculated by control algorithms
Return

APPENDIX C

TELEOPERATION MAP

This section shows the teleoperation signal flow between each component.

MASTER SYSTEM

SLAVE SYSTEM

Robotic Arm

User Interface

GPIO

CEK Switch

PWM

Laser Pointer

Vibration Element

GPIO

MKB

GPIO

ASB Button

GPIO

GPIO

IRQ

KBE (Foot Pedal)

Doctor's Ring

BOSCH BMI160 IMU

SPI

Antenna

DA14583 Microcontroller

Bluetooth 4.1 Low Energy

DRIVERS

System Manager

Communication Handling

Teleoperation Scheme

Control Algorithm

UART

LOG FILE

x6

DMA

ADC

Amplifier Circuit

Bias Reference Voltage Circuit

F/T Sensor

SPI

GPIO

CS

Encoders

SPI

GPIO

CS

Bluetooth Module

Reset

GPIO

IRQ

x9

GPIO

Brakes (in KEY)

GPIO

Brakes (in PEK)

MOSFET Circuit

Motor Driver

PWM

GPIO

Motor Driver

Active Arm

BRAKE_A1

BRAKE_A2

BRAKE_A3

MOTOR_1

MOTOR_2

MOTOR_3

Magnetic Interaction

Magnetic Interaction

Magnetic Interaction

Passive Arm

BRAKE_P1

BRAKE_P2

BRAKE_P3

BRAKE_P4

BRAKE_P5

Magnetic Interaction

Magnetic Interaction

Magnetic Interaction

Magnetic Interaction

Magnetic Interaction

APPENDIX D

AUXILIARY CIRCUITS

In this section, designed auxiliary circuits are presented in order to optimize the system.

D.1. Differential Amplifier Circuit for Force/Torque Sensor

ATI Industrial Automation's Mini45 force/torque sensor (ATI, 2018) has a 10-pin connector in order to be connected a DAQ card or Net F/T (Net Box) which is an interface provides EtherNet/IP and CAN bus communication with the sensor.

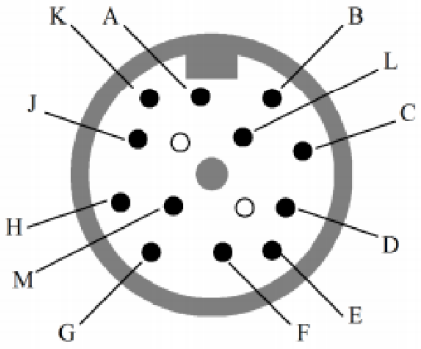

Figure D.1. ATI-IA Mini45 F/T sensor connector pin

A	Not Connected
B	SG4 output
C	SG5 output
D	SG2 output
E	SG3 output
F	SG0 output
G	SG1 output
H	Not Connected
J	SG_{LO} excitation input
K	SG_{HI} excitation input

Table D.1. Strain gauge output map of the ATI-IA Mini45 F/T Sensor

The experimental results shows that the strain gauge outputs shown in D.1 and labeled as in D.1 deliver 10mV difference analog signal between 0N-50N forces. In another words, each unity force (1N) produces about 0.2mV voltage difference on th outputs of the strain gauges. However, soft tissue experiments performed by the control team of NeuRoboScope project show that the exceeding force in order not to harm the tissue is maximum 4N. That means, the microcontroller should be able to detect the analog

signals lower than 1mV.

ADC module embedded to the STM32F407VG provides up to 12-bit resolution, which is 0.8mV error occurs between each bit due to ADC conversion. Therefore, even-though the ADC settings are adjusted to the highest precision, only increasing the ADC resolution is not enough for a precise enough measurement for such a case.

In order to overcome this problem, the differential amplifier circuit using rail-to-rail MCP6022 OPAMP is designed as shown in D.2. Each SGx output pin from the connector is connected to a separate OPAMP circuit from the non-inverting input of the opamp where the bias reference voltage circuit output is connected to inverting input. In order to eliminate the noise at the output, LC-filter is attached as shown in Figure D.2.

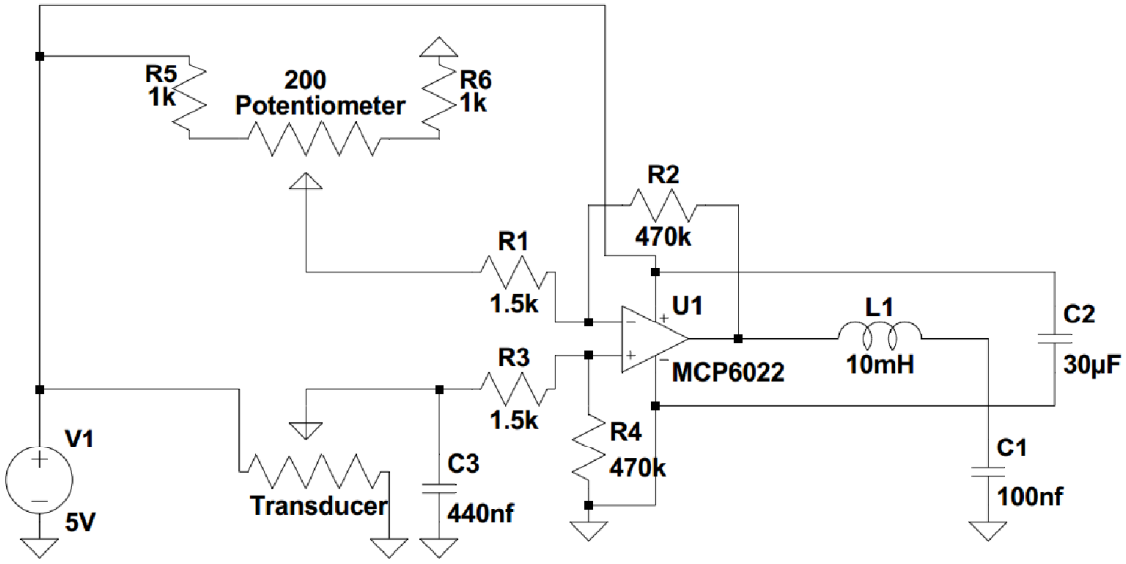

Figure D.2. OPAMP circuit designed to amplify the strain gauge output signals

The differential amplifier gain is calculated as $\frac{R3}{R1} = \frac{470k}{1.5k} = 313.3$. This differential amplifier circuit with 313.3 gain allows us to amplify 0.2mV signal which is produced by 1N applied force to 626.6mV. This value is detectable by STM32F407VG microprocessor's built-in ADC module.

8-bit resolution with 3.3V reference input causes 12.9mV ADC conversion error. This value is acceptable compared to 626.6mV per newton. Choosing lower resolution on ADC reduces the computation time on the processor. That's why as the optimal solution, SGx outputs are amplified by 313.3 and sampled in 8-bit resolution on the ADC module. The conversion on ADC module is read by DMA in order not to pause the microprocessor during conversion period of ADC and allow the system to compute other tasks.

D.2. Encoder Chain

As it is mentioned in Section 3.2.4, MA702 maghetic encoders provide three different outputs to the user. In this system two of these outputs are used for two different purposes as mention in Section 3.2.4 with reasons.

In this section, the connection type of eight encoders on a single SPI line is presented. There are three different SPI modules on STM32F407VG microcontroller. The reason of connected all of the eight encoders on a single line is to reduce the lack of pin and SPI modules. The connection map is presented in Figure D.3. The configuration settings of this connection chain can be found in Appendix A.

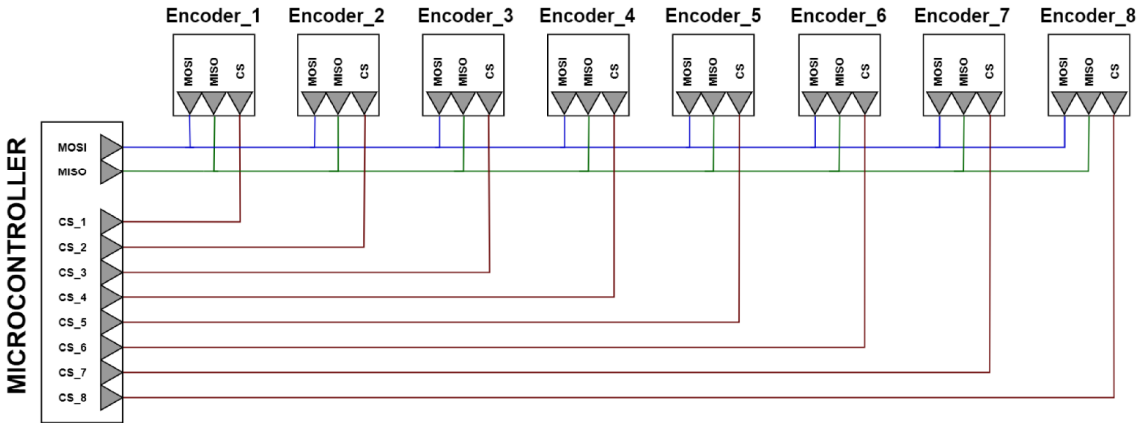

Figure D.3. Eight encoders' connection map with the microprocessor

D.3. MOSFET Driver for the Brakes

The main reason of using a driver circuit is because the microcontroller cannot provide sufficient power to the brakes. The general solution of driving these kind of components is designing a MOSFET circuit. The MOSFET circuit works as a power switch. By triggering its gate pin, the drain and source terminals are short-circuited and let the current flow from drain-to-source. The triggering gate voltage is depend on the MOSFET type. It can be either a negative gate-to-source voltage in p-channel MOSFETs or a positive gate-to-source voltage in n-channel MOSFETs.

The chosen brakes are is given in Section 3.2.7. According to the required power

for the brakes the total current that the system should provide is calculated as:

$$3x0.3A + 2x0.7A + 3x0.2A = 2.9A \tag{D.1}$$

According to the proposed the teleoperation scheme, some motors work synchronous according to operation state (see Appendix E). For that reason, two brakes on the arm structure of PEK, three brakes on the wrist structure of PEK and three brakes on KEY are controlled synchronously. Therefore, the calculation of the required power on three different MOSFET circuits are extended as:

$$3x0.3A = 0.9A \tag{D.2a}$$

$$2x0.7A = 1.4A \tag{D.2b}$$

$$3x0.2A = 0.6A \tag{D.2c}$$

where Equation D.2a is the required MOSFET current on which the driver circuit controlling the the brakes on the wrist of PEK, Equation D.2b is the required MOSFET current on which the driver circuit controlling the brakes on the arm of PEK and Equation D.2c is the required MOSFET current on which the driver circuit controlling the brakes of KEY.

Eventually, IRLR7843 n-channel power MOSFETs from Infineon Technologies are used. It supports up to 30V drain-to-source voltage and up to 161A continuous drain current at 10V. The representative circuit diagram is given in Figure D.4.

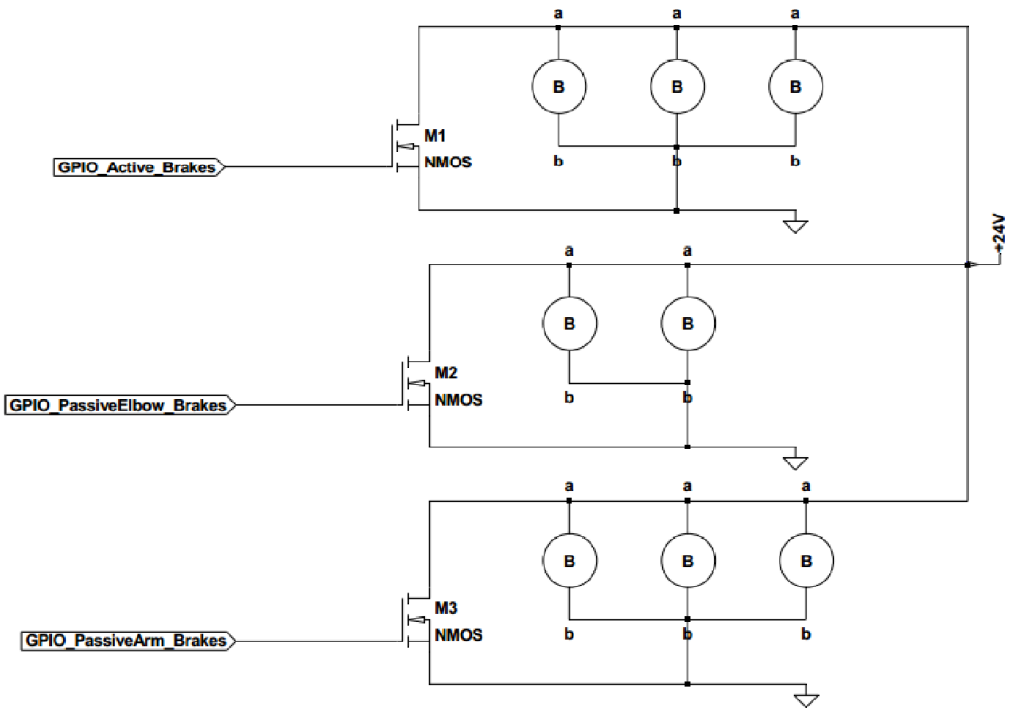

Figure D.4. Driver circuit for the brakes

APPENDIX E

OPERATION STATES

The following chart shows the operation states on the map.

HARDWARE STATES

SOFTWARE STATES

States | Scenarios | Buttons | Lights | Mechanical Systems

SHUT DOWN

The health team has not started to set up the system yet, or the operation has been completed and the system is shut down. All brakes are locked, all subsystems are closed.

AGA	OFF
ADD	x
MKB	x
CEK	x
KBE	x

All the lights are off.

KEY : locked
PEK : locked

AGA Pressed & ADD Pressed

AGA Pressed & ADD Released

CEK

Half pressed → PASSIVE: ENDOSCOPE IS HOLD

Full pressed → **MKB**

MKB ON → MANUAL

MKB OFF → PASSIVE: ENDOSCOPE IS DETACHED

OFF → **MKB**

MKB ON → MANUAL

MKB OFF → ASB Check starts

MANUAL

If the surgeon wishes to use the system as a passive endoscope holder, the system switches to this mode.
The surgeon should press the ASB button for 1 time at the beginning of the operation.

AGA	ON
ADD	Released
CEK	Released
MKB	Pressed
KBE	x

All the lights are off.

KEY : locked
PEK : arm released wrist locked

MKB ON & CEK released → PASSIVE: ENDOSCOPE IS HOLD

CEK half pressed → The surgeon can clean the endoscope without removing it. ALSO, PEK can be driven manually.
Homing may be required afterwards.

AGA	ON
ADD	Released
CEK	Half
MKB	x
KBE	x

CEK vibrator is active

KEY : locked
PEK : all released

CEK released & MKB ON → MANUAL

CEK fully pressed → PASSIVE: ENDOSCOPE IS DETACHED

The surgeon can remove the endoscope.
Homing is performed if necessary.

AGA	ON
ADD	Released
CEK	Pressed
MKB	Released
KBE	x

CEK vibrator is active

KEY : locked
PEK : all locked

MKB ON & CEK pressed → MANUAL

ASB Check starts

CEK released & MKB OFF → MANUAL

CEK released & MKB OFF → PASSIVE: ENDOSCOPE IS HOLD

MKB OFF & CEK released → **Surgery Zone Check (ASB Check)**

ASB button should be pressed

Red LED is blinking

No ← Has ASB set before?

Yes → Is homming required?

No → WAIT

Yes → Is the system is in surgery zone?

No → Red LED is off

wait ~1sec

Homming of KEY starts, Green LED is blinking

Yes → **Homming required. System should be manually moved outside of the surgery zone**

Red LED is on

At this time, the system can be moved out of the surgery zone by either interrupting the MKB or holding down the CEK key. The system changes the mode according to the input.

WAIT

Cerrah endoskobu istediği pozisyona sabitlemiştir.
Sistem Aktif Mod'a geçmek için beklemektedir.
Sistemin en çok bulunacağı moddur.

AGA	ON
ADD	Released
MKB	Released
CEK	Released
KBE	Released

Green LED is on

KEY : locked
PEK : locked

CEK half pressed → WAIT

CEK fully pressed → MKB pressed

KBE single pressed → **ACTIVE: ROTATION**

The surgeon controls the system via ring.
The system allows only pitch and yaw motions.
Control algorithms run in this state.

AGA	ON
ADD	Released
MKB	Released
CEK	Released
KBE	Single Pressed

Green LED is blinking

KEY : released
PEK : locked

KBE released → WAIT

KBE double pressed → **ACTIVE: DOLLY**

The surgeon controls the system via ring.
The system allows only dolly motions.
Control algorithms run in this state.

AGA	ON
ADD	Released
MKB	Released
CEK	Released
KBE	Double Pressed

Green LED is blinking

KEY : released
PEK : locked

KBE released → WAIT

CEK half pressed → WAIT

MKB pressed → WAIT

CEK fully pressed → WAIT

CEK half pressed

MKB Pressed

CEK fully pressed

ADD Pressed

ADD Released

EMERGENCY

System is still back drivable by the relay system connected the brakes on the arm structure of PEK.
The power of the microcontroller is cut.

AGA	ON
ADD	Pressed
MKB	x
CEK	x
KBE	x

All the lights are off

KEY : locked
PEK : arm released wrist locked

APPENDIX F

IMU MEASUREMENTS DURING A REAL SURGERY

The following table shows the maximum and minimum α and β angles in 22 different motions inside the surgical area of an ex-vivo subject. Three different filtering step sizes (5,10 and 40) are applied.

Table F.1. IMU measurements of 22 different motions with various filtering step sizes

No.	Operation	Max β	Min β	Max ω_β	Max α	Min α	Max ω_α
		(deg)	(deg)	(deg/sec)	(deg)	(deg)	(deg/sec)
1	No filtering	-15	-19		34	29	
	5 step	-15	-19	19	35	28	64
	10 step	-15	-19	6.4	35	28	33
	40 step	-16	-18	1.7	34	27	2.8
2	No filtering	-11	-13	5	35	29	5
	5 step	-6	-15	29	35	27	42
	10 step	-7	-14	8.9	35	28	12.7
	40 step	-11	-13	1.3	34	29	2.4
3	No filtering	-7	-15	2.3	38	28	4.6$\sim$6
	5 step	-7	-15	18	39	27	52.3
	10 step	-7	-15	10.3	38	27	23
	40 step	-8	-15	2.5	38	29	3.5
4	No filtering	-9	-14	4$\sim$15	33	29	$\sim$15
	5 step	-8	-14	21.8	37	28	40.5
	10 step	-8	-14	11.7	37	28	16.2
	40 step	-8	-13	1.8	36	29	3.1
5	No filtering	-8	-17	3	34	26	$\sim$20
	5 step	-8	-17	-20.2	34	25	23.8
	10 step	-9	-17	-12.4	34	27	10.5
	40 step	-10	-16	2.3	33	27	3.1
6	No filtering	-11	-15	1.6	35	29	12$\sim$22
	5 step	-10	-16	16	36	29	22.7
	10 step	-10	-16	5.4	35	29	10
	40 step	-10	-15	1.5	35	29	3
7	No filtering	-5	-17	4	44	22	5.2
	5 step	-4	-18	36.7	45	22	29.4
	10 step	-4	-18	21.2	44	22	15
	40 step	-5	-17	4	43	23	7.4

Table F.1. (cont.) IMU measurements of 22 different motions with various filtering step sizes

No.	Operation	Max β	Min β	Max ω_β	Max α	Min α	Max ω_α
		(deg)	(deg)	(deg/sec)	(deg)	(deg)	(deg/sec)
8	No filtering	-3	-10	4	38	23	10∼37
	5 step	-2	-10	48.6	39	22	74.2
	10 step	-3	-10	11	38	23	33.5
	40 step	-3	-10	2.6	38	29	5.7
9	No filtering	-15	-19	5	38	31	3∼6.8
	5 step	-15	-22	42.3	38	30	50.6
	10 step	-15	-20	11	38	31	11.9
	40 step	-15	-19	1.8	37	32	2.1
10	No filtering	-8	-16		30	16	4
	5 step	-4	-20	105∼65	33	12	114
	10 step	-5	-17	34	33	14	40
	40 step	-9	-15	3.2	29	19	7
11	No filtering	-4	-9		30	24	7.5
	5 step	1	-13	111	39	22	102
	10 step	-3	-11	24.8	34	24	28.5
	40 step	-4	-9	2	31	25	2.7
12	No filtering	-12	-15		33	29	
	5 step	-11	-15	13.6	33	28	16.5
	10 step	-12	-15	5.6	33	29	5.5
	40 step	-	-	-	-	-	-
13	No filtering	-8	-14	10	37	30	20
	5 step	-2	-22	42.9	36	25	50.9
	10 step	-4	-21	29.5	35	27	17.7
	40 step	-	-	-	-	-	-
14	No filtering	-14	-16	-	35	30	8∼30
	5 step	-4	-14	50.8	37	23	66.2
	10 step	-5	-12	16	34	24	26
	40 step	-8	-12	2.2	34	26	4.8
15	No filtering	-10	-17	20∼30	35	26	20
	5 step	-10	-18	40.6	36	25	28.8
	10 step	-10	-17	13.4	35	26	16.7
	40 step	-	-	-	-	-	-
16	No filtering			36	26		
	5 step	-2	-22	42.9	36	25	51
	10 step	-4	-21	29.5	35	26	17.7
	40 step	-	-	-	-	-	-
17	No filtering	-7	-12	8	35	25	25
	5 step	-4	-14	50.8	37	23	66.2
	10 step	-5	-12	16	34	24	26
	40 step	-8	-12	2.2	34	26	4.8
18	No filtering	-15	-20		40	36	
	5 step	-16	-20	14.8	40	36	22
	10 step	-17	-20	5.8	40	36	8.5
	40 step	-	-	-	-	-	-

Table F.1. (cont.) IMU measurements of 22 different motions with various filtering step sizes

No.	Operation	Max β	Min β	Max ω_β	Max α	Min α	Max ω_α
		(deg)	(deg)	(deg/sec)	(deg)	(deg)	(deg/sec)
19	No filtering					2	
	5 step	-13	-16	30.7	32	16	94
	10 step	-13	-16	45	31	21	18.2
	40 step	-	-	-	-	-	-
20	No filtering	-9	-12		32	28	
	5 step	-9	-12	11	32	28	13.3
	10 step	-9	-11	2	31	29	3.2
	40 step	-	-	-	-	-	-
21	No filtering	-5	-10		34	31	
	5 step	-3	-11	33.5	34	29	43
	10 step	-4	-10	8.8	34	29	17.5
	40 step	-	-	-	-	-	-
22	No filtering	-10	-14		35	28	$\sim$29
	5 step	-8	-15	39.6	35	27	36.4
	10 step	-9	-14	17.5	34	28	22.4
	40 step	-10	-14	1.9	33	29	3.7
Summary	No filtering	-3	-20	20$\sim$30	44	16	37
	5 step	1	-22	111	45	12	114
	10 step	-3	-21	45	44	14	40
	40 step	-3	-19	4	43	19	7.4